Technische Universität Braunschweig

emg

Monthol Homklintian

# Frequency Dependence of Primary Capacitance Standard in Audio Frequency Range

**Dissertation**
Braunschweig 2012

Berichte aus dem **Institut für Elektrische Messtechnik und Grundlagen der Elektrotechnik**

Band **40**

Hrsg. Prof. Dr. Meinhard Schilling

# Frequency Dependence of Primary Capacitance Standard in Audio Frequency Range

Von der Fakultät für Elektrotechnik, Informationstechnik, Physik der
Technischen Universität Carolo-Wilhelmina zu Braunschweig

zur Erlangung der Würde
eines Doktor-Ingenieurs (Dr.-Ing.)

genehmigte Dissertation

von
Monthol Homklintian

| | |
|---|---|
| aus (Geburtsort): | Samut Prakan, Thailand |
| eingereicht am: | 04.06.2012 |
| mündliche Prüfung am: | 07.08.2012 |
| Referenten: | Prof. Dr. rer. nat. Meinhard Schilling<br>Prof. Dr. rer. nat. Achim Enders<br>Prof. Dr. rer. nat. Marc Tornow (Vorsitz) |

2012

*To my wife, Chompunut Jenajaroen, and*

*to the memory of to my parents*

# Abstract

The Thompson–Lampard theorem is a theorem of electrostatics which describes a so-called cross capacitance independent of its cross sectional dimensions. It is therefore best suited to be used as a capacitance standard for the absolute determination of the unit of capacitance, the farad. As this cross capacitance is defined for DC but must be operated at AC, a frequency correction must be applied the uncertainty of which is one of the largest contributions to the uncertainty budget. The frequency correction can be calculated with a sufficient accuracy using an equivalent circuit model which describes the behavior of the calculable cross capacitor at AC. Calculable cross capacitors are mostly operated at a frequency of 1592 Hz ($\omega = 10^4$ rad/s) which is convenient for the link between the farad and the ohm.

The determination of the frequency behavior of the PTB calculable cross capacitor in the audio frequency range is carried out by applying an equivalent circuit model which considers the influence of distributed admittances and impedances within the calculable cross capacitor. It has been derived taking into account the main currents flowing inside the calculable cross capacitor and the voltage drops caused by these currents.

Most of the circuit parameters of the model were directly measured in the actual configuration of the electrode system with a commercial auto-balancing bridge in a frequency range between 1 kHz and 10 kHz. Owing to the uncertainty of the bridge which is 0.1 % for capacitance measurements and 2 % for inductance measurements, the calculated uncertainty of the frequency correction amounts to a few parts in $10^8$. The capacitances on the calculable cross capacitor were found to be frequency independent, but self-inductances and mutual inductances of the electrodes are frequency dependent and linearly proportional to the inverse square root of the frequency in the examined frequency range.

The frequency dependence of the calculable cross capacitor has been calculated based on the measured circuit parameters. It has been found that the frequency dependence of the cross capacitance is proportional to the square of the frequency, and that the influence of mutual inductances of opposite electrodes dominate the behavior at higher frequencies. At a frequency of 1592 Hz, the correction of the PTB calculable cross capacitor with a value of 1 pF amounts to $9.2\times10^{-8}$ pF with an expanded uncertainty (k=2) of $3.1\times10^{-8}$ pF.

# Zusammenfassung

Das Thompson-Lampard Theorem ist ein Theorem der Elektrostatik, das eine sogenannte Kreuzkapazität beschreibt, die unabhängig von den Querschnittsabmessungen ist. Sie ist daher bestens als Kapazitätsnormal für die Darstellung der Kapazitätseinheit Farad geeignet. Da die Kreuzkapazität für den statischen Fall definiert ist, jedoch bei Wechselstrom betrieben wird, muss eine Frequenzkorrektur angebracht werden, deren Unsicherheit einen wesentlichen Beitrag zum Unsicherheitsbudget des Kondensators leistet. Die Frequenzkorrektur kann mit ausreichender Genauigkeit unter Verwendung eines Wechselstrom-Ersatzschaltbildes für den Kreuzkondensator berechnet werden. Kreuzkondensatoren werden im Allgemeinen bei einer Frequenz von 1592 Hz, entsprechend einer Kreisfrequenz von $10^4$ rad/s betrieben, die für die Ableitung der Widerstandseinheit Ohm aus der Kapazitätseinheit Farad am geeignetsten ist.

Das Frequenzverhalten des PTB Kreuzkondensators im Tonfrequenzbereich wurde unter Anwendung eines Ersatzschaltbildes bestimmt, das den Einfluss der verteilten Impedanzen und Admittanzen im Kondensator berücksichtigt. Es wurde unter Beachtung der wesentlichen Ströme im Kondensator sowie ihrer Spannungsabfälle an den Impedanzen abgeleitet.

Die Mehrzahl der Ersatzschaltbild-Parameter wurde direkt in der originalen Konfiguration des Elektrodensystems mit einer kommerziellen selbst abgleichenden Messbrücke in einem Frequenzbereich von 1 kHz bis 10 kHz bestimmt. Mit der Messunsicherheit der Messbrücke, die 0,1 % für Kapazitätsmessungen und 2% für Induktivitätsmessungen beträgt, ergibt sich für die Frequenzkorrektur eine Unsicherheit von einigen $10^{-8}$. Die Kapazitäten des Kreuzkondensators sind im untersuchten Bereich frequenzunabhängig, während die Selbst- und Gegeninduktivitäten sich linear mit der inversen Quadratwurzel der Frequenz ändern.

Die Frequenzabhängigkeit des Kreuzkondensators wurde auf der Grundlage der gemessenen Ersatzschaltbild-Parameter berechnet. Sie ist proportional zum Quadrat der Frequenz. Den stärksten Einfluss auf das Frequenzverhalten bei höheren Frequenzen haben die Gegeninduktivitäten gegenüberliegender Elektroden. Bei einer Frequenz von 1592 Hz beträgt die Frequenzkorrektur des PTB Kreuzkondensators bei einer Kapazität von 1 pF $9.2\times10^{-8}$ pF mit einer erweiterten Unsicherheit (k=2) von $3.1\times10^{-8}$ pF.

# Contents

# List of Figures

# List of Tables

# Chapter 1

# Introduction

The International System of Units (SI) was established in 1960 by the 11th General Conference on Weights and Measures (CGPM), and in 1971 by the 14th CGPM the present definition of the SI was completed [1]. The SI is a coherent system based on the seven independent physical quantities (base units) and derived quantities (derived units). The base units are the meter (m), the kilogram (kg), the second (s), the ampere (A), the kelvin (K), the mole (mol), and the candela (cd). The derived units are products of powers of the base units. All electrical and magnetic units can be derived from the four base units of electrodynamics as shown in figure 1.

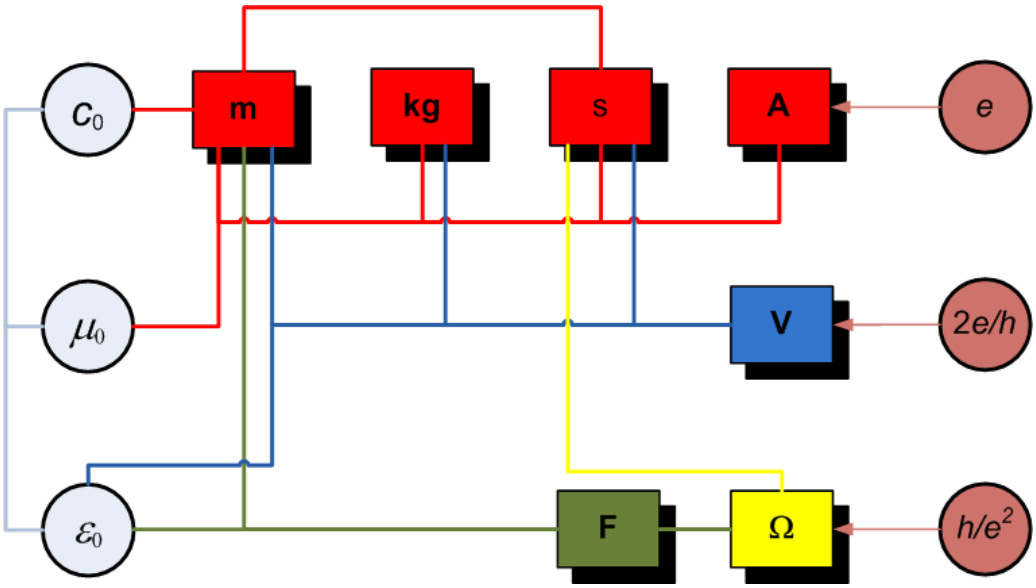


Figure 1.1: The units of electrodynamics.

The definition of the meter fixes the speed of light in vacuum $c_0$, and the definition of the ampere fixes the magnetic constant (also called permeability of vacuum) $\mu_0$. They have exact values without measurement uncertainties as given in [2]. Since the electric constant (also called permittivity of vacuum) $\varepsilon_0$ is related to $\mu_0$ by Maxwell's equation $\varepsilon_0 = 1/\mu_0 c_0^2$, it is also exactly known. The unit of voltage (V) can be derived from the meter, the kilogram and the second and the permittivity of vacuum. It is realized by means of a voltage balance [3]. The farad (F), the unit of capacitance, is derived from the meter and the permittivity of vacuum. It's realized by means of a calculable cross capacitor. The impedance of this capacitor can be compared with a resistance according to the relation $1/\omega C = R$. Therefore, the ohm (Ω) can be also realized by means of a calculable cross capacitor. Ohm's law combines the quantities of voltage, current, and resistance and therewith allows to determine one of the units if the two others are known. It can serve to control the experiments for the determination of the three units.

With the discovery of macroscopic quantum effects, the three units can be reproduced based on fundamental constants. The Josephson effect and the quantized Hall effect (QHE) allow the representation of the volt and the ohm in terms of the Josephson constant $K_J = 2e/h$ and the von Klitzing constant $R_K = h/e^2$, respectively. The ampere can be derived from the elementary charge $e$ and a frequency by means of a single-electron tunneling (SET) device. Therefore, Ohm's law also combines the SET effect, the Josephson effect, and the quantum Hall effect which is known as the so-called quantum metrological triangle (QMT) [4].

Recently a redefinition of the kilogram, the ampere and other base units of the SI by linking them to exact known values of fundamental constants has been proposed [5].

Some NMIs such as NIST, NMIA, LNE and MSL [6–9] still perform absolute measurements of the farad by means of a calculable cross capacitor. Calculable cross capacitors are normally operated at a frequency of 1592 Hz ($\omega = 10^4$ rad/s) which leads to decadic impedance values and is suited for precision AC bridge techniques. The unit of capacitance is maintained at this frequency, too. This frequency is also convenient for the link between the farad and the ohm, because decadic values of capacitance and resistance can directly be compared with each other.

First attempts to determine the frequency dependence of a cross capacitor have been made by Clothier [19] and Jones [9]. In both cases concentrated elements for the equivalent circuit are used. In contrary, this work uses for the first time distributed elements for the equivalent circuit and therewith allows for a better approach to the real capacitor.

The calculable cross capacitor [10] is based on a theorem in electrostatics ($f = 0$) which allows the calculation of the capacitance of a special type of capacitor directly from a single length measurement which can be made traceable to the SI unit of length, but the calculable cross capacitor must be operated at AC to compare it against a resistance standard. Thus, a frequency correction must be applied because internal distributed admittances and

impedances will cause a deviation between the capacitance at DC and AC. As a result, the electrode surfaces of the calculable cross capacitor are no longer at equipotential as assumed in the electrostatic theorem. The frequency correction is one of the dominant parameters in the uncertainty budget for a calculable cross capacitor. It can be calculated with an equivalent circuit model which accurately and sufficiently describes the behavior of the calculable cross capacitor at AC. It is the aim of this thesis to develop such a model for the calculable cross capacitor, to study the frequency dependence of the calculable cross capacitor, and to calculate and discuss the uncertainty for the frequency correction. The circuit model described in this thesis takes the influence of distributed admittances and impedances within the calculable cross capacitor into consideration and evaluates the significant current paths and voltage drops along the circuit components. Any influences resulting from the measuring bridge are not part of this work.

Moreover, the determination of the frequency dependence of the calculable cross capacitor aims at solving some concerns with regard to two possible quantum representations of the farad in the quantum metrology triangle. The first possibility is loading a capacitor with a known number of electrons, which generate a reasonable voltage drop across the capacitor and can be measured against a Josephson voltage standard. If the current is derived from a single electron tunneling (SET) device, the voltage increases linearly with time, i.e., the capacitor is operated at very low frequencies near DC [11, 12]. The second possibility is to measure a quantum Hall resistance (QHR) at AC with a capacitor the value of which is known in SI units. Doing this, the theories on the AC behavior of the quantum Hall effect (AC–QHE), which have been developed in the meantime can be investigated. A comparison is made between a frequency-characterized capacitor and two AC–QHR devices through a quadrature bridge to investigate the frequency dependence observed in QHR devices [13].

This thesis provides an overview of the theory, design, and construction of a calculable cross capacitor in chapter 2. Chapter 3 describes an equivalent circuit model which is used to determine the frequency dependence. The parameters of the equivalent circuit model are determined together with their measurement uncertainties in chapter 4. Finally, in chapter 5 the frequency dependence of the calculable cross capacitor is calculated by means of the parameters of chapter 4, a detailed measurement uncertainty budget is developed and the results are discussed.

# Chapter 2

# Absolute determination of the unit of capacitance

## 2.1 Thompson-Lampard theorem

In 1956, Thompson and Lampard [10] devised a new form of capacitor which they called a cylindrical cross capacitor (shown in figure 2.1). The theory for the new capacitor was developed by Lampard [14], and subsequently extended by Lampard and Cutkosky to investigate the influence of uniform thin films on the electrodes on the cross capacitance [15]. The Thompson-Lampard theorem is a theorem of electrostatics which allows the calculation of the capacitance of a special type of capacitor directly from a single dimension.

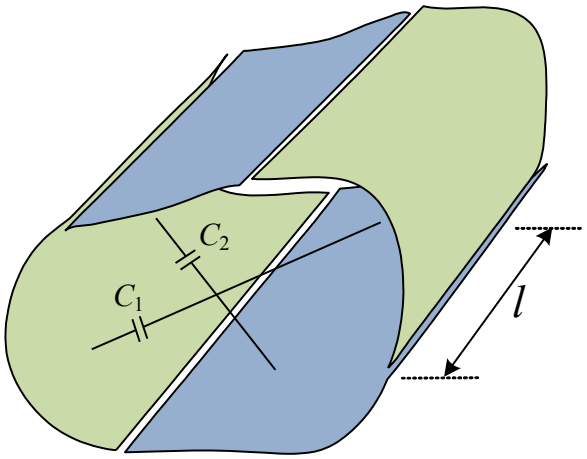


Figure 2.1: Cross section of a cylindrical conducting shell divided into four parts by narrow insulating gaps in parallel to the generators of the cylinder.

Applying Riemann's theorem and after conformal transformation, Lampard converted the arbitrary cross section into the cross section of a cylindrical capacitor the direct capacitance of which can now be computed. The relationship between cross capacitances $C_1$ and $C_2$ per unit length of the infinite system in a vacuum is given by

$$e^{-C_1 \cdot \pi / \varepsilon_0} + e^{-C_2 \cdot \pi / \varepsilon_0} = 1. \tag{2.1}$$

Lampard also showed that the effect of gaps between electrodes is negligibly small, if they are placed in a re-entrent position of the cross section.

In theory, arbitrary cross sections fulfil the theorem, but in practice cylindrical electrode systems are used (see figure 2.2). For a symmetrical calculable cross capacitor where $C_1$ and $C_2$ are equal, the theorem gives a very simple formula (equation (2.2)). In this case, the cross capacitance per unit length, $C_0$, between opposite electrodes in vacuum is given by

$$C_0 = \frac{\varepsilon_0 \ln 2}{\pi}. \tag{2.2}$$

With the defined value for $\varepsilon_0 = 8.854187817 \times 10^{-12}$ F m$^{-1}$, see also chapter 1 and [2], $C_0$ amounts to 1.953 549 043 pF m$^{-1}$ ≈ 2 pF m$^{-1}$.

In practice, due to geometrical imperfections full symmetry can not be achieved. Therefore, $C_1$ and $C_2$ are not equal but differ by $\delta C = C_1 - C_2$, where $\delta C$ is small and can be kept to $<10^{-4}$. In this case, the mean value of the cross capacitances, $C_m$, can be expressed as a potential series and is given by

$$C_m = \frac{C_1 + C_2}{2} = C_0 \left( 1 + \frac{\ln 2}{8} \left( \frac{\delta C}{C_0} \right)^2 - \frac{(\ln 2)^3}{192} \left( \frac{\delta C}{C_0} \right)^4 \pm higher\, order\, terms \right). \tag{2.3}$$

Although the electrode system is not fully symmetric, in practice it is not difficult to adjust the electrode system such that $\delta C/C_0 < 10^{-4}$. Therefore it is sufficient to consider only the quadratic term in equation (2.3) to achieve an uncertainty of less than 1 part in $10^8$.

# 2.2 Design and construction of a calculable cross capacitor

To fulfil the theorem, two requirements must be met. The insulating gaps must be located where they have little effect on the cross capacitance, and the length of the capacitor must be limited without disturbing the homogeneous field in the active area of the capacitor. The effect of the gaps on the cross capacitance can be reduced when the surfaces of adjacent electrodes are highly re-entrant as described in [14; 16]. Therefore, the most suitable design for a cross capacitor uses four cylinders arranged at the corners of a square as shown in figure 2.2. Cylindrical electrodes can be easily manufactured with high geometrical precision.

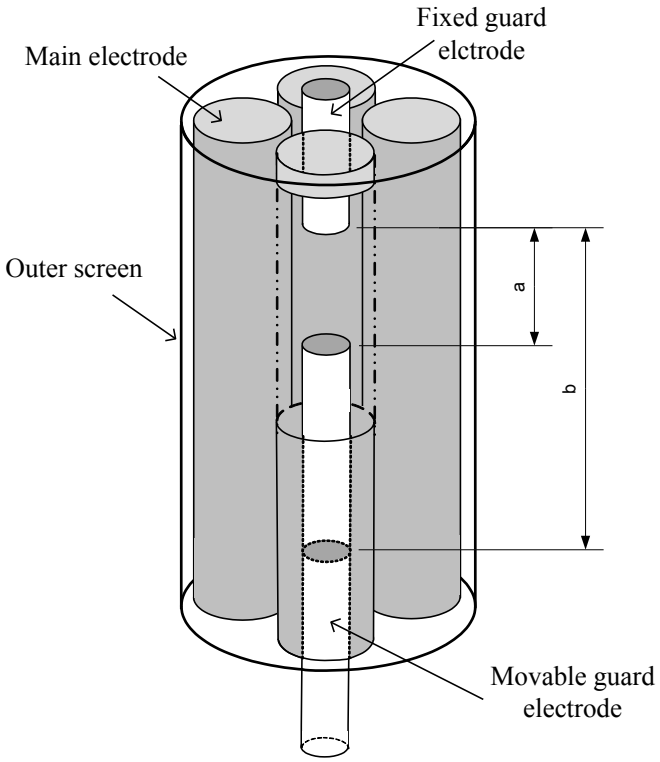


Figure 2.2: Realization of the calculable cross capacitor.

As the electrostatic field does not only expand inside the electrode system but also outside, the outer electrostatic field must be shielded by means of an outer screen surrounding the electrode system. Two so-called guard electrodes limit the internal field except in the region between their opposing ends. One guard electrode is fixed and another can move in a vertical direction. The electrostatic field inside the capacitor can be subdivided into three parts, to inhomogeneous parts around the guard electrodes and a homogeneous part in between. If the distorted edge fields around the guard electrodes do not alter by shifting the movable guard

electrode, the change in capacitance can be determined by the change in the effective length of the capacitor ($\Delta l$) which is the distance between the two positions of the guard electrodes ($b$-$a$), and equation (2.2) can be rewritten as

$$C_b - C_a = \frac{\varepsilon_0 \ln 2}{\pi} \cdot \Delta\ell \,. \tag{2.4}$$

Shifting one of the guard electrodes by $\Delta l$ has the additional advantage, that a length shift can be measured by means of a laser interferometer much more accurately than an absolute length. Figure 2.3 shows the outer view of the PTB calculable capacitor. The design aimed at achieving highest accuracy for a reasonable change of capacitance of 1 pF. These considerations led to a vertically arranged electrode system and a similar design as described in [17]. The diameter of the main electrodes is 85 mm, the diameter of the outer screen 228 mm, and that of the guard electrodes 40 mm. The length of the main electrodes is 850 mm allowing a change in cross capacitance of 1 pF. All generators of the electrodes are straight within 0.5 μm over the full length of 850 mm. The design described above has the advantage that the electrode system can be adjusted under vacuum, and the influence of imperfections of the electrode system on the cross capacitance can be investigated more easily. For this purpose both guard electrodes are supplied with capacitive probes to adjust the electrode system under vacuum before each series of measurements [18].

The principal features of the construction of PTB's cross capacitor are illustrated in figure 2.4. The four main electrodes (a) are freely suspended by means of sliding holders (b) on a mounting plate (c) and brought into position by means of micrometer screws (d). For each electrode, four micrometers are provided and each two of them allow a shift in the radial and tangential directions. Fused silica rods (e) are used for the struts at the tips of the micrometer screws to provide electrical insulation. An outer screen (f) shields the electrode system from external influences. The capacitance is defined by the position of the fixed guard electrode (g) located at the upper mounting plate with regard to the movable guard electrode (h) which is connected to the outer screen by means of a ring of contacts (i). Two guard electrodes provide a "spike" (j) and a capacitive probe (k). The purpose of the spike is to reduce considerably the effects of any irregularities in the electrode system. The calculable cross capacitor is mounted in a vacuum housing ($l$) so that there will be no additional uncertainty arising from the permittivity or the refractive index of the residual gas inside the capacitor. Both guard electrodes are hollow cylinders to allow the laser beam to pass through for measuring the effective length of the capacitor by means of a laser interferometer. At the top and bottom of the vacuum housing anti reflective windows are mounted. An Iodine-stabilized He-Ne laser (m) is used for the interferometer. To determine a possible tilt of the mirrors fixed on the top of each guard electrode an autocollimator (n) located at the top of the calculable cross capacitor is used.

Figure 2.3: PTB's calculable cross capacitor.

All constructional parts that could affect the cross capacitance as a result of their thermal expansion are made of Invar, a FeNi36 alloy. This concerns the whole inner part of the calculable cross capacitor, the electrodes, guard electrodes, the outer screen, the upper and the lower mounting plate, and the micrometers. The coefficient of thermal expansion of Invar is about $1.2 \times 10^{-6}\ \mathrm{K}^{-1}$ and the electrical resistivity amounts to 820 μΩ-mm.

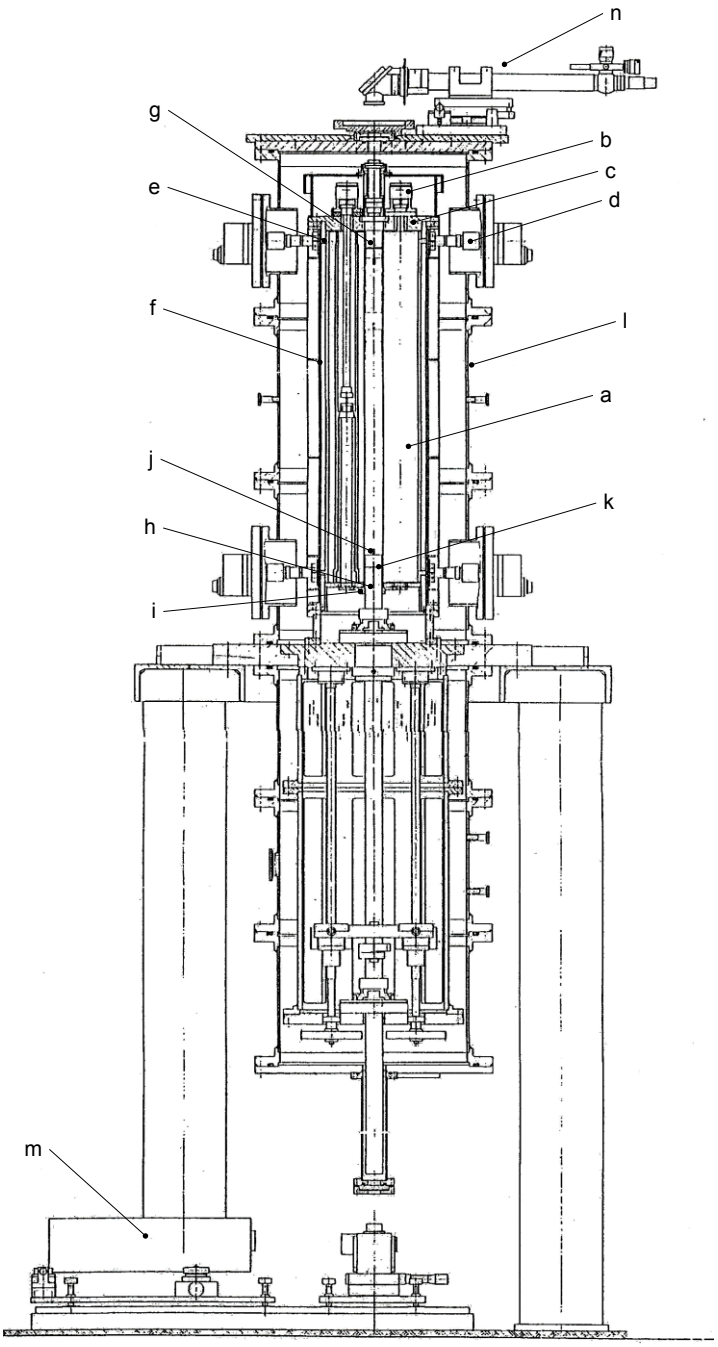


Figure 2.4: PTB calculable cross capacitor assembly. The letters are explained in the text.

The internal electrical connections are made as shown in figure 2.5. They consist of a feedthrough mounted in the vacuum housing and connected to a coaxial cable. This cable ends in a highly flexible piece of wire which avoids any force transfer to the electrode. The conmnection to the electrode is made via a metal pin, which is connected to the top end electrode as shown in figure 2.6.

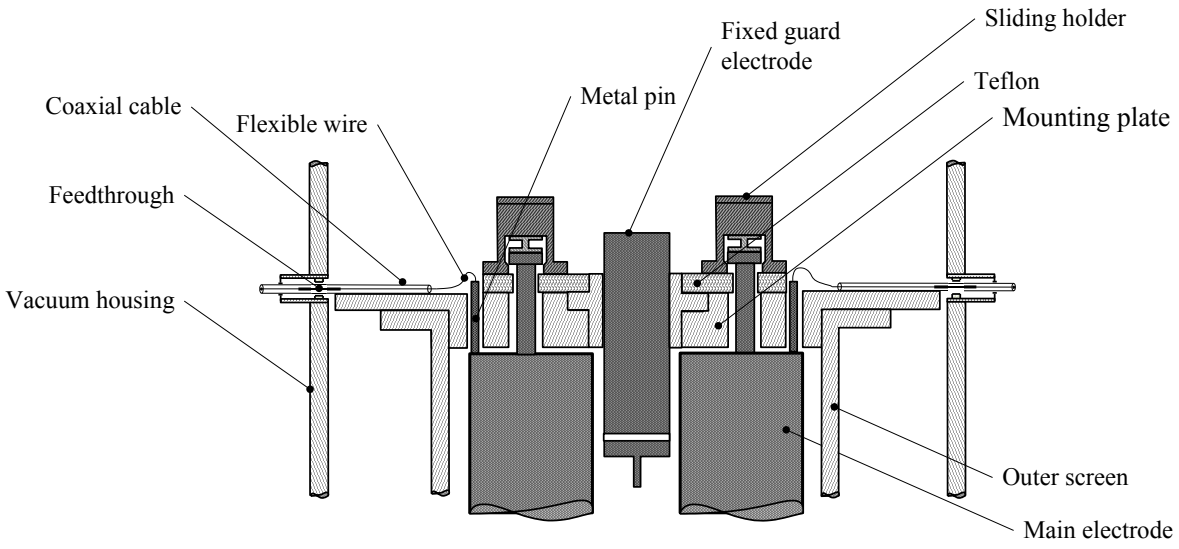


Figure 2.5: Electrical connections between outer connectors and electrodes.

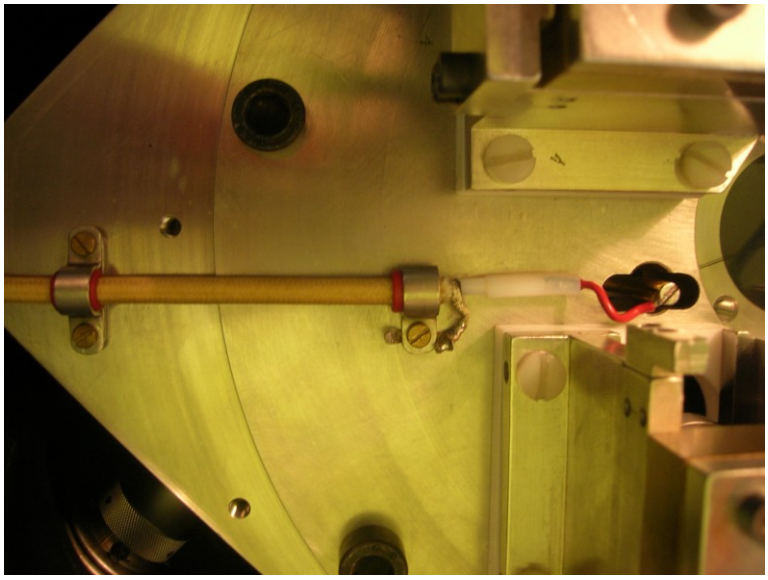

Figure 2.6: Internal connection consisting of a coaxial cable, flexible wire, and metal pin.

Feedthroughs used are triaxial ceramic feedthroughs with three concentric conductors as shown in figure 2.7. The outermost conductor will be mounted in the vacuum housing and other conductors will be connected to a coaxial cable. The three conductors are insulated and separated by a high purity alumina ceramic dielectric, and no connection is made between the vacuum housing and the electrode system of the capacitor.

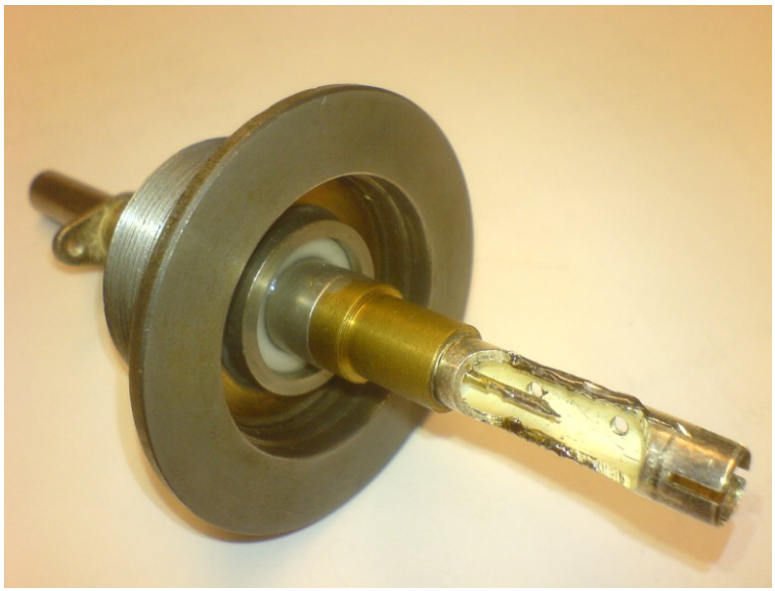

Figure 2.7: Feedthrough.

# 2.3 Imperfections of a calculable cross capacitor

There are a number of errors that limit the accuracy of the capacitance realized by a calculable cross capacitor. At first, we consider the imperfections from an ideal geometric arrangement. The theorem assumes an infinitesimally small gap between the electrodes. In practice, the gaps are not infinitesimally small and give rise to leakage capacitances through the gaps. Three different types of gaps must be considered: Gaps between main electrodes, gaps between main electrodes and guard electrodes, and gaps between main electrodes and the outer shield. If the arcs, in which the outer screen is subdivided, are connected to the electrodes as shown in figure 2.8 (a), the electrode system becomes a fully defined cylindrical cross capacitor described by Clothier [19].

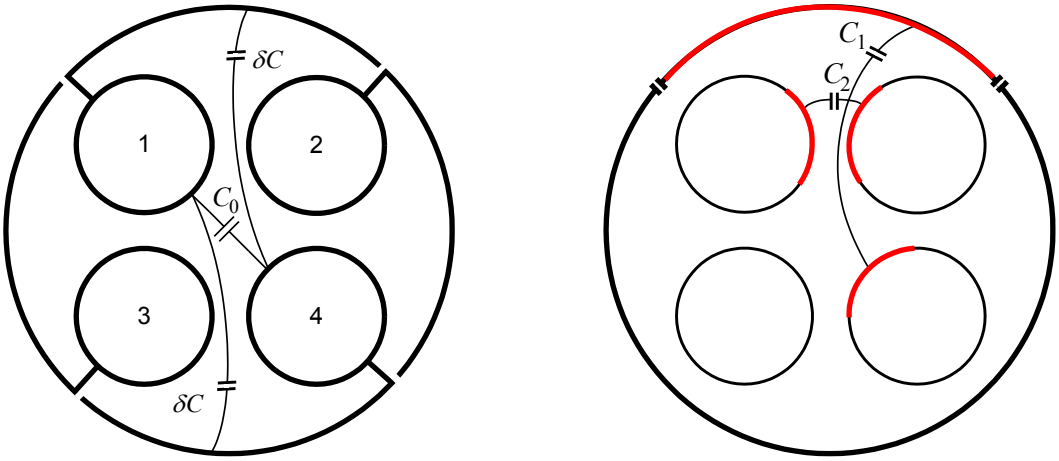


(a) (b)

Figure 2.8: The influence of the gaps between electrodes.

The total cross capacitance is the sum of the main cross capacitance $C_0$ and the two leakage capacitances $\delta C$. The leakage capacitance between the two parts of the outer screen (two gaps in series!) is very small. In practice, the outer screen is undivided and connected to ground. Thus, the relative correction to the cross capacitance due to leakage capacitances is therefore $-2\delta C/C_0$. In figure 2.8 (b), the correction can be obtained from a measurement of the capacitance $C_2$ between adjacent electrodes per unit length and the calculated leakage capacitance $C_1$ by applying the following approximate equation derived from equation (2.1) when $C_1 \langle\langle C_2$,

$$C_1 \approx \frac{\varepsilon_0}{\pi} \cdot e^{-C_2 \cdot \pi / \varepsilon_0} . \tag{2.5}$$

$C_2$ has been directly measured with a model of the calculable cross capacitor. The value is about 59 pF per meter length. The leakage capacitance $C_1$ has been calculated using equation (2.5) to approximately $10^{-22}$ F per meter length corresponding to an error about 1 part $10^9$ in the cross capacitance.

The influence of the gaps between the main electrodes and the guard electrodes can be determined according to figure 2.9. The leakage capacitances $\delta C$ depend on the gaps between main electrodes and guard electrodes. The relative correction is obtained by measuring capacitance $C_2$ and calculating leakage capacitance $C_1$ according to equation (2.5). A similar procedure can be applied for the correction due to the gaps between the electrodes and the outer screen. For the PTB design, the influences of leakage capacitances can be kept below $1 \cdot 10^{-9}$ [18].

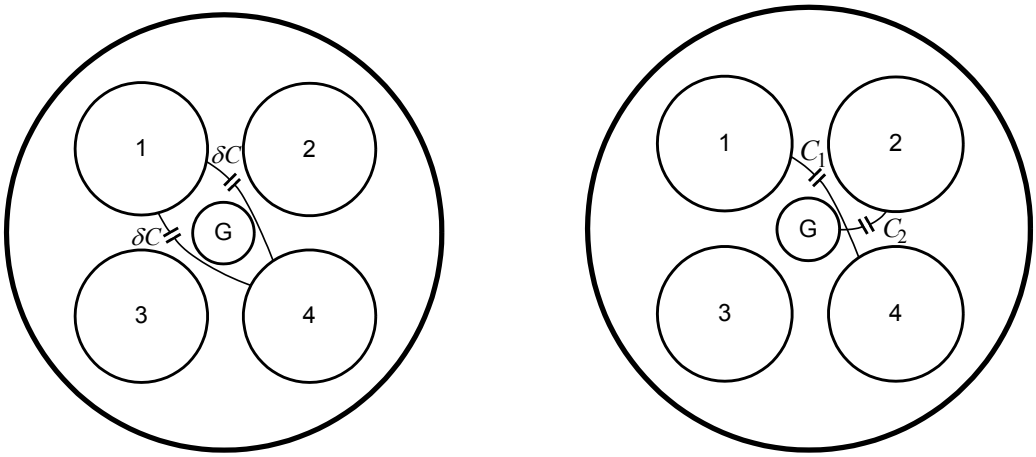


(a) (b)

Figure 2.9: The influence of the gaps between main electrodes and guard electrodes.

The two guard electrodes in figure 2.10 determine the effective length of the capacitor. The electrostatic field of the electrode system consists of three parts. A central part free from end effects corresponding to the field distribution in an infinitely long capacitor, and two parts near the ends of the guard electrodes where the field is considerably distorted. To avoid deviations from the theoretical approach, these edge effects must be kept constant independent from the position of the movable guard electrode. The minimum distance between the two guard electrodes must be large enough to prevent an interlock of the two edge fields and therewith to limit the close approach error to an acceptably small value.

The close approach error can be checked experimentally by extending the path of travel of the movable guard electrode by an increment $\Delta s$, which is a small part of the residual length at the upper position of the movable guard electrode as shown in figure 2.10 and measuring the non-linear component of the change in cross capacitance. The close approach error can be kept well below one part in $10^8$ with the PTB design [20]

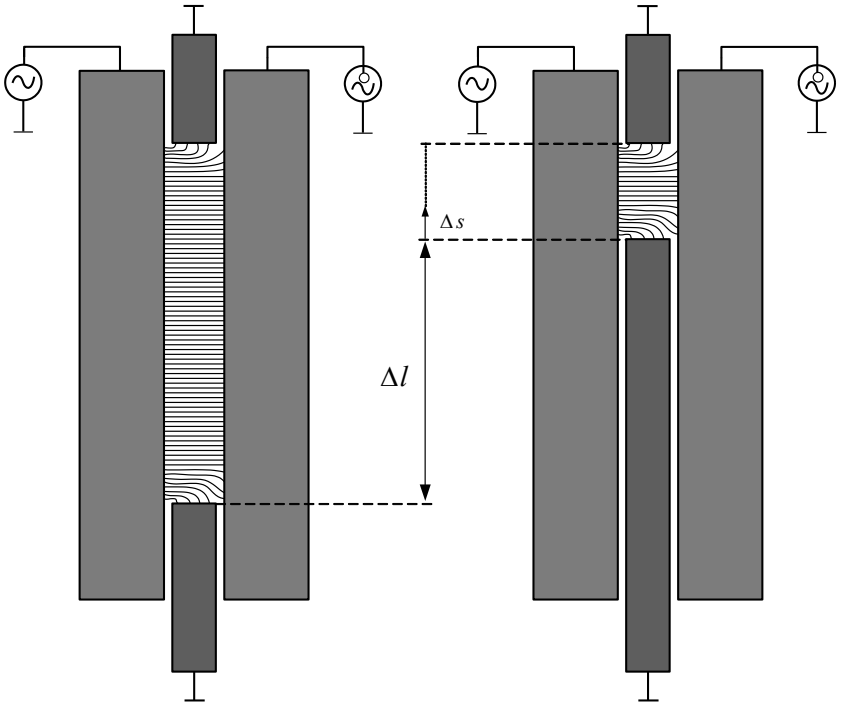


Figure 2.10: The close approach error due to edge effects with the movable guard electrode at the lower position (a) and upper position (b).

A critical condition for the calculable cross capacitor is the invariability of the cross-sectional dimensions of the electrode system along the path of travel of the movable guard electrode. Changes in the geometry cause changes of the inhomogeneous edge field of the movable guard electrode and therewith deviations from a linear change of capacitance with the path of travel. The effect of changing dimensions of the cross section of the cross capacitor can be reduced by so-called spikes at the ends of both guard electrodes by which the influence of a changing geometry is reduced [19; 21].

Finally, all unavoidable deviations from the theoretical assumptions such as finite gap width, inhomogeneous edge fields, taper or other asymmetries in the electrode system etc., do not essentially influence the measuring uncertainty, if the calculable cross capacitor is well designed and properly manufactured. The investigation of the frequency effect on the cross capacitance forms the main part of this thesis and is described in detail in the following chapters.

# 2.4 Principle of capacitance measurement

The cross capacitance ($C_{TL}$) and a fixed unknown capacitor ($C_x$) are compared by using a capacitance bridge as shown in figure 2.11. The bridge uses a two-stage inductive voltage divider (IVD) as a ratio device. The bridge is a combined 10: 1 ratio and substitution bridge which allows the 1 pF change in capacitance of the calculable cross capacitor to be transferred directly to a 10 pF unknown capacitor. In addition, the correction of the bridge ratio amounts to $-18.4\times10^{-9} \pm 5\times10^{-10}$.

In the upper position of the guard electrode, $C_x$ is disconnected from the bridge, and an in-phase balance is made using $T_W$ and $C_1$. The quadrature balance is made by adjusting $\delta U$ with $T_B$ and $C_B$, respectively. In the lower position of the movable guard electrode, $C_x$ is connected to the bridge and the bridge will be balanced again. Before the main bridge balance, a Wagner balance (W) is performed by adjusting W until the potential between the inner and the outer of the coaxial cable at the mid-point of the IVD reaches zero. The Wagner balance reduces the effect of an unbalance of the stray capacitances to ground. A switch box connected between the calculable cross capacitor and the bridge allows to select the corresponding electrode configuration.

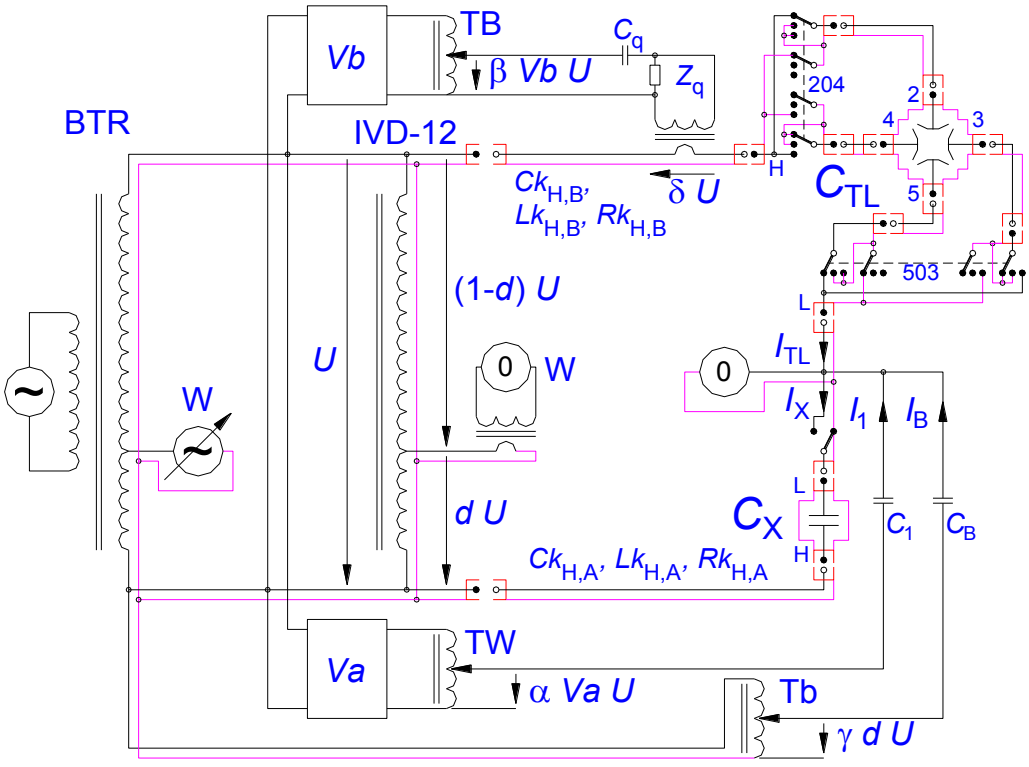


Figure 2.11: Schematic diagram of the capacitance bridge.

# Chapter 3

# Frequency behavior of the calculable cross capacitor

## 3.1 Equivalent circuit model

As mentioned in chapter 2, the theorem of a calculable cross capacitor is a theorem of electrostatics ($f = 0$), but the calculable cross capacitor must be used at AC to compare it against other impedance standards. Therefore, an equivalent circuit model of the calculable cross capacitor for application with AC has been developed and used to specifically derive its frequency correction.

In order to derive an equivalent circuit model of the calculable cross capacitor, it is noted that the return path for all currents flowing along the electrodes and guard electrodes in the calculable cross capacitor is formed by the outer screen of the electrode system of the cross capacitor and the outers of the coaxial cables which connect the capacitor to the measuring bridge. Resistances and conductances are not included in the equivalent circuit model since they mainly influence the quadrature balance of the bridge, and therewith do not essentially influence the capacitance of the cross capacitor.

An equivalent circuit of the calculable cross capacitor is shown in figure 3.1, and the connections apply to the measurement of a cross capacitance $C_{25}$ between electrodes 2 and 5. Electrodes 3 and 4 and the guard electrodes (B) are at ground potential. The external electrical connection to the electrodes is made through coaxial connectors and triaxial ceramic feedthroughs mounted in the vacuum housing. All electrodes are connected to the feedthroughs via a metal pin and a flexible piece of wire to allow for small movements of the electrodes during adjustment on the one hand and to prevent any forces acting on the electrodes through the connecting cables on the other hand.

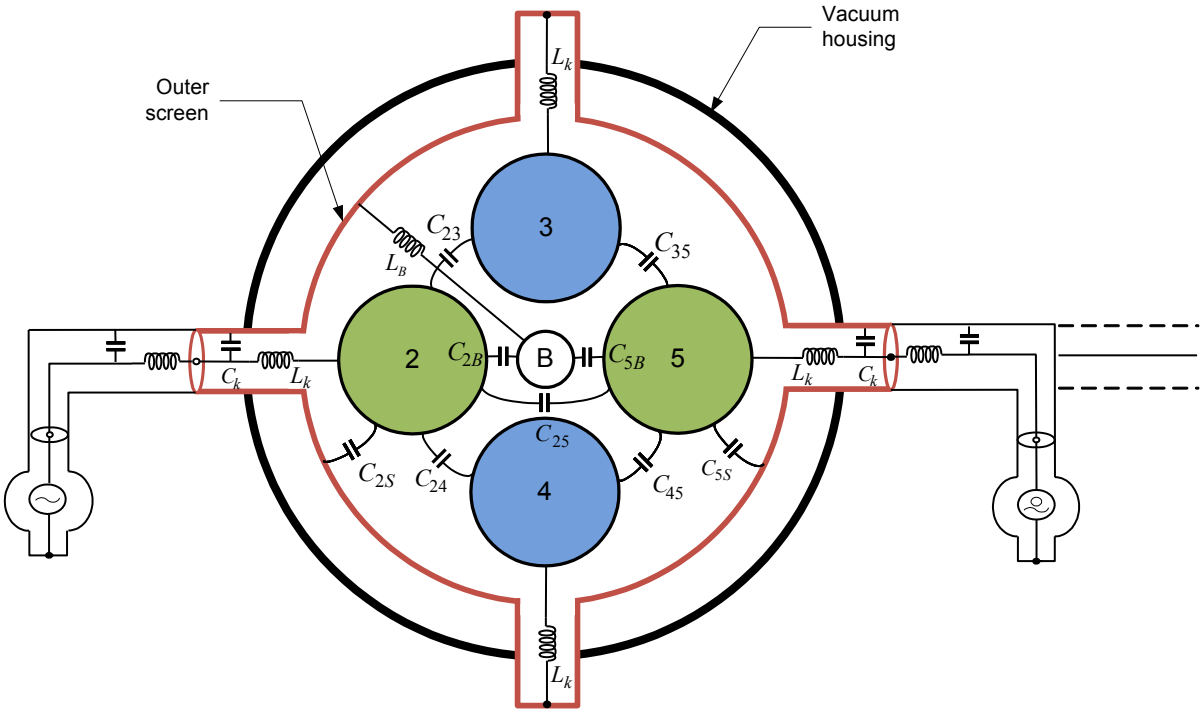


Figure 3.1: Equivalent circuit of a calculable cross capacitor. Dotted lines are connected to unknown capacitor in order to get the complete circuit.

Coaxial cables are used to connect the calculable cross capacitor to the bridge generator and the null detector. This results in a small voltage drop on the cable connecting the calculable cross capacitor and the generator and a small difference in current flowing out of the calculable cross capacitor and into the null detector. As for both effects a correction can be applied quite easily, they are not considered in the following investigation of the frequency influence.

The corrections for the internal coaxial cables between the coaxial connectors and the electrodes will be determined in chapter 3.2. The capacitances $C_{23}$, $C_{24}$, $C_{2S}$, $C_{5S}$, $C_{35}$, $C_{45}$, $C_{2B}$ and $C_{5B}$ cause capacitive currents to flow through the capacitor. These currents cause voltage drops across the self inductances of the main electrodes and guard electrodes and induce voltages in the secondary of the mutual inductances between these electrodes. The effects of capacitances and self inductances will be considered in chapter 3.3, while the influence of the mutual inductances is dealt with in chapter 3.4.

# 3.2 Influence of internal cable connections

Figure 3.2 shows the equivalent circuit for internal cables which connect the electrodes of the calculable cross capacitor to its outer connectors. For reasons mentioned above, resistances and conductances of the cables are neglected, since they do not contribute significantly to the frequency characteristic of a calculable cross capacitor.

$L_{kD}$ and $C_{kD}$ are the inductance and the capacitance of the feedthrough mounted in the vacuum housing of the capacitor. It is connected to a coaxial cable making the connection between the feedthrough and the electrode having an inductance $L_{kcoaxial}$ and a capacitance $C_{kcoa}$, respectively. A highly flexible piece of wire makes the connection between this cable and the electrode to avoid any forces acting on the electrode. It has an inductance $L_{kwire}$ and a capacitance $C_{kwire}$. The cross capacitance $C_{25}$ is independent of frequency. $C_g$ is the total capacitance between the respective electrode and ground.

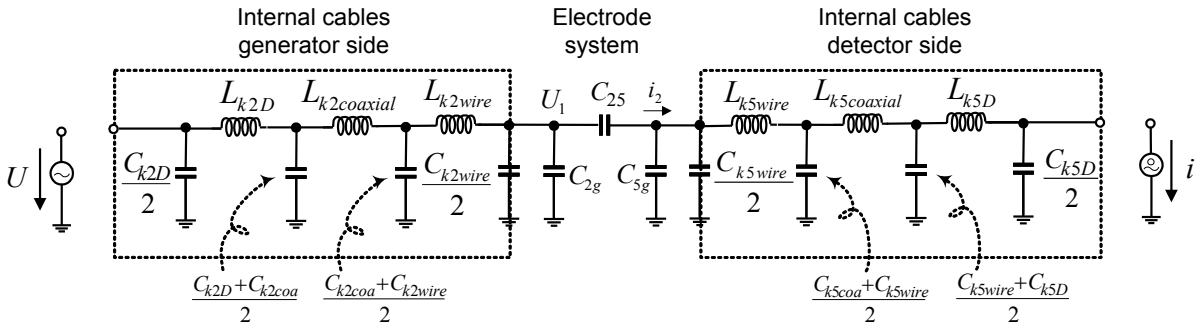


Figure 3.2: Equivalent circuit for internal cables (subscript numbers describe the electrodes in use).

As a cross capacitor is a highly symmetrical device, the stray inductances and capacitances of the internal cables for the generator side and the detector side as well as the internal capacitances of the cross capacitor differ only by a very small amount. Therefore, it is allowed to replace the individual components by their mean values to simplify the calculation. It is also convenient to refer the change in cross capacitance $\Delta C_{25}$ to the mean value of the cross capacitance $C_0$ to apply the corresponding correction to the cross capacitance. The change in cross capacitance is given by

$$\frac{\Delta C_{25}}{C_0} = 2\omega^2 \left\{ \left( C_A + \frac{C_{kwire}}{2} \right) L_{kwire} + \left( C_A + C_{kwire} + \frac{C_{kcoa}}{2} \right) L_{kcoaxial} + \left( C_A + C_{kwire} + C_{kcoa} + \frac{C_{kD}}{2} \right) L_{kD} \right\} \quad .(3.1)$$

whereby $C_A \cong C_{25} + C_{2g} \cong C_{25} + C_{5g}$,

$C_{2g} = C_{23} + C_{24} + C_{2B} + C_{2S}, C_{5g} = C_{53} + C_{54} + C_{5B} + C_{5S}$

$C_{kwire} \cong C_{k2wire} \cong C_{k5wire}$, $C_{kcoa} \cong C_{k2coa} \cong C_{k5coa}$, $C_{kD} \cong C_{k2D} \cong C_{k5D}$,

$L_{kwire} \cong L_{k2wire} \cong L_{k5wire}$, $L_{kcoaxial} \cong L_{k2coaxial} \cong L_{k5coaxial}$, and

$L_{kD} \cong L_{k2D} \cong L_{k5D}$

# 3.3 Influence of self - inductances and stray capacitances

To compensate the effect of small asymmetries in the electrode system of a calculable cross capacitor, the cross capacitance must be calculated as mean of the cross capacitances for the two electrode configurations ($C_{25}$+$C_{34}$)/2 (see equation (2.3)). However, for the determination of the frequency dependence it will be sufficient to consider only one configuration (for example $C_{25}$), because the cross capacitance $C_{34}$ for the other electrode configuration will give nearly identical results. Figure 3.3 shows the equivalent circuit for determining the influence of the capacitances $C_{23}$, $C_{35}$, $C_{2s}$, $C_{3s}$, and $C_{5s}$ and the self-inductances $L_2$, $L_3$ and $L_5$ on the frequency behavior of $C_{25}$. A similar configuration can be used to determine the influence of $C_{24}$, $C_{45}$, $C_{2s}$, $C_{4s}$, and $C_{5s}$ and the self-inductances $L_2$, $L_4$ and $L_5$.

The coupling capacitances and stray inductances cause additional currents flowing from electrode 2 to electrode 5:

- The capacitive current flowing through $C_{23}$ to electrode 3 causes a voltage drop across the self- inductance $L_3$ which drives a current through $C_{35}$ to electrode 5 and the detector.
- The capacitive current flowing through $C_{24}$ to electrode 4 causes a voltage drop across the self- inductance $L_4$ which drives a current through $C_{45}$ to electrode 5 and the detector.
- The capacitive current flowing through $C_{2B}$ to the movable guard causes a voltage drop across the self-inductance $L_B$ which drives a current through $C_{5B}$ to electrode 5 and the detector.

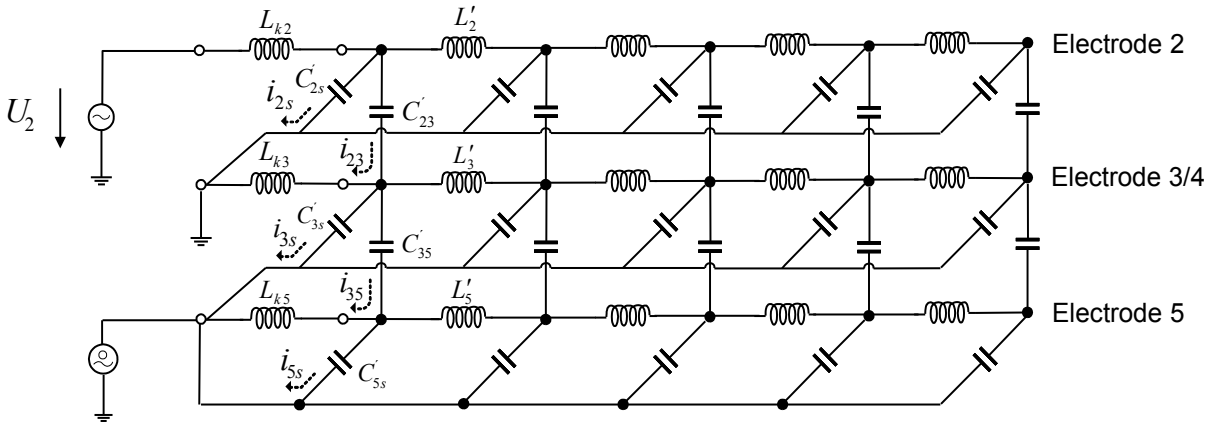


Figure 3.3: Equivalent circuit for determining the influence of the capacitances $C_{23}$, $C_{35}$, $C_{2s}$, $C_{3s}$, and $C_{5s}$ and the self-inductances $L_2$, $L_3$ and $L_5$ on the frequency behavior of $C_{25}$. $L'$ and $C'$are self-inductances and capacitances per unit length.

The circuit can be considerably simplified if the influence of the current $i_{2s}$ on the voltage $U_2$ and of currents $i_{3s}$, and $i_{35}$ on $i_{23}$ are estimated. The maximum voltage drop caused by $i_{2s}$ on $L_2$ is about $10^{-8}\cdot U_2$, therefore the influence of $i_{2s}$ on $U_2$ can be neglected. Due to the small voltage drop of current $i_{23}$ across $L_3$ the currents $i_{3s}$ and $i_{35}$ amount to only $10^{-7}\cdot i_{23}$ and can also be neglected. For the same reasons, the influence of $i_{5s}$ can also be neglected. Taking this into consideration, the equivalent circuit in figure 3.3 can be simplified as shown in figure 3.4. $L_{k2}$, $L_{k3}$, and $L_{k5}$ describe the inductances of the internal cables connected to the electrodes 2, 3 and 5. $L'_2$, $L'_3$, and $L'_5$ are the self-inductances per unit length of electrodes 2, 3 and 5, and $C'_{23}$ and $C'_{35}$ are coupling capacitances per unit length between electrodes 2and 3 and 3 and 5 respectively.

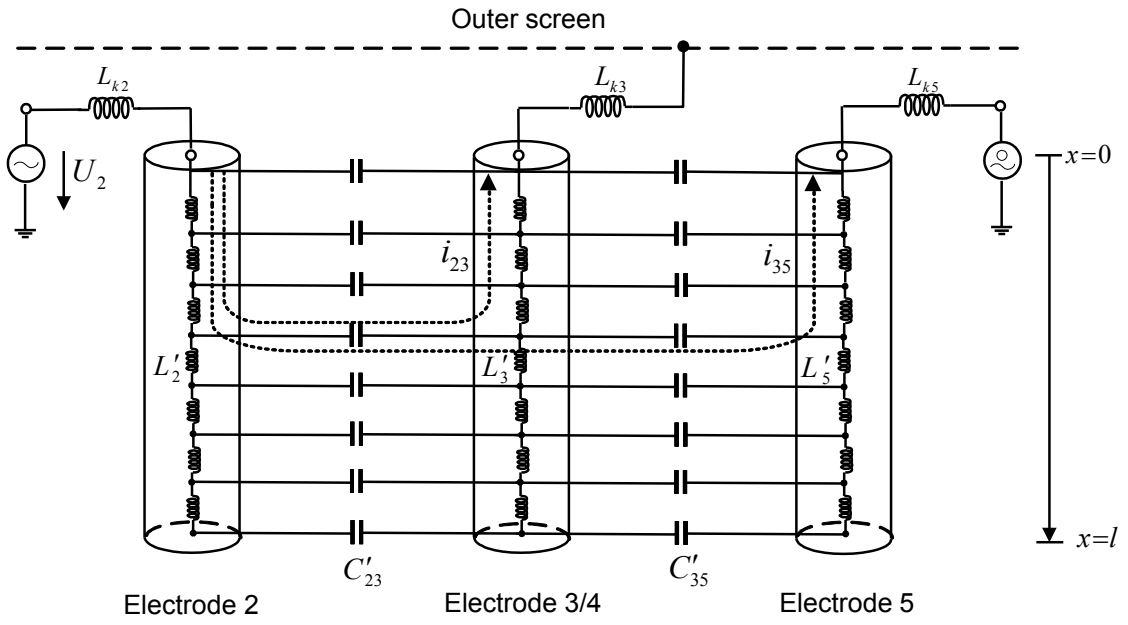


Figure 3.4: Coupling capacitances $C_{23}$ and $C_{35}$.

$U_2$ drives a capacitive current $i_{23}$ through $C_{23}$, the current $i_{23}$ generates a voltage drop $U_3$ along the self-inductance of electrode 3 and this voltage causes a capacitive current $i_{35}$ through $C_{35}$ as shown in figure 3.4.

The current $i_{23}$ decreases over the length of electrode 2 according to $di_{23} = -U_2 \cdot j\omega C'_{23} dx$. Therefore, the total current as a function of distance $x$ from the top of the electrode is given by

$$i_{23} = U_2 \cdot j\omega C_{23}\left(1 - \frac{x}{l}\right). \tag{3.2}$$

The total voltage drop $U_3$ is calculated by integrating current $i_{23}$ along electrode 3 and adding the constant voltage drop of this current across $L_{k3}$, giving

$$U_3 = -U_2\omega^2 L_3 C_{23}\left(\frac{L_{k3}}{L_3} + \frac{x}{l} - \frac{1}{2}\left(\frac{x}{l}\right)^2\right). \tag{3.3}$$

The decrease of current $i_{35}$ over the length of electrode 5 is $di_{35} = -U_3 \cdot j\omega C'_{35} dx$ and the total current as a function of the distance x from the top of electrode 5 amounts to

$$i_{35} = -j\omega C_{35} \cdot U_2 \cdot \omega^2 C_{23}\left[\left(L_{k3} + \frac{1}{3}L_3\right) - L_{k3}\frac{x}{l} - \frac{1}{2}L_3\frac{x^2}{l^2} + \frac{1}{6}L_3\frac{x^3}{l^3}\right]. \tag{3.4}$$

The change in capacitance $\Delta C_{25}$ can be calculated by comparing the current through $\Delta C_{25}$ with the current $i_{35}$ at $x = 0$: $j\omega\Delta C_{25} = -j\omega C_{35} \cdot \omega^2 C_{23}\left(L_{k3} + \frac{1}{3}L_3\right)$.

This gives

$$\Delta C_{25} = -C_{35} \cdot \omega^2 C_{23}\left(L_{k3} + \frac{1}{3}L_3\right) \tag{3.5}$$

and, if referred to the mean cross capacitance $C_0$,

$$\frac{\Delta C_{25}}{C_0} = -\frac{C_{35}}{C_0}\omega^2 C_{23}\left(L_{k3} + \frac{1}{3}L_3\right). \tag{3.6}$$

For the coupling capacitances $C_{24}$ and $C_{45}$ together with $L_4$, $\Delta C_{25}/C_0$ can be calculated correspondingly, so that the change in $C_{25}$ due to $C_{24}$, $C_{45}$ and $L_4$ is given by

$$\frac{\Delta C_{25}}{C_0} = -\frac{C_{45}}{C_0}\omega^2 C_{24}\left(L_{k4} + \frac{1}{3}L_4\right). \tag{3.7}$$

The conditions for $C_{2B}$, $C_{5B}$, and the self-inductance of the movable guard electrode, $L_B$, are shown in figure 3.5. The calculation of the influence of the coupling capacitances $C_{2B}$ and $C_{5B}$ and the inductance $L_B$ of the movable guard electrode must take into consideration that the coupling capacitances do not have an effect over the whole length of the electrodes and that this length also depends on the position of the movable guard electrode (lower position $l_1$ and upper position $l_2$). For convenience, the variable "$x$" therefore counts from the lower to the upper end of the electrodes. $U_2$ drives a capacitive current $i_{2B}$ through $C_{2B}$, this current generates a voltage drop $U_B$ across the self-inductance of the movable guard electrode $L_B$ causing a capacitive current $i_{5B}$ through $C_{5B}$ as shown in figure 3.5.

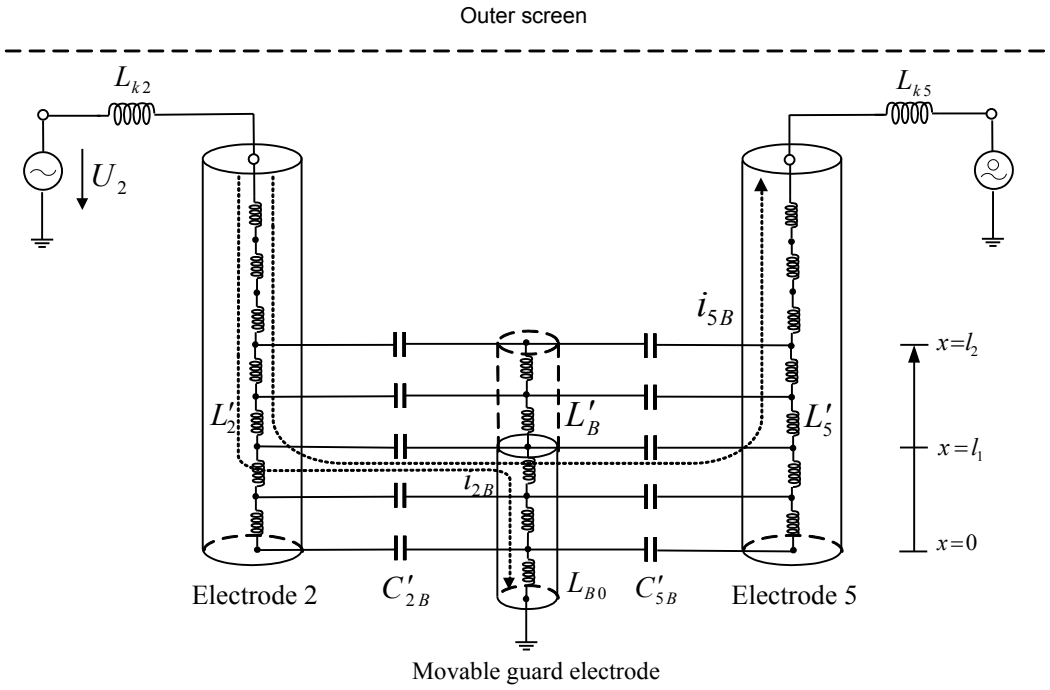


Figure 3.5: Coupling capacitances $C_{2B}$ and $C_{5B}$.

The current $i_{2B}$ decreases over the length $x$ according to $di_{2B} = -U_2 \cdot j\omega C'_{2B} dx$. $i_{2B}$ can be obtained by integrating $di_{2B}$ over the length of the guard electrode

$$i_{2B} = U_2 \cdot j\omega C_{2B}\left(1 - \frac{x}{l_1}\right). \tag{3.8}$$

The total voltage drop $U_B$, is calculated by integrating current $i_{2B}$ along the movable guard electrode and adding the constant voltage drop of this current across $L_{B0}$, giving

$$U_B = -U_2 \omega^2 L_B C_{2B}\left(\frac{L_{B0}}{L_B} + \frac{x}{l_1} - \frac{1}{2}\left(\frac{x}{l_1}\right)^2\right). \tag{3.9}$$

The current $i_{5B}$ driven by $U_B$ through $C_{5B}$ can be derived from $di_{5B} = U_B \cdot j\omega C'_{5B} dx$

$$i_{5B} = -j\omega C_{5B} \cdot U_2 \cdot \omega^2 L_B C_{2B}\left[\frac{L_{B0}}{L_B}\frac{x}{l_1} + \frac{1}{2}\frac{x^2}{l_1^2} - \frac{1}{6}\frac{x^3}{l_1^3}\right]. \tag{3.10}$$

The change in capacitance $\Delta C_{25}$ can be calculated by comparing the current through $\Delta C_{25}$ with the current $i_{5B}$ at $x = l_1$: $U_2 \cdot j\omega\Delta C_{25} = -U_2 \cdot j\omega C_{5B} \cdot \omega^2 C_{2B}\left(L_{B0} + \frac{1}{3}L_B\right)$.

This gives

$$\Delta C_{25} = -C_{5B} \cdot \omega^2 C_{2B}\left(L_{B0} + \frac{1}{3}L_B\right) \tag{3.11}$$

and, if referred to the mean cross capacitance $C_0$,

$$\frac{\Delta C_{25}}{C_0} = -\frac{C_{5B}}{C_0}\omega^2 C_{2B}\left(L_{B0} + \frac{1}{3}L_B\right). \tag{3.12}$$

Equation (3.12) can be used to calculate the change in capacitance for the lower position of the movable guard electrode ($L_B$ (LMG) at $x=l_1$) and its upper position ($L_B$ (UMG) at $x=l_2$).

There is no need to take the influence of the fixed guard electrode into consideration, because the cross capacitance is calculated as the difference of the two cross capacitances in the lower and upper position of the movable guard electrode. As the contribution of the fixed guard electrode to the two capacitances is the same for both positions of the movable guard electrode, it is cancelled out by calculating the difference.

# 3.4 Influence of mutual inductances and stray capacitances

Currents flowing in the electrodes 2, 3 and 4 as well as the movable guard electrode will generate voltages in electrode 5 according to the mutual inductances $M_{25}$, $M_{35}$, $M_{45}$ and $M_{5B}$. These voltages together with the capacitance of electrode 5 to ground cause currents which influence the balance of the bridge null detector.

To calculate the influence of the mutual inductance $M_{25}$, the total current $i_2$ flowing in electrode 2 must be considered because it induces a voltage in electrode 5 due to $M_{25}$. The current $i_2$ driven by $U_2$ is composed of five parts, a current $i_0$ flowing through the cross capacitance $C_{25}$, a current $i_{23}$ flowing through $C_{23}$ to electrode 3, a current $i_{24}$ flowing through $C_{24}$ to electrode 4, a current $i_{2B}$ flowing through $C_{2B}$ to the movable guard electrode and a current $i_{2S}$ flowing through $C_{2S}$ to the outer screen $s$ of the calculable cross capacitor as is shown in figure 3.6.

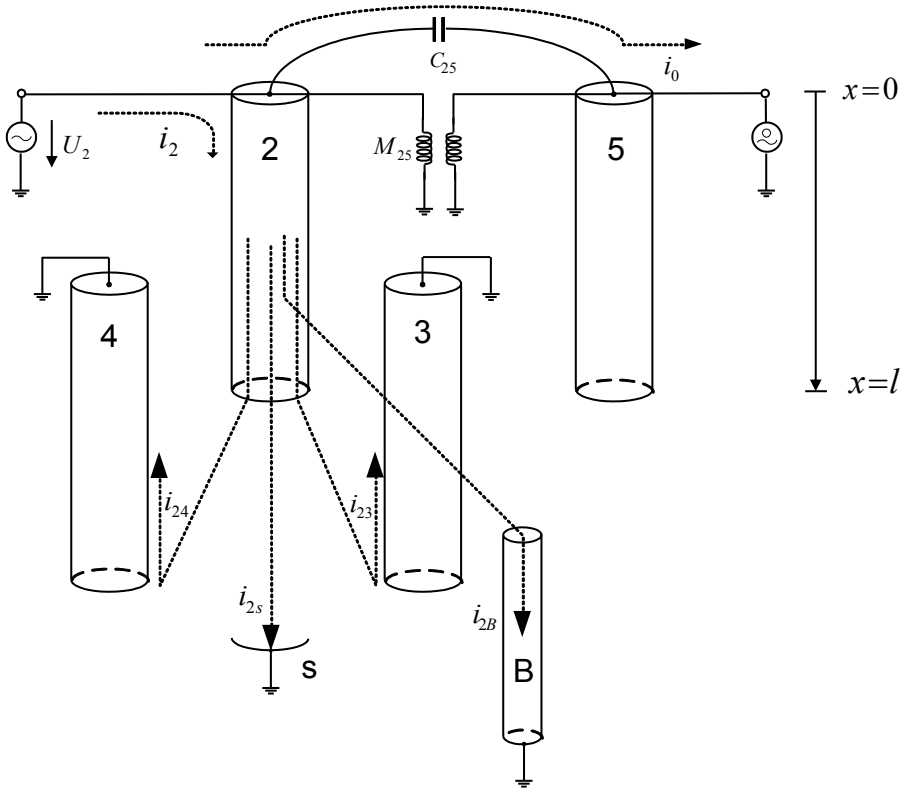


Figure 3.6: Mutual inductance.

$U_2$ drives a total current $i_2$ through electrode 2 which induces a voltage in electrode 5 according to $M_{25}$. The induced voltage in electrode 5 drives a current $i_5$ through electrode 5 as shown in figure 3.7. The current $i_2$ decreases with $x$ according to $di_2 = -U_2 \cdot j\omega C'_2 dx$, thus,

$$i_2 = U_2 \cdot j\omega C_2 \left(1 - \frac{x}{l}\right), \tag{3.13}$$

where

$$C_2 = C_{23} + C_{24} + C_{2B} + C_{2s}. \tag{3.14}$$

The induced voltage in electrode 5 is derived from $dU_5 = -i_2 \cdot j\omega M'_{25} dx$, hence,

$$U_5 = U_2 \cdot \omega^2 C_2 M_{25} \left(\frac{x}{l} - \frac{1}{2}\frac{x^2}{l^2}\right). \tag{3.15}$$

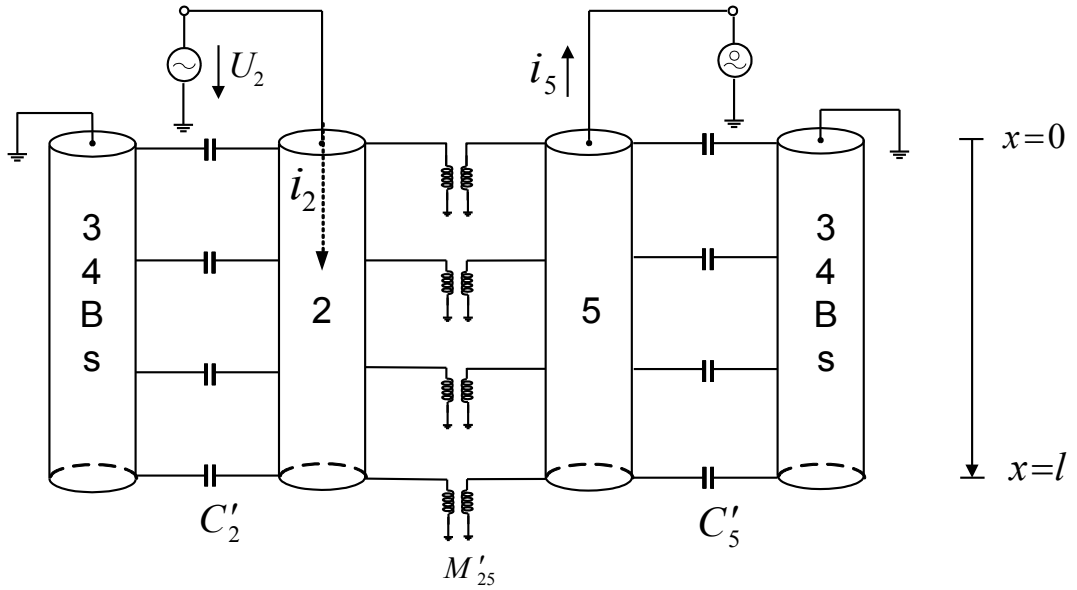


Figure 3.7. Mutual inductance $M'_{25}$ per unit length between electrodes 2 and 5. Coupling capacitances $C'$ per unit length between active electrode and electrodes 3, 4, movable guard (B), and screen ($s$).

The current $i_5$ derived from $U_5$ is given by $di_5 = -U_5 \cdot j\omega C'_5 dx$

$$i_5 = -U_2 \cdot j\omega C_5 \cdot \omega^2 C_2 M_{25} \left(\frac{1}{2}\frac{x^2}{l^2} - \frac{1}{6}\frac{x^3}{l^3} - \frac{1}{3}\right), \tag{3.16}$$

where

$$C_5 = C_{35} + C_{45} + C_{5B} + C_{5s}. \tag{3.17}$$

The change in capacitance can be calculated by comparing $i_5$ ($x = 0$) and the current through $C_{25}$.

$$\Delta C_{25} = \frac{1}{3} C_5 \omega^2 C_2 M_{25}. \tag{3.18}$$

Referred to $C_0$ one gets

$$\frac{\Delta C_{25}}{C_0} = \frac{1}{3} \frac{C_5}{C_0} \omega^2 C_2 M_{25}. \tag{3.19}$$

The calculation of $i_2$ does not take into consideration that the current $U_2 \cdot j\omega C'_{2B}$ is not distributed uniformly over the whole length of electrode 2, because the movable guard electrode does not cover the whole length of the electrode. But for simplicity we consider both lengths as equal which will only cause a second order effect error.

The mutual inductances between electrodes 3 and 5 and between electrodes 4 and 5 can be calculated in a similar manner. Taking into account the opposite direction of the current flow in electrodes 3 and 4, the change in capacitance due to $M_{35}$ is given by

$$\frac{\Delta C_{25}}{C_0} = -\frac{1}{3} \frac{C_5}{C_0} \omega^2 C_{23} M_{35}, \tag{3.20}$$

and the change in capacitance due to $M_{45}$ is

$$\frac{\Delta C_{25}}{C_0} = -\frac{1}{3} \frac{C_5}{C_0} \omega^2 C_{24} M_{45}. \tag{3.21}$$

For the calculation of the influence of $M_{5B}$ it must be considered that the mutual inductance is not effective over the entire length of the movable guard electrode and electrode 5. $U_2$ drives a capacitive current $i_{2B}$ through $C_{2B}$, which induces a voltage drop in the movable guard electrode and therewith caused by $M_{5B}$ in electrode 5, too. The induced voltage in electrode 5 drives a current $i_5$ through $C_5$ as shown in figure 3.8. The length of the movable guard electrode changes with its position ($l_1$ and $l_2$), and even in the upper position, the length is smaller than the length of the electrode. For convenience, the variable "$x$" therefore counts from the lower end of the electrodes.

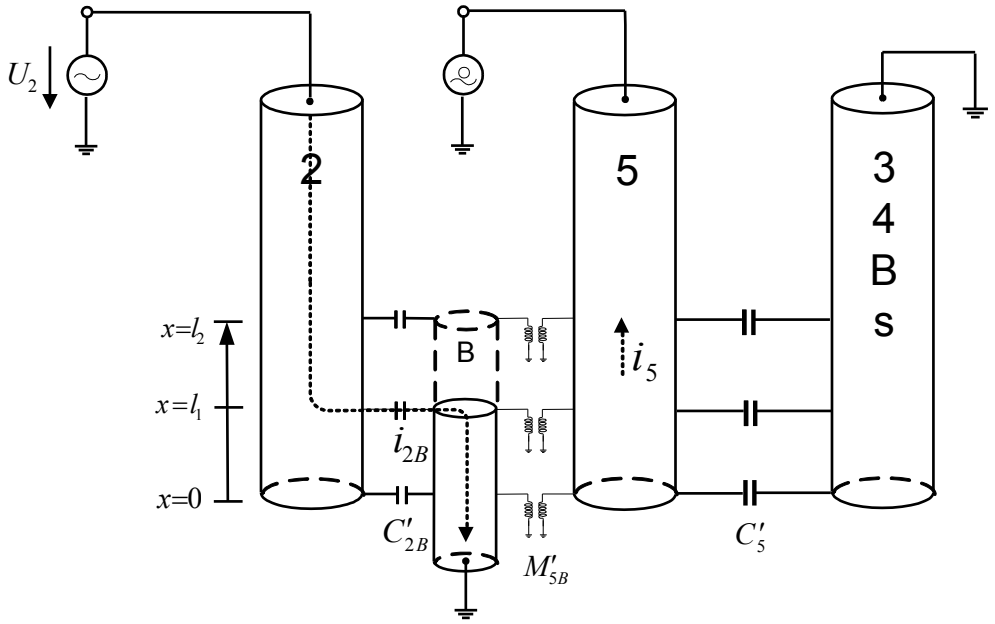


Figure 3.8: Mutual inductance between electrode 5 and the movable guard electrode.

The current $i_{2B}$ is derived from $di_{2B} = -U_2 \cdot j\omega C'_{2B} dx$, thus,

$$i_{2B} = U_2 \cdot j\omega C_{2B}\left(1 - \frac{x}{l_1}\right). \tag{3.22}$$

The induced voltage in electrode 5 is derived from $dU_5 = i_{2B} \cdot j\omega M'_{5B} dx$, hence,

$$U_5 = U_2 \cdot \omega^2 C_{2B} M_{5B}\left(\frac{1}{2} - \frac{x}{l_1} + \frac{1}{2}\frac{x^2}{l_1^2}\right). \tag{3.23}$$

The current $i_5$ is derived from $di_5 = U_5 \cdot j\omega C'_5 dx$, thus,

$$i_5 = U_2 \cdot j\omega C_5 \cdot \omega^2 C_{2B} M_{5B}\left(\frac{l_1}{l}\right)\left(\frac{1}{2}\frac{x}{l_1} - \frac{1}{2}\frac{x^2}{l_1^2} + \frac{1}{6}\frac{x^3}{l_1^3}\right). \tag{3.24}$$

As the length ratio between the movable guard electrode and electrode 5 is $l_1/l$, the current $i_5$ must be multiplied with this length ratio. This factor is automatically included in $C_{2B}$ and $M_{2B}$, because they are measured in the two positions of the movable guard electrode.

The total current flowing through the detector is equal to $i_5$ at $x = l_1$ ($l_2$ in the upper position of the movable guard electrode). The change in capacitance due to the mutual inductance between electrode 5 and the movable guard electrode at $x = l_1$ is given by

$$\frac{\Delta C_{25}}{C_0} = \frac{1}{6}\frac{C_5}{C_0}\frac{l_1}{l}\omega^2 C_{2\mathrm{B}} M_{5\mathrm{B}} \ . \tag{3.25}$$

According to equation (3.17), $C_5$ consists of four parts. While three of them are uniformly distributed over the whole length of the electrode, $C_{5\mathrm{B}}$ is restricted to the length of the movable guard electrode. Therefore, equation (3.17) must be slightly modified and becomes

$$C_5 = \left(C_{35} + C_{45} + C_{5s}\right)\frac{l_1}{l} + C_{5B}, \tag{3.26}$$

and thus,

$$\frac{\Delta C_{25}}{C_0} = \frac{1}{6}\left[C_5\frac{l_1}{l} + C_{5B}\left(1 - \frac{l_1}{l}\right)\right]\frac{\omega^2}{C_0} C_{2B} M_{5B}. \tag{3.27}$$

In a similar way, the influence of the mutual inductances can be calculated for the other electrode configuration (electrodes 3 and 4).

# 3.5 Superposition of the change in capacitance of the calculable cross capacitor

For the electrode combination 2 and 5, the total change in capacitance resulting from self-inductances, stray capacitances, and mutual inductances can be calculated by summing up the results of equations (3.6), (3.7), (3.12), (3.19), (3.20), (3.21), and (3.27). For the lower position of the movable guard electrode ($x$=$l_1$) it amounts to

$$\Delta C_{25low} = -2\omega^2 C_e^2 L_{ek} - \omega^2 C_B^2 L_m + \left(\frac{1}{3}\right)\omega^2 C_g^2 M_0 - \left(\frac{2}{3}\right)\omega^2 C_g C_e M_e + \frac{1}{6}\omega^2 C_B M_B \left[ C_g \frac{l_1}{l} + C_B \left(1 - \frac{l_1}{l}\right)\right], \quad (3.28)$$

and for the upper position of the movable guard electrode ($x = l_2$) it is given by

$$\Delta C_{25up} = -2\omega^2 C_e^2 L_{ek} - \omega^2 C_B^2 L_m + \left(\frac{1}{3}\right)\omega^2 C_g^2 M_0 - \left(\frac{2}{3}\right)\omega^2 C_g C_e M_e + \frac{1}{6}\omega^2 C_B M_B \left[ C_g \frac{l_2}{l} + C_B \left(1 - \frac{l_2}{l}\right)\right], \quad (3.29)$$

where $C_g \cong C_2 \cong C_5$, $C_e \cong C_{23} \cong C_{35} \cong C_{24} \cong C_{45}$, $C_B \cong C_{2B} \cong C_{5B}$,

$L_{ek} \cong \left(L_{k2} + \frac{1}{3}L_2\right) \cong \left(L_{k5} + \frac{1}{3}L_5\right)$, $L_m \cong \left(L_{B0} + \frac{1}{3}L_B\right)$, $M_e \cong M_{35} \cong M_{45}$,

$M_0 \cong M_{25}$, and $M_B \cong M_{5B}$.

It must be mentioned that most of the inductances and capacitances change with the position of the movable guard electrode. This is especially true for the cross capacitance and the components related to the movable guard electrode. Combining the internal cable correction (equation (3.1)) with the change due to stray capacitances, self-inductances and mutual inductances yields for the lower position of the movable guard electrode

$$\Delta C_{25low} = -2\omega^2 C_e^2 L_{ek} - \omega^2 C_B^2 L_m + \left(\frac{1}{3}\right)\omega^2 C_g^2 M_0 - \left(\frac{2}{3}\right)\omega^2 C_g C_e M_e + \frac{1}{6}\omega^2 C_B M_B \left[ C_g \frac{l_1}{l} + C_B \left(1 - \frac{l_1}{l}\right)\right] + 2\omega^2 C_0 \left\{ \left( C_A + \frac{C_{kwire}}{2}\right) L_{kwire} + \left( C_A + C_{kwire} + \frac{C_{kcoa}}{2}\right) L_{kcoaxial} + \left( C_A + C_{kwire} + C_{kcoa} + \frac{C_{kD}}{2}\right) L_{kD} \right\}, \quad (3.30)$$

and for the upper position

$$\Delta C_{25up} = -2\omega^2 C_e^2 L_{ek} - \omega^2 C_B^2 L_m + \left(\frac{1}{3}\right)\omega^2 C_g^2 M_0 - \left(\frac{2}{3}\right)\omega^2 C_g C_e M_e + \frac{1}{6}\omega^2 C_B M_B \left[ C_g \frac{l_2}{l} + C_B \left(1 - \frac{l_2}{l}\right)\right] + 2\omega^2 C_0 \left\{ \left( C_A + \frac{C_{kwire}}{2} \right) L_{kwire} + \left( C_A + C_{kwire} + \frac{C_{kcoa}}{2} \right) L_{kcoaxial} + \left( C_A + C_{kwire} + C_{kcoa} + \frac{C_{kD}}{2} \right) L_{kD} \right\} \quad . (3.31)$$

Finally, the change in capacitance of the calculable cross capacitor is given by

$$\Delta C_0 = \Delta C_{25low} - \Delta C_{25up} \, . \quad (3.32)$$

# Chapter 4

# Measurement of equivalent circuit parameters

## 4.1 Auto balancing bridge and its verification

The auto balancing bridge was used to perform the measurements of the circuit parameters. The principle of the bridge is shown in figure 4.1. The current $I_x$ through the unknown impedance $Z$ is balanced by the current $I_r$ which flows through the range resistor $R_r$, driven by an I–V converter. The potential at the "Low" point is kept at zero. The unknown impedance $Z$ is calculated from the voltage at the "High" terminal $V_x$, the voltage across $R_r$ and the range resistor $R_r$, $Z = (V_x / V_r) \cdot R_r$ [22].

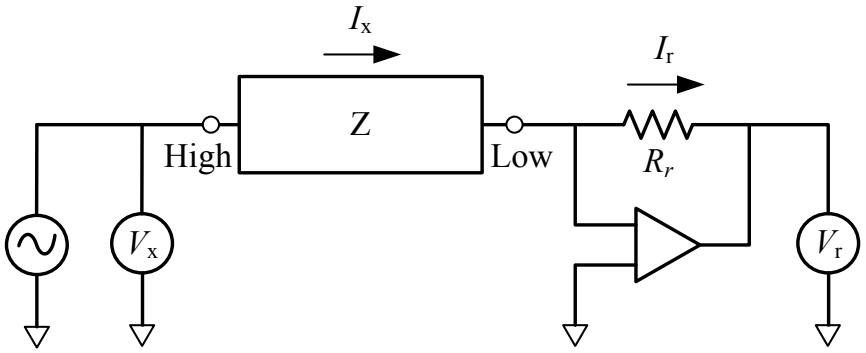


Figure 4.1: The auto-balancing bridge method.

According to the performance test required by the manufacturer, the bridge is calibrated with standard capacitors and standard resistors. For the measurement of the circuit parameters, the bridge is also used or inductance measurements. Therefore, it must also be verified with standard inductors. Three standard inductors of value 1 μH, 10 μH, and 50 μH were calibrated using a Maxwell-Wien bridge [23] at the frequencies 1 kHz, 2 kHz, 10 kHz,

20 kHz, and 100 kHz for 1 μH and 10 μH and 100 Hz, 400 Hz, and 1 kHz for 50 μH. The measurement results performed with the auto balancing bridge were compared with the values obtained by calibrating the standards with the Maxwell bridge. The results are shown in figure 4.2. The bars show the expanded uncertainties (black for the calibrated standards and red for the results of the auto balancing bridge). The results show that the bridge gives the correct results within its expanded uncertainty. Before performing a measurement, open/short compensation should be used to reduce the additional errors due to test fixtures and cables. In addition, open compensation capability cancels errors due to stray admittances and short compensation cancels errors due to residual impedances.

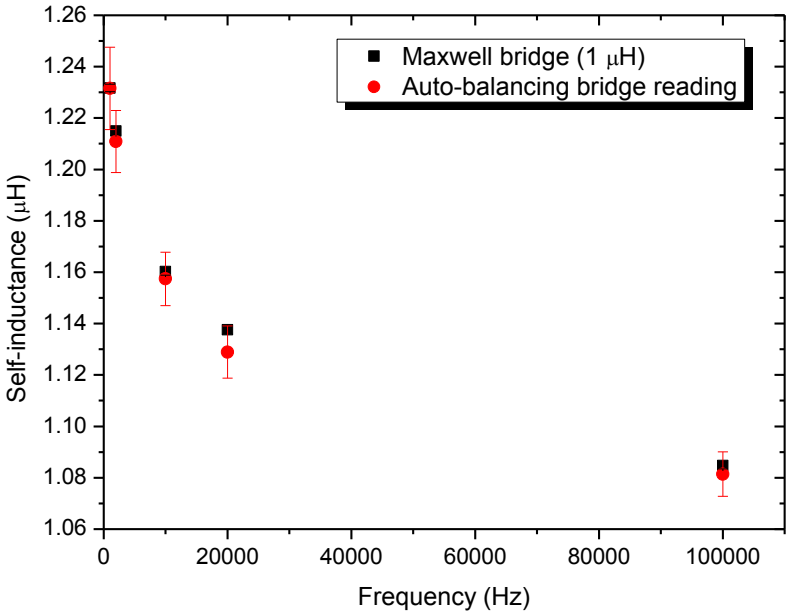


Figure 4.2 (a): Verification of the auto-balancing bridge for 1 μH.

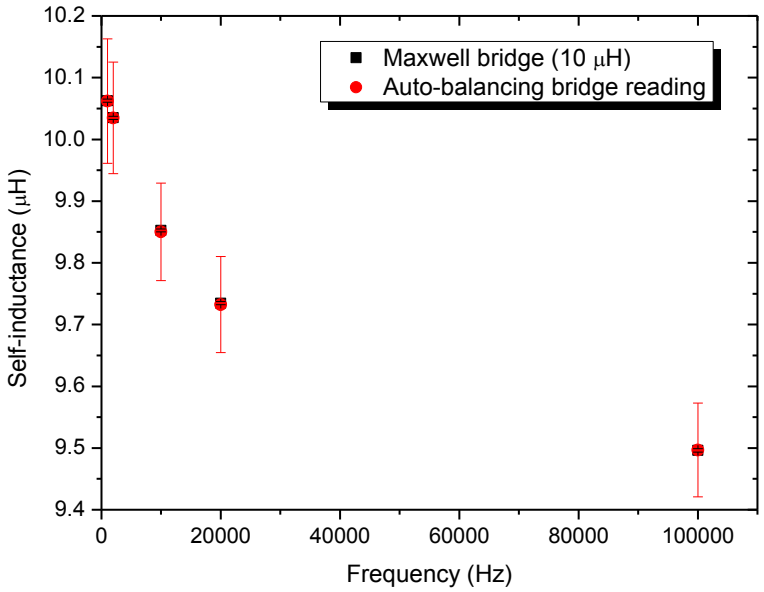


(b)

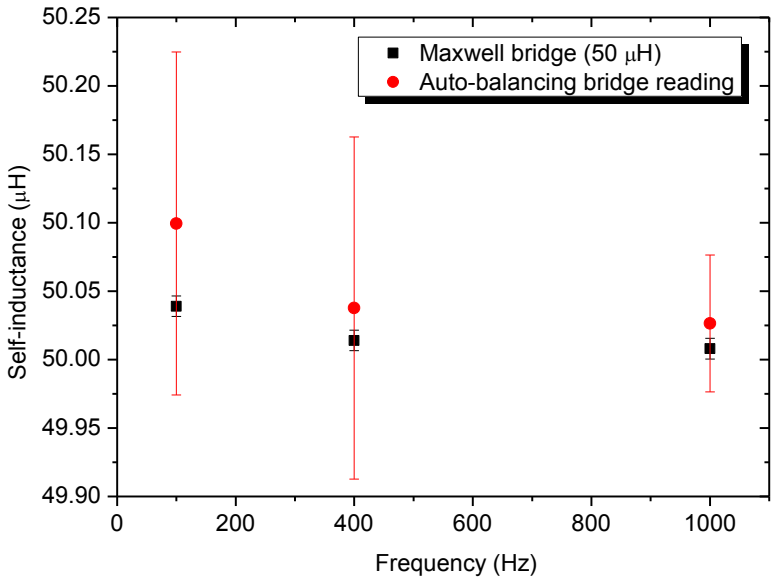


(c)

Figure 4.2: Verification of the auto-balancing bridge (b) for 10 μH and (c) for 50 μH

Moreover, the auto-balancing bridge also can be verified by measuring a circular loop inductor. The measurement results are shown in Appendix A.1.

# 4.2 Measurement techniques and calculations

There are different techniques to measure impedances. Each of them has advantages and disadvantages. The measurement techniques employed also depend on the terminal configuration of the device under test and the desired accuracy. Some parameters of the equivalent circuit such as the coupling capacitances between the main electrodes and the movable guard electrode could not be measured directly. They were calculated as the capacitance of two parallel cylinders. Moreover, the calculations may confirm the results of the measurements.

## 4.2.1 Two-terminal measurement technique

The two-terminal measurement technique is the simplest method but it contains many sources of error due to lead inductances $L_L$, lead resistances $R_L$, contact resistances $R_c$, and stray capacitance $C_{stray}$ as shown in figure 4.3. All additional errors are added to the measured impedance $Z$. However, these errors due to the leads and the test fixtures can be eliminated by the open/short compensation.

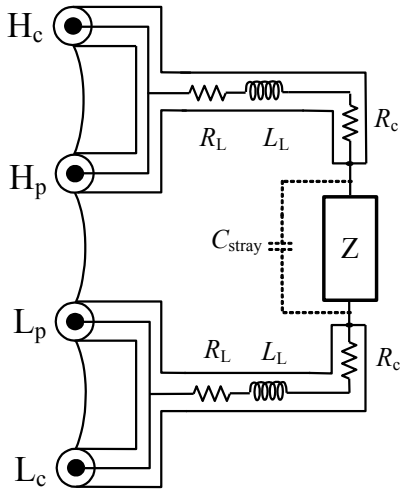


Figure 4.3: Two-terminal measurement technique.

## 4.2.2 Shielded two-terminal measurement technique

The shielded two-terminal measurement technique uses coaxial cables for connecting the unknown impedance to the bridge to reduce the effects of the stray capacitance. The outer conductors of the coaxial cables are connected to the guard terminal. Using this method, the measurement accuracy can be improved especially for the measurement of higher impedances

but not for lower impedances, because the lead impedances ($R_L$ and $L_L$) and the contact resistances $R_C$ still remain (see figure 4.4). However, the influence of the leads and the test fixtures can be eliminated by open/short compensation.

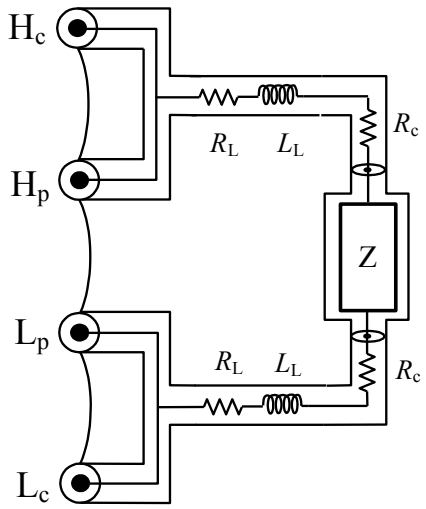


Figure 4.4: Shielded two-terminal measurement technique.

### 4.2.3 Four-terminal measurement technique for measuring self-inductance

In figure 4.5, the four-terminal measurement technique can reduce the effects resulting from lead impedances ($R_L$ and $L_L$) and contact resistances ($R_C$) because the signal current path and the voltage sensing leads are separated from each other. The impedances on the voltage sensing leads do not affect the measurement, because the signal current does not flow through these leads. Therefore, measurement errors due to the lead impedances and contact resistances are eliminated.

However, the measurement accuracy for higher impedances is not improved, because the stray capacitance $C_{stray}$ between the leads still remain. Moreover, there is some disadvantage because the signal currents flowing through the current leads generate external magnetic fields around the leads. These magnetic fields induce error voltages due to magnetic coupling $M$ in the adjacent voltage sensing leads resulting in measurement errors. The magnetic couplings can be eliminated by twisting together in current and voltage leads [24]. The four-terminal measurement technique is especially suited for low impedance measurements.

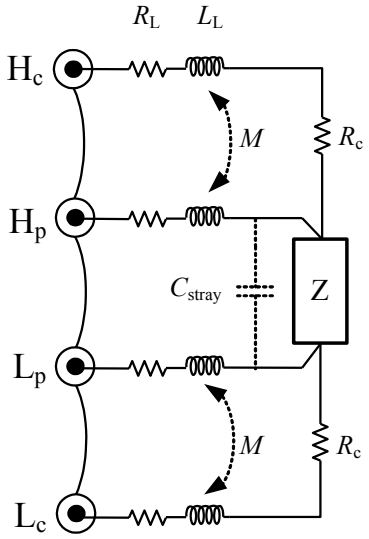


Figure 4.5: Four-terminal measurement technique.

### 4.2.4 Four-terminal measurement technique for measuring mutual inductance

The four-terminal measurement technique can also be used to measure mutual inductances with a configuration as shown in figure 4.6. The value of the mutual inductance is directly obtained from the bridge reading. When the current $I$ flows through the primary winding, the voltage across the secondary winding is given by $V = \omega M \times I$. Therefore, the mutual inductance can be calculated from the ratio between the secondary voltage ($V$) and the primary current ($I$). This method can also be applied to the calculable cross capacitor, if instead of the two windings the electrodes are connected to the auto balancing bridge according to figure 4.6.

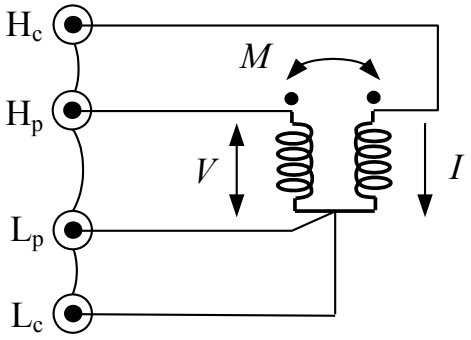


Figure 4.6: Measurement principle for the mutual inductance.

## 4.2.5 Calculation of capacitance for two parallel cylinders

The capacitance [25] between two parallel cylinders with the same radius $a$, separated by $D > 2a$ and with a length $l >> D$ is given by

$$C = \frac{\pi \varepsilon_0 l}{\ln\left[(D/2a) + \sqrt{(D/2a)^2 - 1}\right]}. \tag{4.1}$$

If the cylinders have different radii $a$ and $b$, but the same separation $D$ and length $l$ the capacitance is given by

$$C = \frac{2\pi \varepsilon_0 l}{\ln\left[x + \sqrt{(x)^2 - 1}\right]}, \tag{4.2}$$

with

$$x = \left| \frac{D^2 - a^2 - b^2}{2ab} \right|.$$

## 4.2.6 Calculation of inductance and capacitance for coaxial cables

For a coaxial cable which the current flowing in the outer equal in magnitude but opposite in direction to the inner conductor, Grover [26] gives the following equation for the inductance of a coaxial cable (in nH)

$$L = 2l\left[\ln\frac{b}{a} + \frac{\mu}{4}T\right] \tag{4.3}$$

As the outer conductor is usually very thin, its internal inductance can be neglected. In equation (4.3), $l$ is the length of the cable in centimeter and $a$ and $b$ are the inner and outer radius (in centimeter). T is a function which takes the skin effect into account. It can be taken from a table given by Grover. The permeability $\mu$ will be unity for copper.

The capacitance of a coaxial cable is given by

$$C = \frac{2\pi \varepsilon_0 \varepsilon_r l}{\ln\left(\frac{b}{a}\right)}. \tag{4.4}$$

## 4.2.7 Calculation of mutual inductance

Grover [26] gives a general equation for the mutual inductance (in μH) of two parallel cylinders of the same length and radius as

$$M = 0.002l\left[\ln\left(\frac{2l}{d}\right) - \ln k - 1 + \frac{d}{l} - \frac{1}{4}\left(\frac{d}{l}\right)^2\right], \tag{4.5}$$

The length of the cylinders is $l$ and the distance between their axis $d$ (both expressed in centimeters). The value for $\ln k$ which represents a geometric mean distance can be taken from tables given by Grover. The mutual inductance of parallel cylinders of unequal length ($l$ and $m$ in centimeter) is given by

$$2M = (M_l - M_m) - M_{l-m}. \tag{4.6}$$

# 4.3 Stray capacitance measurements

For low values of capacitance, the admittance becomes relatively small and the parallel resistance component is more significant. Therefore, for measuring the stray capacitances of the electrode system the parallel capacitance circuit mode of the bridge has been used. The capacitances have been measured in two-terminal and shielded two-terminal technique except the capacitance between the movable guard electrode and the main electrodes which has been calculated using equations (4.1) and (4.2). The capacitances were measured in a frequency range from 1 kHz to 10 kHz with a voltage of 1 V. The capacitance between the main electrodes and the movable guard electrode can also be extrapolated from the capacitance of the probe at the top of the guard electrode extrapolated to the length of the movable guard electrode. This will be more accurate, because it takes the real geometry into consideration.

## 4.3.1 Internal cables ($C_k$)

Figure 3.2 shows the equivalent circuit for the internal cables. The circuit parameters have been measured using a two-terminal measurement technique. The errors due to measuring leads and test fixtures are compensated by open/short compensation. The capacitance $C_{kD}$ of the feedthrough could not be directly measured. Therefore it has been determined using a spare part identical to that mounted in the calculable cross capacitor. The coaxial cable $C_{kcoa}$ connected to the feedthrough is about 13.5 cm long with an inner radius of 0.35 mm and an outer radius of 2.33 mm. The measured capacitance is 10.4 pF, and the calculated value applying equation (4.4) is about 9.1 pF. The capacitance $C_{kwire}$ is the capacitance of the flexible wire and the metal pin connecting the internal coaxial cable and the main electrode. Figure 4.7 shows the mean value of the internal capacitances with expanded uncertainties.

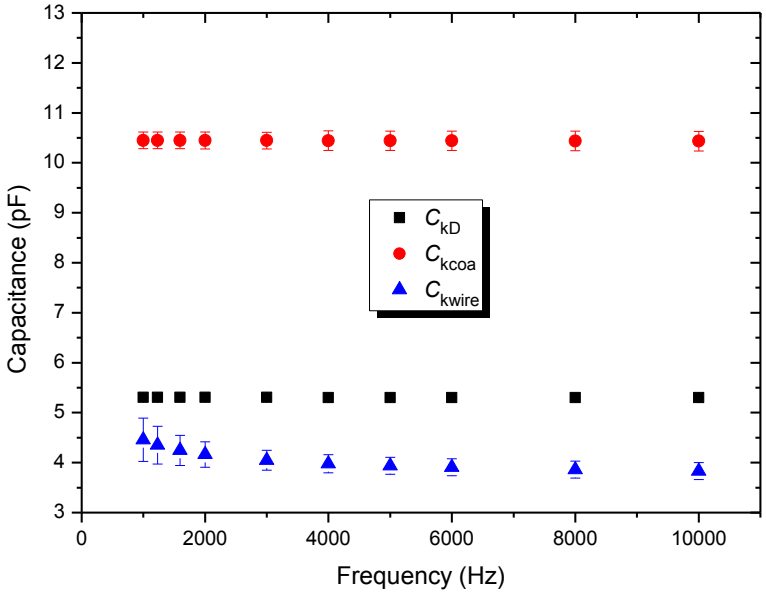


Figure 4.7.: Capacitances of the internal cables with expanded uncertainties.

## 4.3.2 Main electrodes

The stray capacitances of the main electrodes consist of two parts, the capacitances $C_e$ between adjacent electrodes and the capacitances $C_g$ between the main electrode and the shield. For both of them different measurement techniques have been used. The shielded two-terminal measurement technique was employed for $C_e$, and the two-terminal measurement technique was used for $C_g$.

### 4.3.2.1 Coupling capacitances between adjacent electrodes ($C_e$)

The capacitance $C_e$ between adjacent electrodes such as $C_{23}$ has been measured with the electrodes 4 and 5 at ground potential as shown in figure 4.8. The shielded two-terminal measuring method was employed. The effects from leads and test fixtures can be eliminated by open/short compensation. Additional errors due to lead impedances and stray admittances inside the capacitor can be estimated

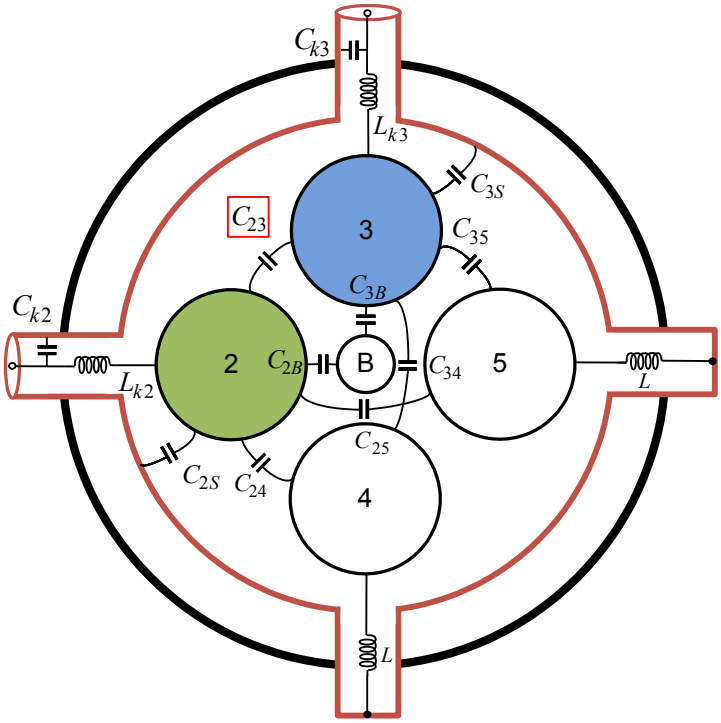


Figure 4.8: Capacitance $C_{23}$.

using a simple equivalent circuit as shown in figure 4.9. $C_{\Sigma g}$ is total stray capacitance between the electrode and ground and includes the internal cable capacitances, and $L_k$ is the inductance of the internal cables and the electrodes.

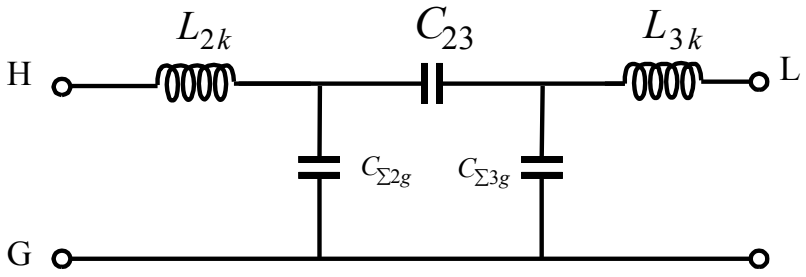


Figure 4.9: A simple equivalent circuit for the coupling capacitance $C_{23}$.

For the PTB calculable cross capacitor, $C_{\Sigma g}$ is about 1 nF and $L_k$ is about 1 µH. The relative error of $C_{23}$ expressed by the term $\omega^2 \cdot L_k \cdot C_{\Sigma g}$, thus gives a value of less than $10^{-7}$ which can be neglected compared to the accuracy of the bridge. Therefore, the measured values of the capacitances $C_{23}$ must not be corrected. Figure 4.10 shows the capacitance between adjacent electrodes for the lower (LMG) and upper position (UMG) of the movable guard electrode. The difference of the two measured capacitances can be explained by the

screening effect of the movable guard electrode which results in a decrease of the capacitance in the upper position of the movable guard electrode. The bars show the expanded measurement uncertainties which mainly come from the asymmetry of the electrode system.

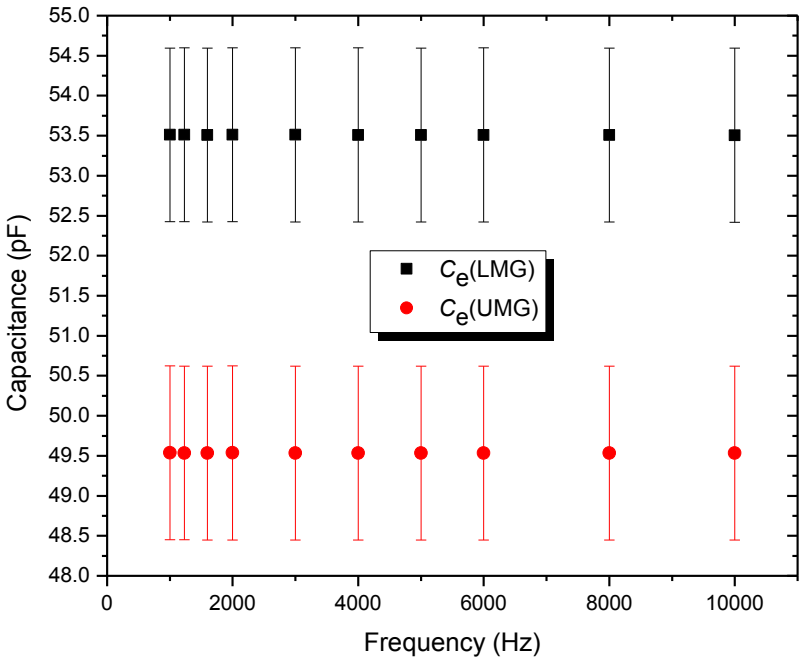


Figure 4.10: Mean capacitance between adjacent electrodes at LMG and UMG with expanded uncertainties.

For convenience, the frequency dependence of the cross capacitance has been calculated using the mean values of capacitances and inductances. The uncertainty could be reduced, if instead of using the mean value the actual values of the capacitances had been used, but to the expense of a much more complicated calculation with only little effect on the result. The expanded uncertainty (about 2%) of adjacent electrode capacitances contributes to the uncertainty of the frequency dependence of the cross capacitance only with $6\times10^{-9}$.

## 4.3.2.2 Capacitances between main electrodes and ground ($C_g$)

Figure 4.11 shows the configuration of the electrode system for measuring the capacitance between a main electrode and the shield of the capacitor. The two-terminal measurement technique is used**.** Additional errors due to leads and test fixtures can be eliminated by open/short compensation The measured value of the capacitance between electrode 2 and ground ($C_{m2g}$) is the sum of capacitances $C_k$, $C_{23}$, $C_{2B}$, $C_{25}$, $C_{24}$, and $C_{2S}$.

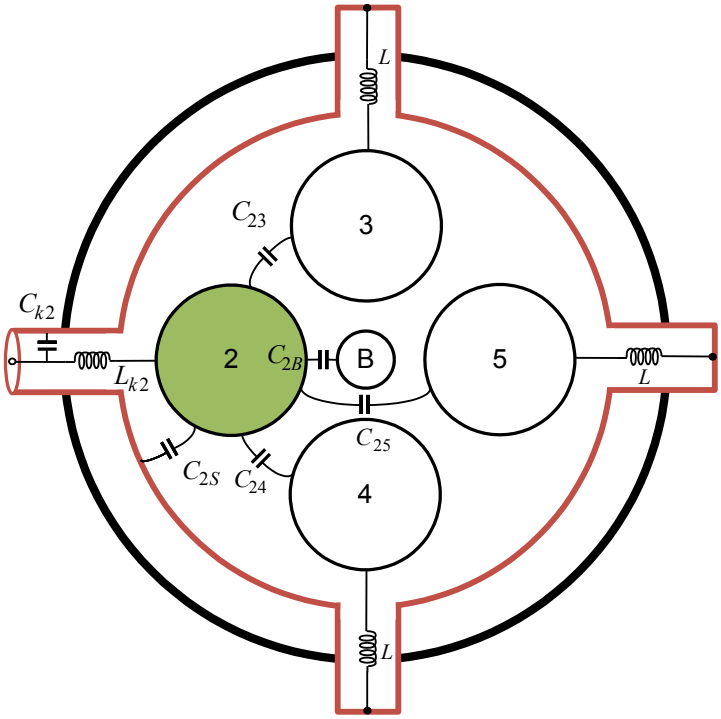


Figure 4.11: Capacitance between electrode 2 and ground.

A simple equivalent circuit of the measurement set-up is shown in figure 4.12. $L_{2k}$ is the inductance of the internal cable and the electrode. The error can be expressed by the term $\omega^2 L_{2k} C_{m2g}$. As $L_{2k}$ is about 1 µH and $C_{m2g}$ is about 1 nF, the error can be neglected with regard to the accuracy of the bridge.

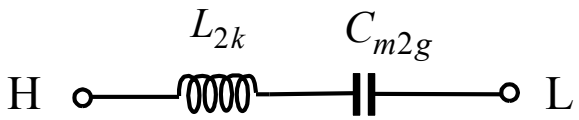


Figure 4.12: Equivalent circuit for the capacitance between electrode 2 and ground.

$C_2$ is defined in equation (3.14) as $C_2 = C_{23} + C_{24} + C_{2B} + C_{2s}$. Thus, $C_2 = C_{m2g} - C_k - C_{25}$. In figure 4.13, the mean capacitance between electrode and ground for the lower (LMG) and upper position (UMG) of the movable guard electrode is shown. As expected, the capacitance in the upper position of the movable guard electrode is higher than the capacitance in the lower position of the movable guard electrode due to the increasing capacitance between the movable guard electrode and the main electrode. The bars show the measurement

uncertainties which mainly come from the basic accuracy of the bridge and asymmetry of the electrode system.

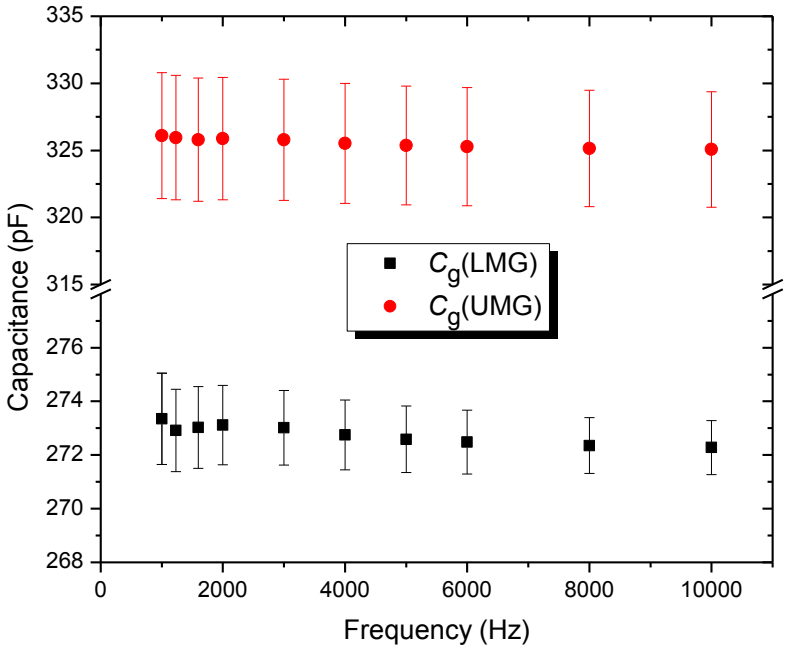


Figure 4.13: Mean capacitance between the main electrode and ground for the movable guard electrode in the lower and upper position (LMG and UMG) with expanded uncertainties

## 4.3.3 Capacitance between main electrode and movable guard electrode ($C_B$)

As described in chapter 2.2**,** both guard electrodes are equipped with capacitive probes for the adjustment of the electrode system. The capacitance $C_B$ between the movable guard electrode and main electrode can be obtained by measuring the capacitance of the capacitive prove ($C_{pBmea}$) and multiplying it with the length ratio $l_B/l_{Probe}$. The shielded two-terminal measurement technique has been used and additional errors due to leads and test fixtures have been eliminated by open/short compensation. The errors due to stray admittances and residual impedances inside the electrode system are by far less than the accuracy of the bridge and can therefore be neglected. As shown in figure 4.14, the guard electrode is equipped with a spike at its end which is a short cylindrical extension to reduce the influence of imperfections of the electrode system.

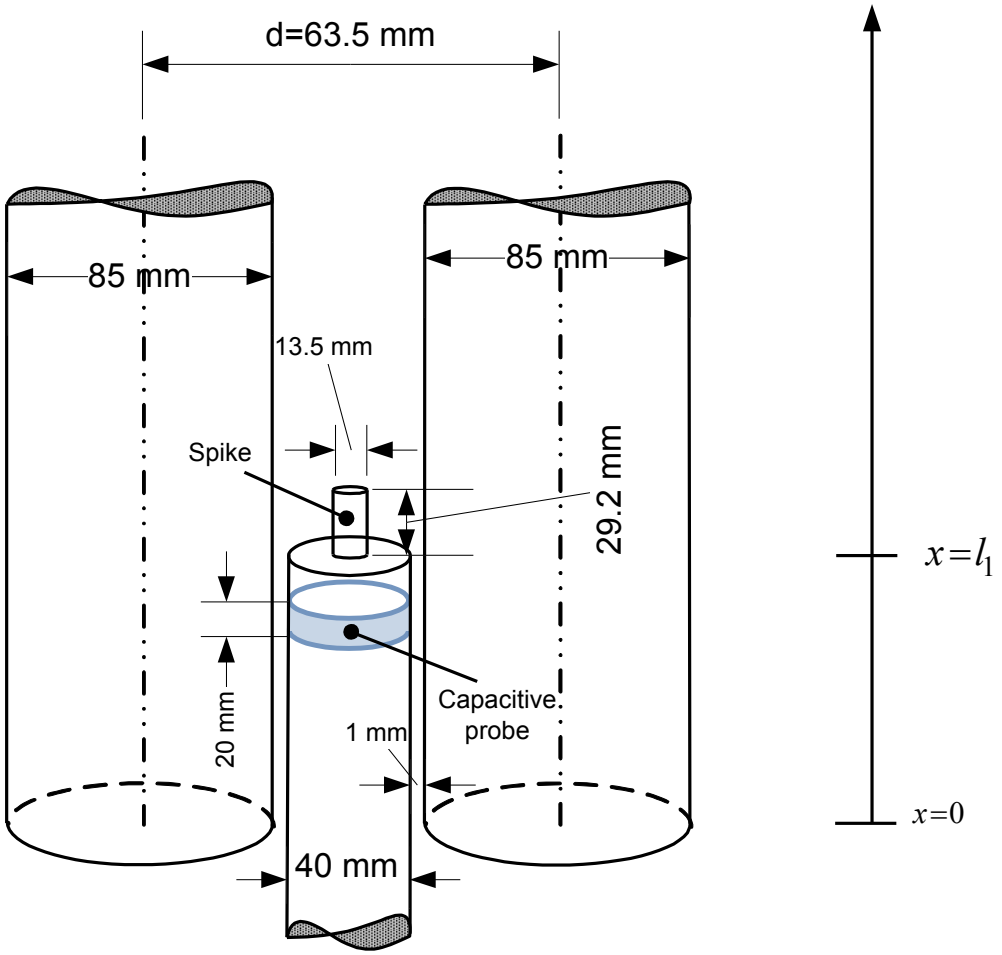


Figure 4.14: Capacitive probe and spike on the movable guard electrode.

The probe capacitance $C_{pB}$ and the capacitance of the spike $C_{sp}$ calculated from equations (4.1) and (4.2) with dimensions given in figure 4.14 yield values of 2.91 pF and 0.81 pF, respectively. As the measurement value of the probe $C_{pBmea}$ is lower than the calculated value $C_{pB}$ (ratio $C_{pBmea}/ C_{pB} = 0.88$), the calculated value of $C_{sp}$ has been multiplied by this factor giving 0.71 pF for the spike capacitance. In figure 4.15, the measurement results for $C_B$ including spike capacitance for the upper and lower position of the movable guard electrode are given.

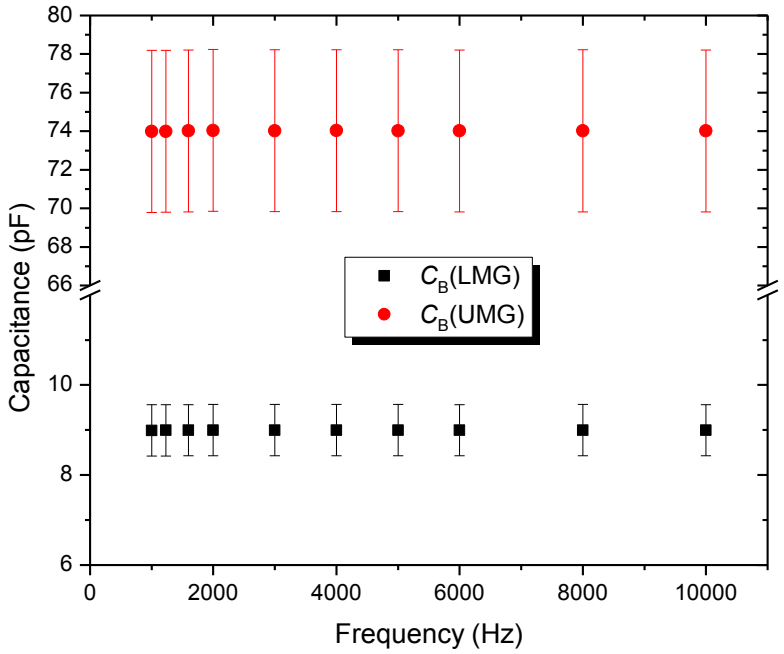


Figure 4.15: Mean capacitance between movable guard electrode and main electrode at LMG and UMG with expanded uncertainties

# 4.4 Self-inductance measurements

For low values of inductance, the reactance becomes relatively small and the series resistance component is more significant. Therefore, it is appropriate to choose the series inductance circuit mode setting of the bridge for the measurements. Before measurements are made, additional errors due to stray admittances and residual impedances of the test fixture and leads must be compensated by performing open/short compensation. A four-terminal measurement technique is not required, because the errors due to leads and test fixtures can be eliminated by the measurement technique as described in chapter 4.2.3. However, these errors can be checked by determining the residual impedances with a zero measurement (short-circuited leads). The self-inductance values were measured in actual use in a frequency range from 1 kHz to 10 kHz with a constant current of 10 mA.

## 4.4.1 Internal cables ($L_k$)

Figure 3.2 shows the equivalent circuit for the internal cables. All inductances of internal cables were measured in a frequency range between 1 kHz and 10 kHz with a constant current of 10 mA. In addition, the inductance of the coaxial cables was calculated according to equation (4.3). The inductance $L_{kD}$ of the feedthrough could not be directly measured. Therefore it has been determined using a spare part identical to that mounted in the calculable cross capacitor. The two-terminal measurement technique was employed to measure the inductance of the feedthrough. The coaxial cable $L_{kcoa}$ connected to the feedthrough is about 13.5 cm long with inner radius of 0.35 mm and outer radius of 2.33 mm. By applying equation (4.3) and taking function T from table given by Grover [25] (0.9999 for 1 kHz and 0.9997 for 10 kHz), the calculated inductance of the coaxial cable is 58 nH for DC up to 10 kHz. Inductance measurements of the flexible wires and metal pins ($L_{kwire}$) were performed by sequential measurements with shorts made at the different connecting points. In figure 4.16, the mean inductances of internal cables connected to the electrodes are shown. The material of the feedthroughs $L_{kD}$ is made of ferromagnetic material for the purpose of an optimal vacuum behavior while $L_{kcoa}$ and $L_{kwire}$ are the inductances of coaxial cables and pieces of wire made from copper. The frequency behavior of $L_{kD}$ can be explained by the properties of the material.

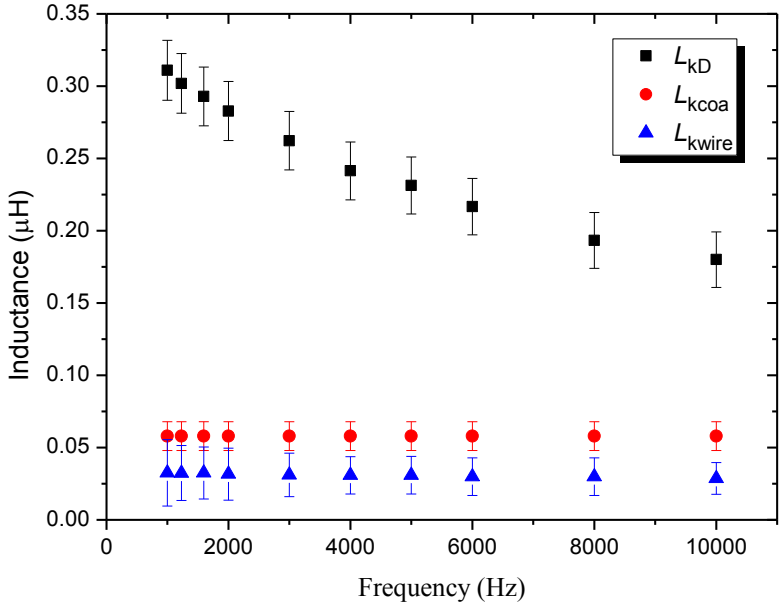


Figure 4.16: Measured inductances of internal cables with expanded uncertainties.

## 4.4.2 Main electrodes ($L_e$)

The electrode system is vertically arranged and made of Invar, a FeNi36 alloy. To measure the very low impedance of the electrodes, four-terminal measurement technique has been employed as described in chapter 4.2.3. The challenge of the measurement is eliminating the small magnetic coupling between the current and voltage circuits. Therefore, unshielded wires are used, and the low current ($L_C$) and high current ($H_C$) leads are tightly twisted together and kept apart from the similarly twisted low potential ($L_P$) and high potential ($H_P$) leads as shown in figure 4.17. The outer screen of the electrode system is used as a return path for the current. This configuration is similar to the actual use of the calculable capacitor, where the capacitive current flows down the main electrode and returns through the outer screen. The $L_C$ connection was made at the top of the outer screen. The main electrode is shorted by a small piece of metal directly at the bottom of the outer screen. The $H_C$ and $H_P$ connections were made to the flexible wire normally used to connect the electrode and the inner coaxial cable. The $L_P$ connection was made at the movable guard electrode which is connected directly to the outer screen by means of a ring of contacts. The $L_P$ lead runs outside the outer screen in order to minimize the induced error voltages caused by the magnetic flux generated by the current loop. The three other main electrodes were kept at ground potential, as in the intended use of the calculable capacitor by connecting them separately to the current low of the measuring instrument so that any currents in them do not flow through the measured

impedance. Before performing the measurement, a zero measurement has been made to measure the residual impedances in the measurement setup. They are less than 0.01 μH and 0.5 mΩ for the desired frequency range.

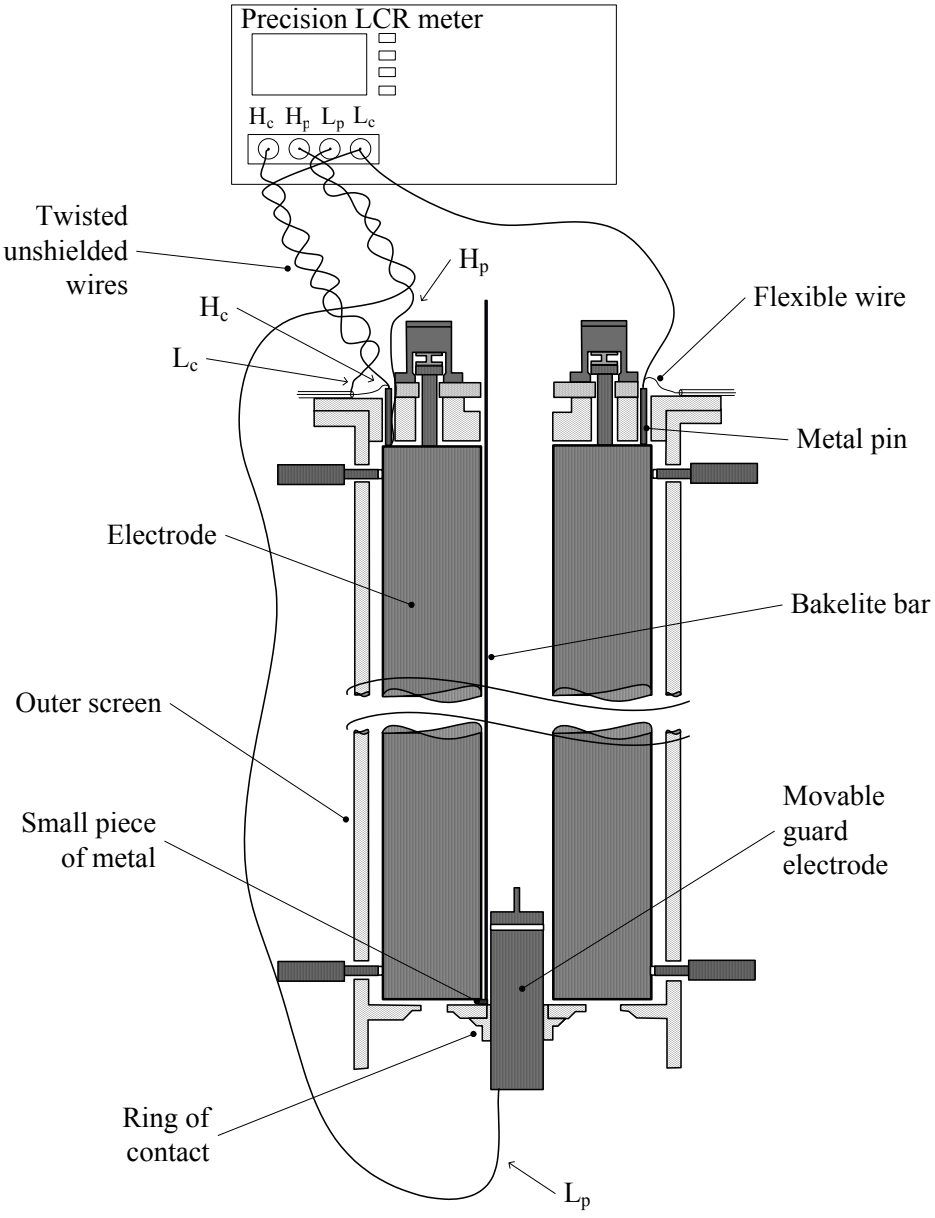


Figure 4.17: Measurement setup for measuring the self-inductance of the main electrodes.

In the measurement setup, a small piece of metal has been used to make a short connection between the main electrode and the outer screen at the bottom. The inductance and resistance of the metal piece calculated from [26] are about 5 nH and 80 μΩ, respectively, and will only

contribute with less than 3 % and 1 %, respectively to the inductance and resistance of the main electrode. These error contributions have been taken into account in the uncertainty of measurement. The impedance of the electrodes is very low compared to the admittance of the distributed capacitance between the electrodes and ground (less than 1 nF). Therefore, the effect of the distributed capacitances on the measured inductances can be neglected. The four main electrodes used in the calculable cross capacitor have the same geometry so that their inductance and resistance values are almost the same.

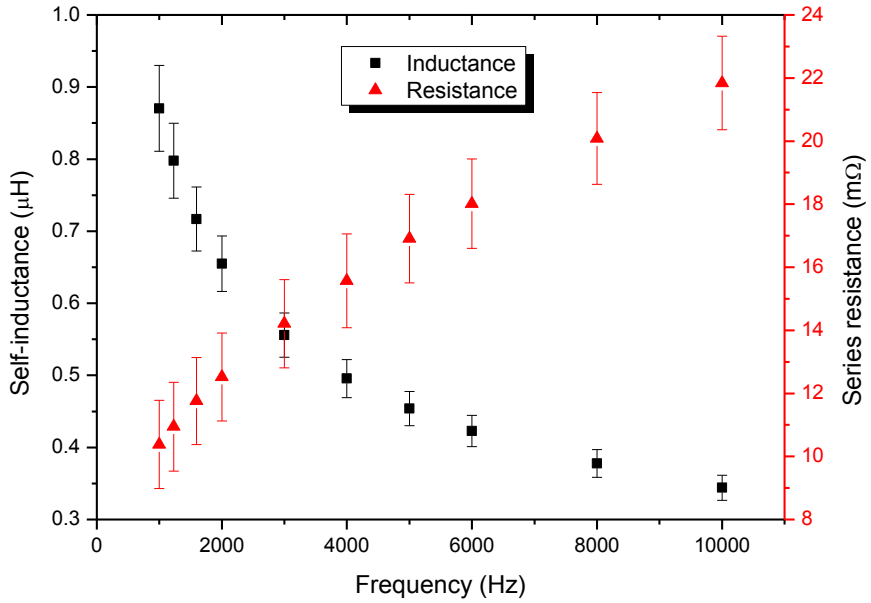


Figure 4.18: Mean value of the series self-inductance and series resistance of main electrodes with the movable guard electrode in the lower position with expanded uncertainties.

Figure 4.19 shows the series self-inductance and series resistance of electrode 5 for the two positions of the movable guard electrode (upper position (UMG) and lower position (LMG)). The measurement results differ by less than 0.02 μH and 1 mΩ in the whole frequency range. Therefore, the influence of the position of the movable guard electrode on the inductance and resistance of the main electrode can be neglected with regard to the uncertainty of measurement. For measuring the DC resistance of electrode 5, the measurement set up is the same as it has been used for the self-inductance measurement of the main electrodes in figure 4.17 but the Precision LCR meter is replaced by a 3458A Digital Multimeter.

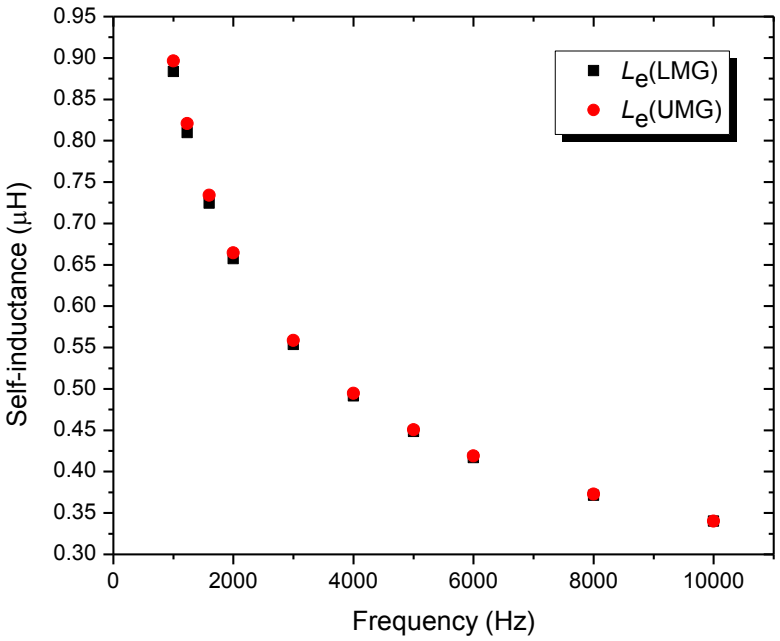


Figure 4.19 (a): Self-inductance of main electrode 5 for the two positions of the movable guard electrode.

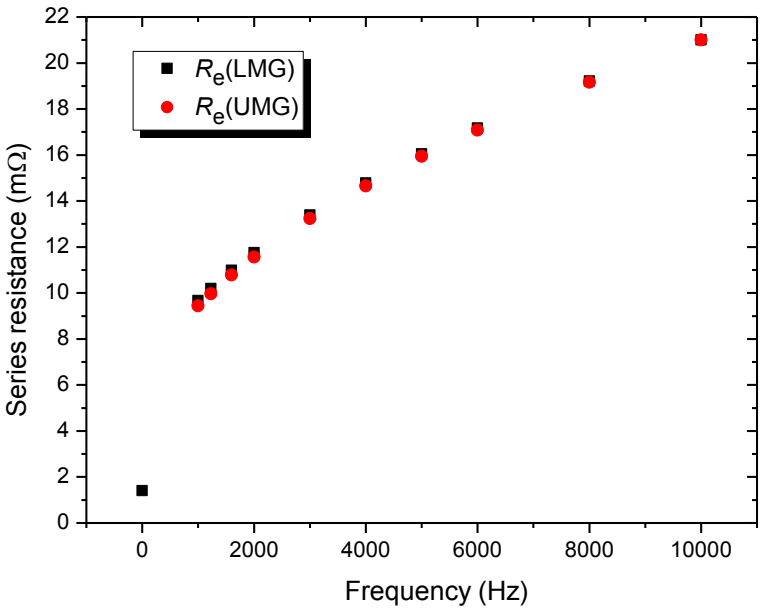


Figure 4.19 (b): Resistance of main electrode 5 for the two positions of the movable guard electrode.

### 4.4.3 Movable guard electrode ($L_B$)

The measurement set up for measuring the series inductance and resistance of the movable guard electrode is almost the same as that for the main electrode and is shown in figure 4.20. An extension tube with a clamp has been used to make a connection to the top of the movable guard electrode. The $H_C$ is connected to the clamp of the extension tube and must be kept in the same plane of the mounting plate when the movable guard electrode is at its lower and upper position. The $H_C$ lead is routed in a horizontal plane along the upper mounting plate (the clamp must be adjusted correspondingly). The $L_C$ lead is connected to the outer screen, and the $L_P$ connection is made to the movable guard electrode and returns outside the screen to reduce induced error voltages caused by a small flux generated by the current loop. The $H_P$ connection is made to the top end of the movable guard electrode, and should be routed inside the hollow extension tube in order to minimize induced error voltages on $H_P$. All main electrodes were at zero potential by connecting them separately to the current low of the measuring instrument. The inductance of the movable guard electrode, $L_B$, can not be measured directly, but its value per unit length can be calculated from two differential measurements. The self-inductance $L_B$ and series resistance $R_B$ of the movable guard electrode are shown in figure 4.21. $L_{B0}$ is the residual inductance of the movable guard electrode for the distance between the lower end of the main electrodes and the ring of contacts. $L_B$ (LMG) and $L_B$ (UMG) are the inductances of the movable guard electrode at its lower and upper position. There is no need to measure the inductance of the fixed guard electrode, because the cross capacitance is calculated as the difference of the two cross capacitances in the lower and upper position of the movable guard electrode. As the contribution of the fixed guard electrode to the two capacitances is the same, it cancels out by forming the difference. For measuring the DC resistance of the moveable guard electrode the Precision LCR meter in figure 4.20 is replaced by a 3458A Digital Multimeter.

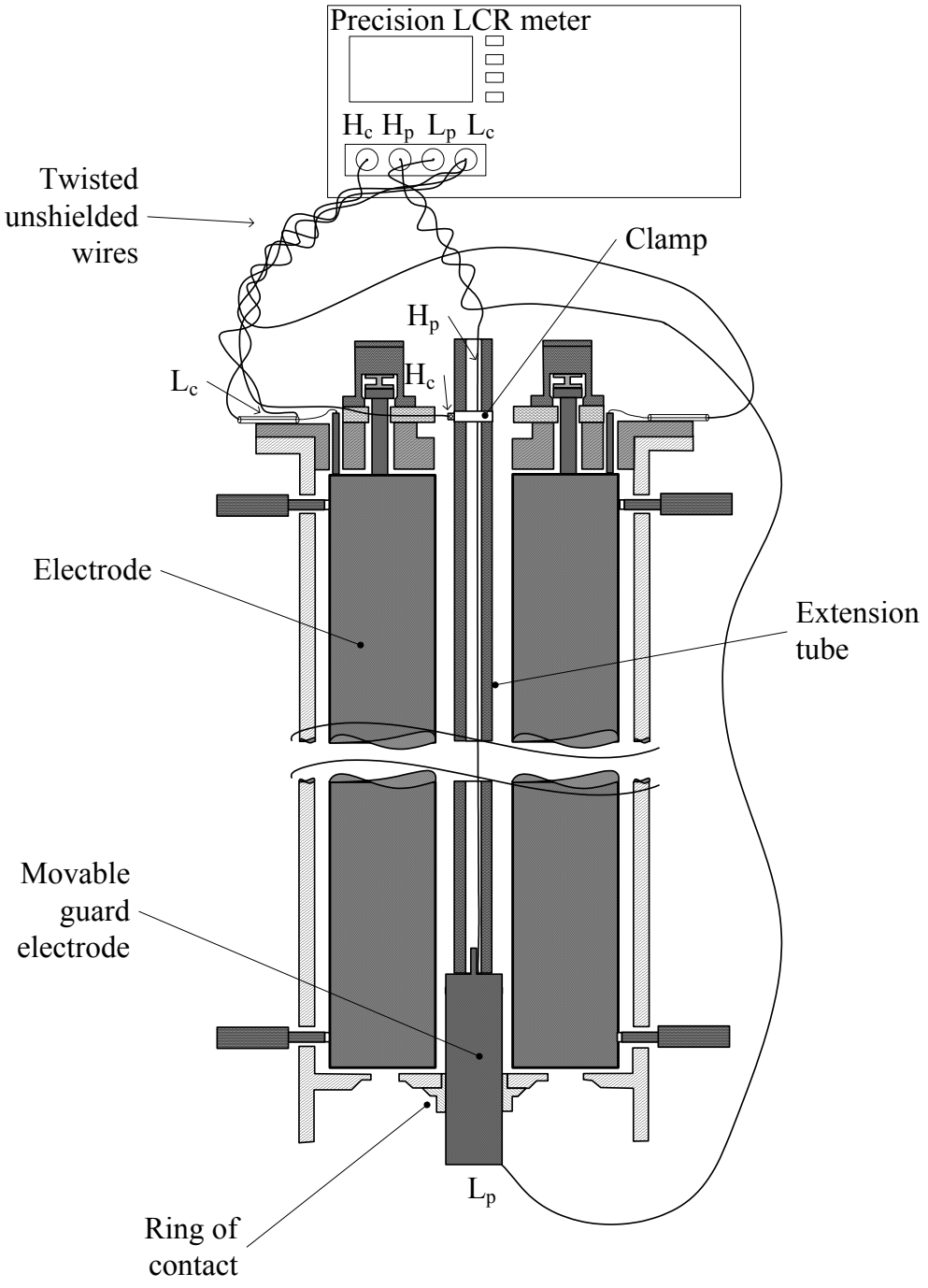


Figure 4.20: Measurement setup for measuring movable guard electrode.

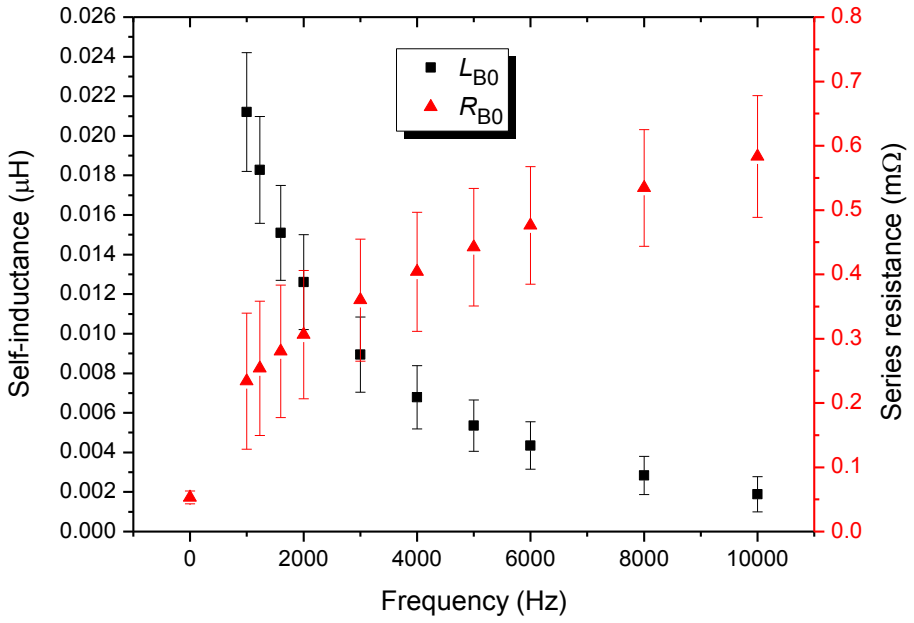


Figure 4.21 (a): Self-inductance and series resistance of the movable guard electrode at distance between the lower end of the main electrodes and the ring of contacts with expanded uncertainties.

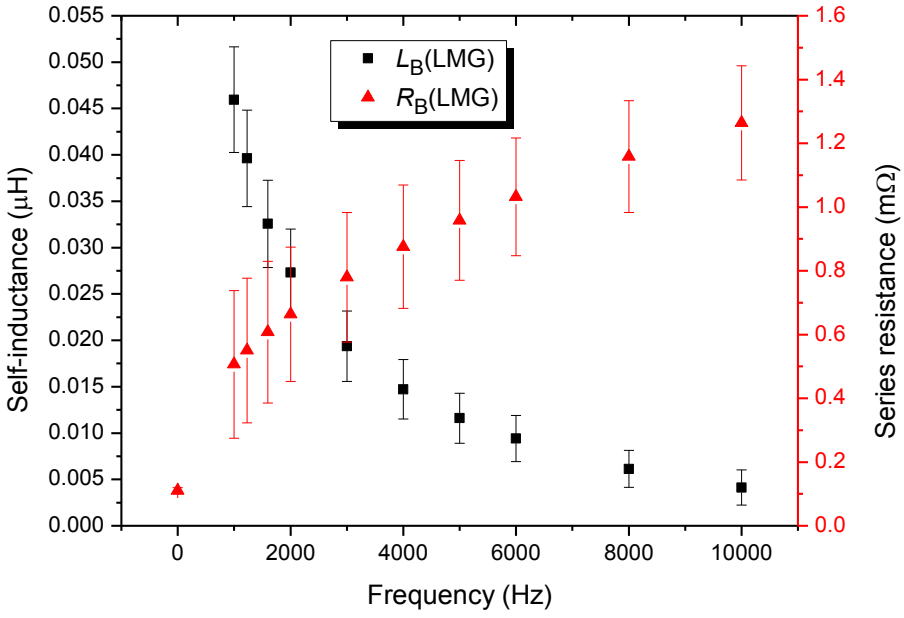


Figure 4.21 (b): Self-inductance and series resistance of the movable guard electrode at lower position (LMG) with expanded uncertainties.

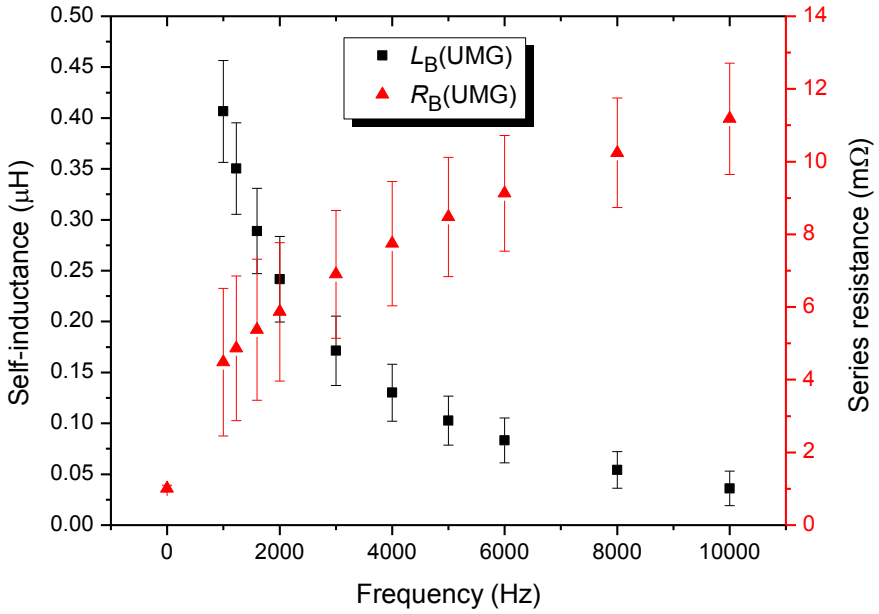


Figure 4.21 (c): Self-inductance and series resistance of the movable guard electrode at upper position (UMG) with expanded uncertainties.

# 4.5 Mutual inductance measurements

For the measurement of the mutual inductances the four-terminal measurement method has been used as described in chapter 4.2.4. The mutual inductances are measured with a constant current of 10 mA in the original configuration of the calculable cross capacitor for frequencies ranging from 1 kHz to 10 kHz. The mutual inductances are directly obtained from the bridge readings. The internal cables do not contribute to the mutual inductances, because the currents in the inner and outer conductors are equalized, so that they do not generate external magnetic fields.

## 4.5.1 Main electrodes ($M_0$ and $M_e$)

Unshielded wires are used for the connection of the capacitor to the bridge. $L_C$ and $H_C$ leads are tightly twisted together and kept apart from the similarly twisted $L_P$ and $H_H$ leads as shown in figure 4.22. The electrode current flows through the main electrode and back along the outer screen. The $L_C$ connection is made at the top of the outer screen. The electrodes are shorted by means of a small metal piece at the bottom of two main electrodes. The $H_P$ connection is made at the top end of the second main electrode, and the $L_P$ connection is made at the movable guard electrode which is connected directly to the outer screen by means of a ring of contacts. The $L_P$ lead should go outside the outer screen to reduce induced error voltages caused by a small flux from the current return loop. The other two main electrodes are at zero potential as in the actual use of the calculable cross capacitor by connecting them separately to the low current terminal of the measuring bridge, so that currents flowing in these electrodes do not have any influence on the measured mutual inductance.

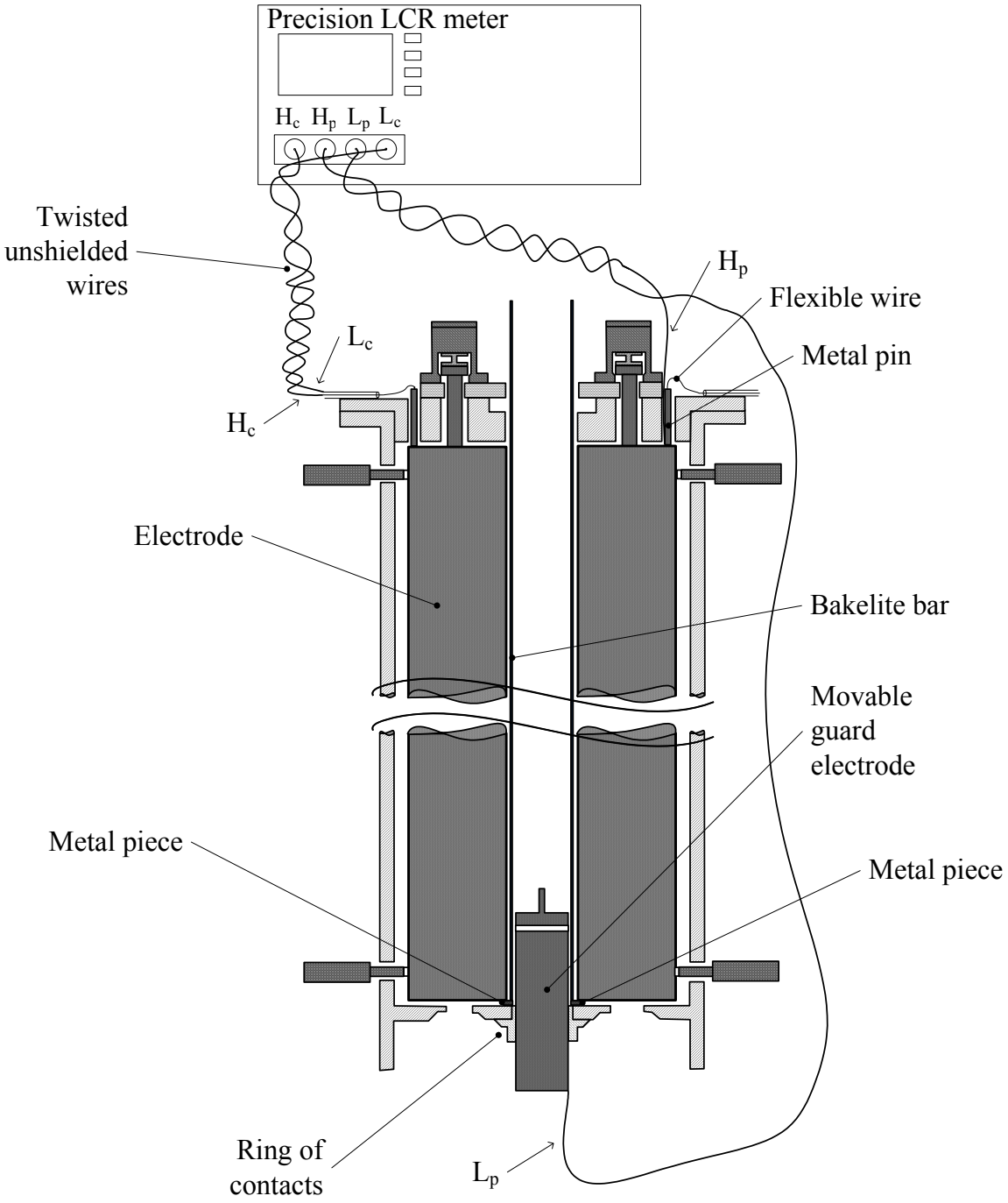


Figure 4.22: Measurement setup for measuring the mutual inductance between two main electrodes.

$M_{25}$, $M_{52}$, $M_{34}$ and $M_{43}$ are the mutual inductances between opposite electrodes ($M_o$), for instance, $M_{25}$ is the mutual inductance between electrode 2 and electrode 5, measured by applying a current to electrode 2. $M_{35}$, $M_{53}$, $M_{45}$, $M_{54}$, $M_{24}$, $M_{42}$, $M_{23}$ and $M_{32}$ are the mutual

inductances between adjacent electrodes ($M_e$). Figure 4.23 clearly show that due to the highly symmetric electrode system of the calculable cross capacitor, $M_{25} \cong M_{34} \cong M_o$ and $M_{35} \cong M_{45} \cong M_{24} \cong M_{23} \cong M_e$. As the mutual inductance between two parallel electrodes of the same geometry strongly depends on the distance between the two electrodes, the mutual inductance between adjacent electrodes is larger than that of opposite electrodes as is clearly shown in figure 4.23.

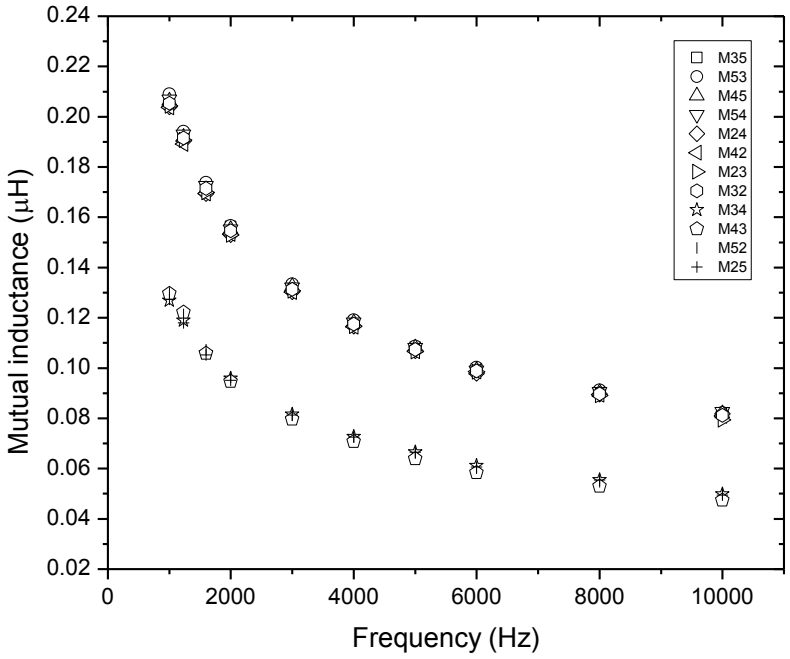


Figure 4.23: Mutual inductances between opposite electrodes and adjacent electrodes with the movable guard electrode in the lower position.

In figure 4.24, the dependence of the mutual inductance between opposite electrodes from the position of the movable guard electrode in the lower (LMG) and upper position (UMG) is shown. The differences can be explained by the screening effect of the movable guard electrode which results in a slight decrease of mutual inductance for the upper position of the movable guard electrode. The bars show the measurement uncertainties which mainly come from the basic accuracy of the bridge.

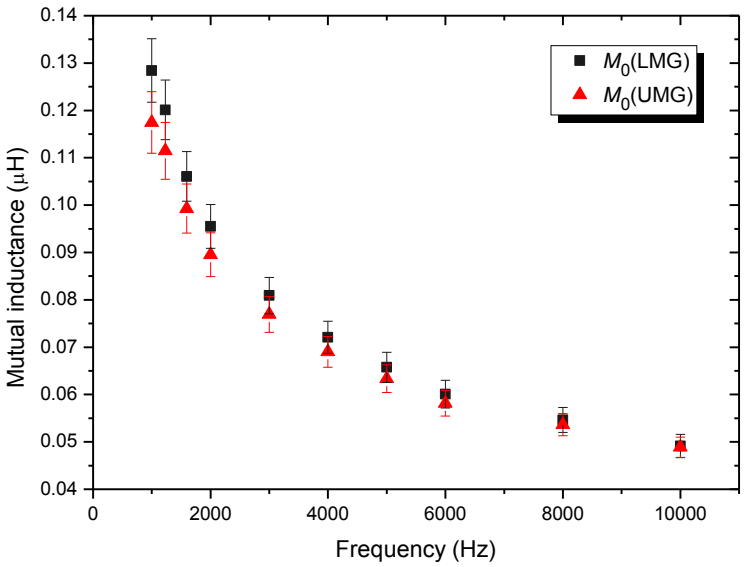


Figure 4.24: Mean mutual inductance between opposite electrodes for the lower (LMG) and upper (UMG) position of the movable guard electrode with expanded uncertainties.

The mutual inductances of adjacent electrodes for the different positions of the movable guard electrode (LMG and UMG) are shown in figure 4.25. As in this case the screening effect of the movable guard electrode is very small, the measurement results do not depend on the position of the movable guard electrode within the measurement uncertainty.

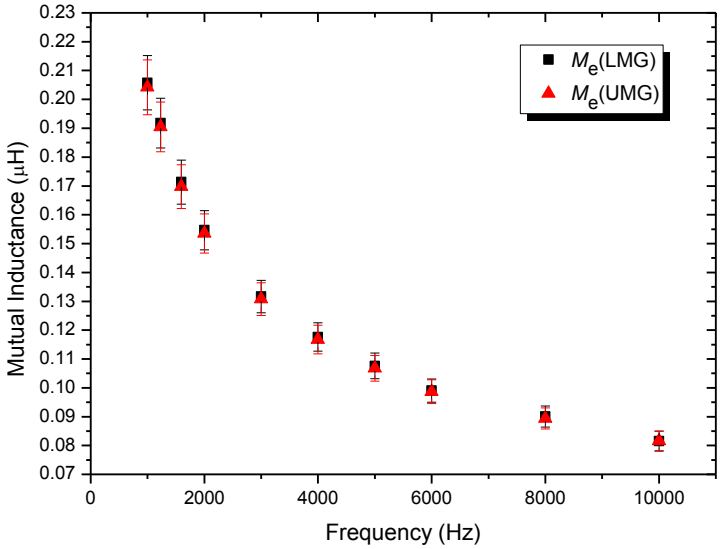


Figure 4.25: Mean mutual inductance between adjacent electrodes for the lower (LMG) and upper (UMG) position of the movable guard electrode with expanded uncertainties.

For comparison, the mutual inductances $M_o$, and $M_e$ can be calculated using equation (4.5) and the dimensions as given in chapter 2.2 .The calculated mutual inductances are about 0.30 μH for $M_o$ and 0.35 μH for $M_e$. The calculated and measured values agree satisfactorily, taking into consideration that the calculation neglected screening effects, distributed currents, skin effect, etc., and are calculated for very low frequencies.

## 4.5.2 Movable guard electrode ($M_B$)

The mutual inductance between the main electrodes and movable guard electrode can not be measured in a similar way as for the main electrodes due to the construction of the calculable cross capacitor, but it can be determined as the mutual inductance per unit length. The measurement set up is shown in figure 4.26. A clamp together with an extension tube has been used. The clamp is used to make an electrical connection between the $H_P$ lead and the extension tube, it must be kept in the same plane of the mounting plate when the movable guard electrode is at the lower and the upper position. The $L_C$ and $H_C$ connections are made in the same way as for measuring the mutual inductance between two main electrodes. The main electrode is shorted at the outer screen by means of a small metal piece. The $H_P$ connection is made at the clamp of the extension tube, and the $L_P$ connection is made at the lower end of the movable guard electrode which is connected directly to the outer screen by a ring of contacts. The $L_P$ lead should go outside the outer screen to reduce induced error voltages caused by the small flux from the current loop. The other main electrodes are at zero potential by connecting them separately to the low current terminal of the measuring bridge. The induced error voltages on the $H_P$ lead connected to the clamp caused by the flux of the $L_C$ lead will be cancelled due to the differential measurement in the lower and upper position of the movable guard electrode. The effect coming from the current loop has been proved by moving the $L_P$ lead around the outer screen. It did not show any effect on the measurement results within the given accuracy. There is no need to measure the mutual inductance of the fixed guard electrode, because the capacitance is calculated as the difference of the two capacitances in the lower and upper position of the movable guard electrode. As the contribution of the fixed guard electrode to the two capacitances is the same, it will be cancelled out by forming the difference.

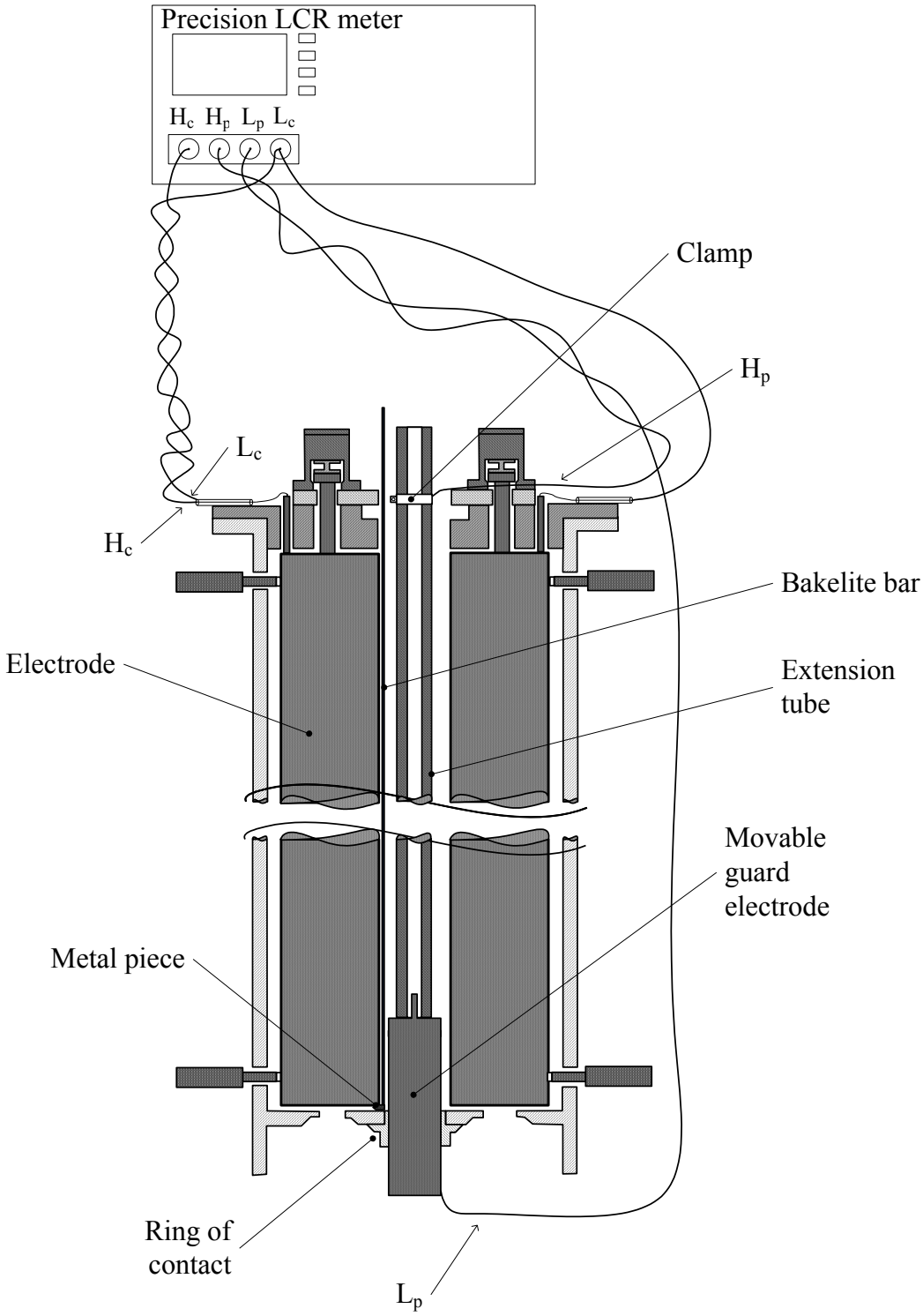


Figure 4.26: Measurement setup for measuring the mutual inductance between a main electrode and the movable guard electrode.

The results for $M_B$ are shown in figure 4.27 for the upper and lower position of the movable guard electrode (LMG and UMG).

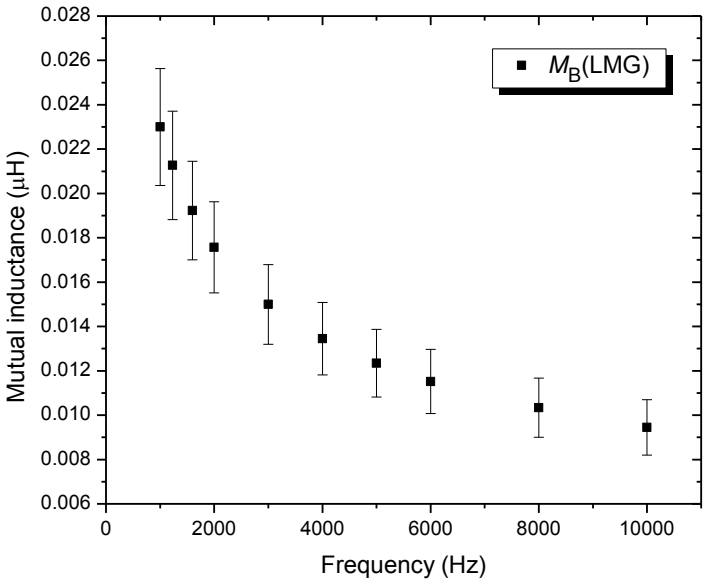


Figure 4.27 (a): Mean mutual inductance between the movable guard electrode and a main electrode for the lower position (LMG) of the movable guard electrode with expanded uncertainties.

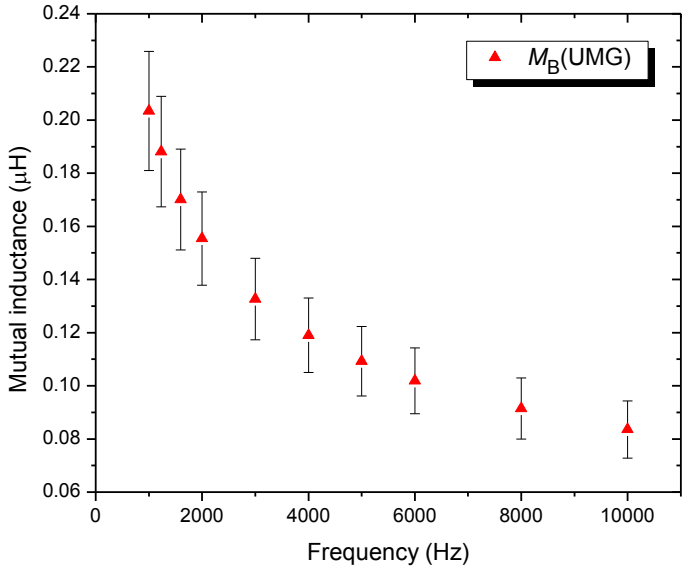


Figure 4.27 (b): Mean mutual inductance between the movable guard electrode and a main electrode for the upper position (UMG) of the movable guard electrode with expanded uncertainties.

The $M_B$ can also be calculated according to equation (4.6) with dimensions as given in chapter 2.2. The calculated mutual inductances are about 0.023 μH for $M_B$ at the lower (LMG) and 0.28 μH for $M_B$ at the upper (UMG) position of the movable guard electrode. The agreement is satisfying taking into consideration that any screening effects, distributed currents, skin effect, etc. were neglected for the calculation, and that the calculated values are only valid for very low frequencies.

# 4.6 Summary

For determining the frequency dependence of the circuit parameters, they were either measured by an auto-balancing bridge or calculated by equations given in the literature. The circuit parameters are capacitances, inductances, mutual inductances, resistances and conductances. All of the capacitances were found to be frequency independent, because the error terms described by $\omega^2 \cdot L \cdot C$ are less than the accuracy of the bridge. However, the accuracy of the bridge is sufficient to determine the frequency dependence of the calculable cross capacitor. The self-inductances, mutual inductances, and resistances of the electrodes show a frequency dependence which is predominant with regard to the accuracy of the bridge. Furthermore, self-inductance and mutual inductance were found to be linearly proportional to the inverse square root of the frequency in the examined frequency range. Two phenomena dominate the frequency dependence. Firstly, the current distribution over the cross section of the electrode is influenced by the skin effect resulting from eddy currents induced in the electrodes. For higher frequencies, the skin effect causes a concentration of the current near the outer surfaces of the electrodes, and the eddy currents – as the result of the skin effect – will suppress flux linkages so that the inductance decreases and the resistance increases at higher frequencies. The eddy currents are large, if the electrical conductivity is high [26]. Secondly, as the electrodes are made of ferromagnetic material having a high relative permeability, the inductances strongly decrease with frequency due to the skin effect resulting from eddy currents induced in the magnetic material. Due to the material and magnetic properties of the electrodes, the transition between weak and strong skin effect, $\omega_{weak} \ll 2/(r^2 \cdot \mu \cdot \sigma) \ll \omega_{strong}$, already occurs at very low frequencies ($\omega = 0.23$ rad/s for $\mu_r = 3000$). These effects are much higher than the accuracy of the bridge. The self-inductances and mutual inductances were found to be linearly proportional to the inverse square root of the frequency in the examined frequency range. In addition, the investigation of the influence of the electrode material is shown in Appendix A2.

# Chapter 5

# Calculation of the frequency behavior

## 5.1 Uncertainty evaluation

In chapter 4, the measurement of the circuit parameters has been discussed. The measurements were performed directly with an auto-balancing bridge, whereby the main uncertainty components come from the basic accuracy of the bridge, which has been verified by means of known standards before. The basic accuracy of the bridge amounts to 0.1 % for capacitance measurements and 2 % for inductance measurements [27]. The uncertainty calculation also includes the uncertainty components coming from the asymmetry of the electrode system (standard deviation of the mean of the equivalent circuit elements), the imperfection of the open/short compensation, and the metal piece used for making the connection to the electrodes. Normally, a calculable cross capacitor is operated at a frequency of 1592 Hz ($\omega = 10^4$ rad/s), the frequency which is also used for making the link between the farad and the ohm. The uncertainty evaluation of the frequency dependence of the cross capacitor is presented in this chapter.

### 5.1.1 Mathematical model

The frequency behavior of the calculable cross capacitor is calculated by means of the mathematical model in chapter 3 (equation (3.32)) and the parameters as determined in chapter 4 :

$$\Delta C_0 = \Delta C_{0low} - \Delta C_{0up}$$

where

$$\Delta C_{0low} = -2\omega^2 C_e^2 L_{ek} - \omega^2 C_B^2 L_m + \left(\frac{1}{3}\right)\omega^2 C_g^2 M_0 - \left(\frac{2}{3}\right)\omega^2 C_g C_e M_e + \frac{1}{6}\omega^2 C_B M_B \left[ C_g \frac{l_1}{l} + C_B \left(1 - \frac{l_1}{l}\right)\right] +$$

$$2\omega^2 C_{0LMG} \left\{ \left( C_A + \frac{C_{kwire}}{2} \right) L_{kwire} + \left( C_A + C_{kwire} + \frac{C_{kcoa}}{2} \right) L_{kcoaxial} + \left( C_A + C_{kwire} + C_{kcoa} + \frac{C_{kD}}{2} \right) L_{kD} \right\}$$

and $\Delta C_{0up} = -2\omega^2 C_e^2 L_{ek} - \omega^2 C_B^2 L_m + \left(\frac{1}{3}\right)\omega^2 C_g^2 M_0 - \left(\frac{2}{3}\right)\omega^2 C_g C_e M_e + \frac{1}{6}\omega^2 C_B M_B \left[ C_g \frac{l_2}{l} + C_B \left(1 - \frac{l_2}{l}\right)\right] +$

$$2\omega^2 C_{0UMG}\left\{\left(C_A + \frac{C_{kwire}}{2}\right)L_{kwire} + \left(C_A + C_{kwire} + \frac{C_{kcoa}}{2}\right)L_{kcoaxial} + \left(C_A + C_{kwire} + C_{kcoa} + \frac{C_{kD}}{2}\right)L_{kD}\right\}$$

$\Delta C_0$ : Change in capacitance of the calculable cross capacitor

$\Delta C_{0low}$ : Change in capacitance of the calculable cross capacitor at the lower position (low) of the movable guard electrode

$\Delta C_{0up}$ : Change in capacitance of the calculable cross capacitor at the upper position (up) of the movable guard electrode

$C_k$ : Internal cable capacitances ($C_{kwire}$, $C_{kcoa}$, and $C_{kD}$)

$C_A$ : Coupling capacitance between electrode and ground ($C_0$ and $C_g$)

$C_0$ : Cross capacitance taken from the difference of the capacitance at the lower and upper position of the movable guard electrode ($C_{0LMG}$ and $C_{0UMG}$)

$C_e$ : Coupling capacitance between adjacent electrodes

$C_B$ : Coupling capacitance between electrode and movable guard electrode

$L_k$ : Internal cable inductances ($L_{kwire}$, $L_{kcoaxial}$, and $L_{kD}$)

$L_{ek}$ : Self-inductance of the main electrode and internal cable inductance ($L_e$ and $L_k$)

$L_m$ : Self-inductance of the movable guard electrode ($L_{B0}$ and $L_B$)

$M_0$ : Mutual inductance between opposite electrodes

$M_e$ : Mutual inductance between adjacent electrodes

$M_B$ : Mutual inductance between movable guard electrode and main electrode

$l$ : Length of main electrode

$l_1$ : Length of movable guard electrode at lower position (LMG)

$l_2$ : Length of movable guard electrode at upper position (UMG)

ω : Angular frequency

The $C_B$, $C_g$, $L_m$, $M_0$, and $M_B$ will change with the length of the movable guard electrode.

## 5.1.2 Uncertainty calculation

The uncertainty calculation is performed according to the Guide to the Expression of Uncertainty in Measurement, the GUM [28]. The measurand ($y$) is a particular quantity subject to the measurement. It depends on a number of input quantities $x_i$ (i = 1, 2, …, N) according to the functional relationship

$$y = f(x_i,\ x_i, \ldots, x_N).$$

Applied to the calculable cross capacitor, one gets

$$\Delta C_0 = f(C_e, C_0, C_{kwire}, C_{kcoa}, C_{kD}, C_g, C_B, L_e, L_{kwire}, L_{kcoaxial}, L_{kD}, L_k, L_{B0}, L_B, M_0, M_e, M_B, l, l_1, l_2)$$

An estimate of the measurand is obtained from the mathematical model and the estimates of the input quantities. The standard uncertainty of the output quantity can be calculated from the standard uncertainties of the input quantities determined from their known probability distributions. If the input quantities are uncorrelated, the combined standard uncertainty $u_c(y)$ is given by

$$u_c(\Delta C_0) = \sqrt{\begin{aligned} &c_1^2u^2(C_{eLMG}) + c_2^2u^2(C_{eUMG}) + c_3^2u^2(C_{0LMG}) + c_4^2u^2(C_{0UMG}) + c_5^2u^2(C_{kwire}) + c_6^2u^2(C_{kcoa}) \\ &+ c_7^2u^2(C_{kD}) + c_8^2u^2(C_{BLMG}) + c_9^2u^2(C_{BUMG}) + c_{10}^2u^2(C_{gLMG}) + c_{11}^2u^2(C_{gUMG}) + c_{12}^2u^2(L_e) \\ &+ c_{13}^2u^2(L_{kwire}) + c_{14}^2u^2(L_{kcoa}) + c_{15}^2u^2(L_{kD}) + + c_{16}^2u^2(L_{B0}) + c_{17}^2u^2(L_{BLMG}) + c_{18}^2u^2(L_{BUMG}) \\ &+ c_{19}^2u^2(M_{0LMG}) + c_{20}^2u^2(M_{0UMG}) + c_{21}^2u^2(M_{eLMG}) + c_{22}^2u^2(M_{eUMG}) + c_{23}^2u^2(M_{BLMG}) \\ &+ c_{24}^2u^2(M_{BUMG}) + c_{25}^2u^2(l) + c_{26}^2u^2(l_1) + c_{27}^2u^2(l_2) \end{aligned}}.$$

The $c_i$'s are the sensitivity coefficients which are calculated in Appendix A. 3.

The change in capacitance of the calculable cross capacitor and its uncertainty has been calculated by means of the GUM Workbench [29] as given in Appendix A. 4. As an example, the uncertainty budget of the change in capacitance at a frequency of 1592 Hz ($\omega = 10^4$ Hz) is given in table 5.1.

**Table 5.1:** Example for the uncertainty budget for a change in capacitance of 1 pF at 1.6 kHz.

| Quantity | Value | Standard Uncertainty | Sensitivity Coefficient | Uncertainty Contribution |
|---|---|---|---|---|
| $C_{eLMG}(\omega)$ | $53.500 \cdot 10^{-12}$ F | $332 \cdot 10^{-15}$ F | $-16 \cdot 10^{-9}$ | $-5.5 \cdot 10^{-21}$ F |
| $L_{kwire}(\omega)$ | $33.00 \cdot 10^{-9}$ H | $8.45 \cdot 10^{-9}$ H | $-30 \cdot 10^{-15}$ | $-250 \cdot 10^{-24}$ F |
| $L_{kcoa}(\omega)$ | $59.00 \cdot 10^{-9}$ H | $5.00 \cdot 10^{-9}$ H | $-28 \cdot 10^{-15}$ | $-140 \cdot 10^{-24}$ F |
| $L_{kD}(\omega)$ | $293.0 \cdot 10^{-9}$ H | $10.2 \cdot 10^{-9}$ H | $-26 \cdot 10^{-15}$ | $-270 \cdot 10^{-24}$ F |
| $L_{e}(\omega)$ | $717.0 \cdot 10^{-9}$ H | $21.5 \cdot 10^{-9}$ H | $-27 \cdot 10^{-15}$ | $-590 \cdot 10^{-24}$ F |
| $C_{BLMG}(\omega)$ | $9.000 \cdot 10^{-12}$ F | $285 \cdot 10^{-15}$ F | $-35 \cdot 10^{-12}$ | $-9.9 \cdot 10^{-24}$ F |
| $L_{B0}(\omega)$ | $15.10 \cdot 10^{-9}$ H | $1.12 \cdot 10^{-9}$ H | $540 \cdot 10^{-15}$ | $610 \cdot 10^{-24}$ F |
| $L_{BLMG}(\omega)$ | $32.60 \cdot 10^{-9}$ H | $2.09 \cdot 10^{-9}$ H | $-2.7 \cdot 10^{-15}$ | $-5.6 \cdot 10^{-24}$ F |
| $C_{gLMG}(\omega)$ | $273.000 \cdot 10^{-12}$ F | $517 \cdot 10^{-15}$ F | $1.4 \cdot 10^{-9}$ | $730 \cdot 10^{-24}$ F |
| $M_{0LMG}(\omega)$ | $106.10 \cdot 10^{-9}$ H | $2.65 \cdot 10^{-9}$ H | $2.5 \cdot 10^{-12}$ | $6.6 \cdot 10^{-21}$ F |
| $M_{eLMG}(\omega)$ | $171.30 \cdot 10^{-9}$ H | $3.80 \cdot 10^{-9}$ H | $-970 \cdot 10^{-15}$ | $-3.7 \cdot 10^{-21}$ F |
| $M_{BLMG}(\omega)$ | $19.20 \cdot 10^{-9}$ H | $1.05 \cdot 10^{-9}$ H | $4.4 \cdot 10^{-15}$ | $4.6 \cdot 10^{-24}$ F |
| $C_{kwire}(\omega)$ | $4.240 \cdot 10^{-12}$ F | $104 \cdot 10^{-15}$ F | $74 \cdot 10^{-12}$ | $7.6 \cdot 10^{-24}$ F |
| $C_{kcoa}(\omega)$ | $10.4500 \cdot 10^{-12}$ F | $57.6 \cdot 10^{-15}$ F | $65 \cdot 10^{-12}$ | $3.7 \cdot 10^{-24}$ F |
| $C_{kD}(\omega)$ | $5.31000 \cdot 10^{-12}$ F | $9.00 \cdot 10^{-15}$ F | $29 \cdot 10^{-12}$ | $260 \cdot 10^{-27}$ F |
| $C_{eUMG}(\omega)$ | $49.500 \cdot 10^{-12}$ F | $332 \cdot 10^{-15}$ F | $16 \cdot 10^{-9}$ | $5.3 \cdot 10^{-21}$ F |
| $C_{BUMG}(\omega)$ | $74.00 \cdot 10^{-12}$ F | $2.10 \cdot 10^{-12}$ F | $890 \cdot 10^{-12}$ | $1.9 \cdot 10^{-21}$ F |
| $L_{BUMG}(\omega)$ | $289.0 \cdot 10^{-9}$ H | $18.4 \cdot 10^{-9}$ H | $180 \cdot 10^{-15}$ | $3.4 \cdot 10^{-21}$ F |
| $C_{gUMG}(\omega)$ | $325.80 \cdot 10^{-12}$ F | $1.39 \cdot 10^{-12}$ F | $-1.8 \cdot 10^{-9}$ | $-2.4 \cdot 10^{-21}$ F |
| $M_{0UMG}(\omega)$ | $99.30 \cdot 10^{-9}$ H | $2.60 \cdot 10^{-9}$ H | $-3.5 \cdot 10^{-12}$ | $-9.2 \cdot 10^{-21}$ F |
| $M_{eUMG}(\omega)$ | $169.80 \cdot 10^{-9}$ H | $3.80 \cdot 10^{-9}$ H | $1.1 \cdot 10^{-12}$ | $4.1 \cdot 10^{-21}$ F |
| $M_{BUMG}(\omega)$ | $170.00 \cdot 10^{-9}$ H | $9.50 \cdot 10^{-9}$ H | $-300 \cdot 10^{-15}$ | $-2.9 \cdot 10^{-21}$ F |
| $C_{0UMG}(\omega)$ | $0.23 \cdot 10^{-12}$ F | | | |
| $C_{0LMG}(\omega)$ | $1.23 \cdot 10^{-12}$ F | | | |
| $l_1$ | 0.065 m | | | |
| $l_2$ | 0.575 m | | | |
| $l$ | 0.85 m | | | |
| $\omega$ | 10000.0 Hz | | | |
| $\pi$ | 3.1415926535898 | | | |
| $f$ | 1591.549430919 Hz | | | |
| $\Delta C_0(\omega)$ | $-92.4 \cdot 10^{-21}$ F | $15.7 \cdot 10^{-21}$ F | | |

| Quantity | Value | Expanded Uncertainty | Coverage factor | Coverage |
|---|---|---|---|---|
| $\Delta C_0(\omega)$ | $-92 \cdot 10^{-21}$ F | $31 \cdot 10^{-21}$ F | 2.00 | 95% |

($\omega$) means that components depend on frequency.

## 5.2 Results and discussion

As mentioned in chapter 3, the circuit model describes only the influence of distributed admittances and impedances within the calculable cross capacitor and evaluates their influence on the cross capacitance. All influences resulting from the measuring bridge, the outer cable connections included are not part of this work.

The change in capacitance due to frequency and the associated measurement uncertainty of the PTB calculable cross capacitor in the audio frequency range (1 kHz to 10 kHz) carried out by applying equation 3.32, using the measured circuit parameters in chapter 4, and uncertainty evaluation in chapter 5.1 is shown in table 5.1.

According to the equivalent circuit model, the change in capacitance is caused by six different influences: the influence of electrode inductances and adjacent electrode capacitances ($\xi_1$), the influence of the movable guard electrode inductance and the movable guard electrode capacitance ($\xi_2$), the influence of mutual inductances of opposite electrodes and capacitances-to-ground ($\xi_3$), the influence of mutual inductances in adjacent electrodes and capacitances-to-ground ($\xi_4$), the influence of mutual inductances between electrode and the movable guard electrode and the movable guard electrode capacitance ($\xi_5$), and the influence of internal cables ($\xi_6$). The changes in capacitance due to each influence are shown in table 5.2 and in figure 5.1 for frequencies from 1 kHz to 10 kHz.

**Table 5.2:** The changes in capacitance for each influence type of the calculable cross capacitor between 1 kHz and 10 kHz with the total change and its standard uncertainty (1σ).

| Influence | Relative capacitance change at 1 pF $\Delta C_0/C_0$ ($\times 10^{-8}$) | | | | | | | | | |
|---|---|---|---|---|---|---|---|---|---|---|
| | **1 kHz** | **1.23 kHz** | **1.6 kHz** | **2 kHz** | **3 kHz** | **4 kHz** | **5 kHz** | **6 kHz** | **8 kHz** | **10 kHz** |
| **$\xi_1$: ($L_{ek}$ and $C_e$)** | -2.3 | -3.3 | -5.1 | -7.9 | -16.4 | -26.9 | -39.5 | -53.8 | -87.2 | -126.3 |
| **$\xi_2$: ($L_m$ and $C_B$)** | 3.4 | 4.4 | 6.1 | 8.0 | 12.8 | 17.3 | 21.3 | 24.9 | 28.9 | 30.3 |
| **$\xi_3$: ($M_0$ and $C_g$)** | -3.8 | -5.8 | -8.8 | -12.5 | -25.3 | -41.1 | -60.0 | -80.2 | -136.2 | -200.7 |
| **$\xi_4$: ($M_e$ and $C_g$)** | 0.8 | 1.1 | 1.6 | 2.3 | 4.4 | 7.0 | 10.0 | 13.8 | 21.5 | 33.5 |
| **$\xi_5$: ($M_B$ and $C_B$)** | -2.4 | -3.4 | -5.1 | -7.4 | -14.2 | -22.6 | -32.4 | -43.5 | -69.4 | -99.1 |
| **$\xi_6$ : (Cables)** | 0.9 | 1.3 | 2.2 | 3.4 | 7.4 | 12.4 | 18.4 | 25.2 | 41.1 | 59.9 |
| **Total** | **-3.5** | **-5.6** | **-9.2** | **-14.1** | **-31.2** | **-54** | **-82** | **-114** | **-201** | **-302** |
| **Standard Uncertainty ($\times 10^{-8}$)** | **0.8** | **1.1** | **1.6** | **2.3** | **4.3** | **7** | **10** | **13** | **21** | **30** |

The results in the table 5.2 represent the changes in capacitance at AC referred to the capacitance $C_0$ according to the Thompson-Lampard theorem. The correct value can be achieved by applying the correspondent corrections. Neglecting the frequency dependence of $L$ and $M$ and taking the measured values at 1 kHz as constant would alter the relative capacitance change $\Delta C_0/C_0$ by only 12 %.

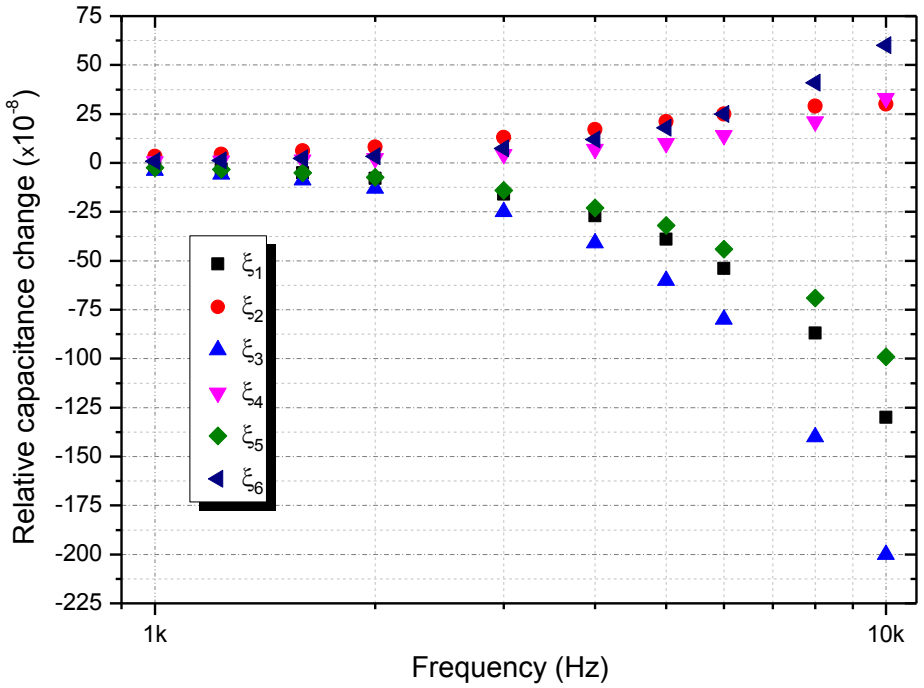


Figure 5.1: The changes in capacitance applied to each influence of the calculable cross capacitor 1 pF between 1 kHz and 10 kHz.

Figure 5.1 clearly shows that the influence of the electrode inductances and adjacent electrode capacitances ($\xi_1$) and the influence of the mutual inductances in opposite electrodes and capacitances-to-ground ($\xi_3$) are the predominant terms for the capacitance change at higher frequencies. It also shows that the capacitance is approximately proportional to the square of frequency as expected from the model.

The corrections of the frequency errors are shown in figure 5.2.

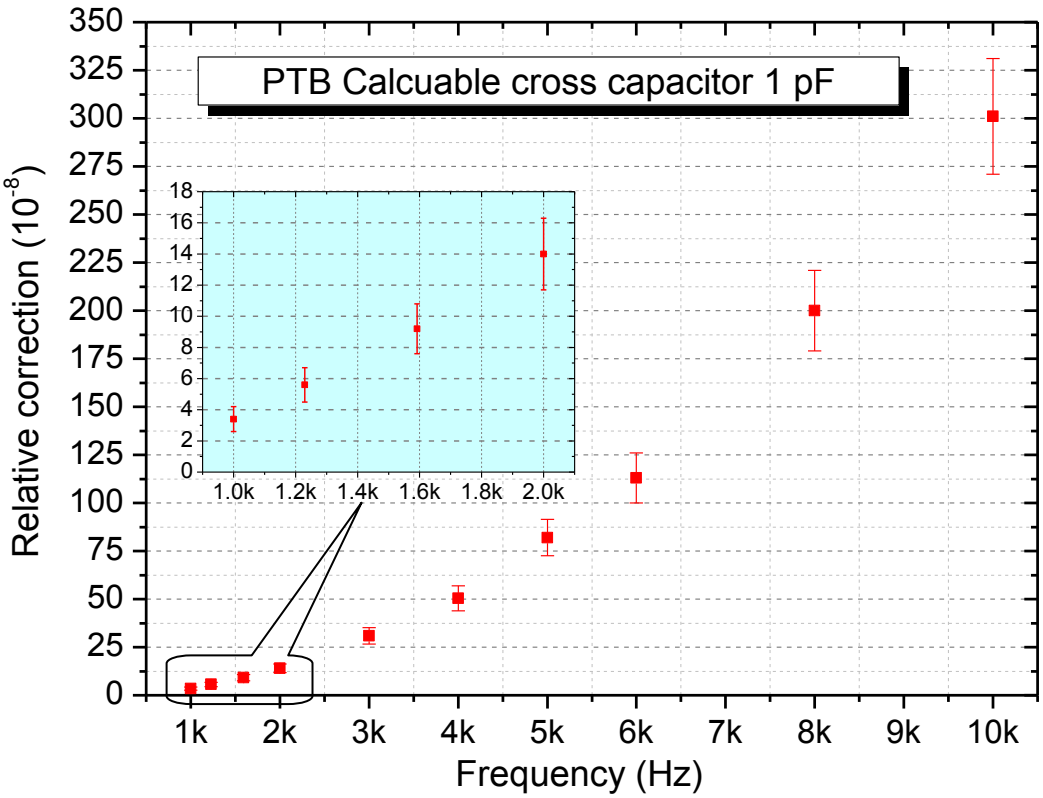


Figure 5.2: Frequency behavior of the PTB calculable cross capacitor 1 pF in audio frequency range (1 kHz to 10 kHz) and its standard uncertainty (1σ).

Considering the uncertainty calculation in Appendix A.4, the dominant uncertainty contributions are the standard uncertainties of the adjacent electrode capacitances and mutual inductances of opposite electrodes. According to chapter 4.3.2.1, the standard uncertainty of the adjacent electrode capacitances mainly results from the standard deviation of the asymmetry of the electrode system. It contributes to the expanded uncertainty to about 20 %. The standard uncertainty of the mutual inductances for opposite electrodes contributes to the expanded uncertainty to about 30 % mainly coming from the bridge accuracy as described in chapter 4.5.1. Figure 5.2 clearly shows that the capacitance change is approximately proportional to the square of frequency (see also equations 3.30 to 3.32).

# Chapter 6

# Conclusion and outlook

An equivalent circuit model has been developed to describe the frequency behavior of the calculable cross capacitor. The circuit model described considers only the influence of distributed admittances and impedances within the calculable cross capacitor and has been derived from the main currents flowing inside the capacitor and the voltage drops caused by these currents. Resistances and conductances are not included in the equivalent circuit model since they mainly influence the quadrature balance of the bridge, and therewith do not essentially influence the frequency behavior of the capacitance of the calculable cross capacitor. Any influences resulting from the measuring bridge can be easily corrected and therefore are not considered.

The circuit parameters of the model mainly are directly measured with a commercial auto-balancing bridge in a frequency range between 1 kHz and 10 kHz. The accuracy of the bridge limits the uncertainty of the frequency correction for the calculable cross capacitor. The accuracy of the bridge has been confirmed by the verified standards before making the measurements. The accuracy of the bridge is 0.1 % for capacitance measurements and 2 % for inductance measurements. With these accuracies, the calculated uncertainty of the frequency correction amounts to a few parts in $10^8$.

The measurement techniques applied for the determination of the circuit parameters depend on the terminal configuration of the device under test and the desired accuracy. Two-terminal and shielded two-terminal measurement techniques have been used for capacitance measurements and four-terminal measurement techniques for the measurement of inductances and mutual inductances. For the four-terminal measurement technique, the small magnetic couplings between the current and voltage circuits have been eliminated by twisting the unshielded current and potential cables.

The additional errors due to test fixtures and cables can be reduced by performing open/short compensation except for the four-terminal measurement technique. However, additional errors caused by the four-terminal measurement technique can be checked by measuring the residual impedances with a zero measurement (short-circuited leads).

The open compensation capability of the bridge cancels errors due to stray admittances and the short compensation cancels errors due to residual impedances.
All parameters were measured in the actual configuration of the electrode system. For each measurement technique, an equivalent circuit has been derived.

The stray capacitances of the capacitor were found to be frequency independent. The self-inductances and mutual inductances of the electrodes show strong frequency dependence which can be explained by the skin effect and magnetic properties of the electrodes. Due to the material and magnetic properties of the electrodes, the transition between weak and strong skin effect, $\omega_{weak} \ll 2/(r^2 \cdot \mu \cdot \sigma) \ll \omega_{strong}$, already occurs at very low frequencies ($\omega = 0.23$ rad/s for $\mu_r = 3000$). These effects are much higher than the accuracy of the bridge. The self-inductances and mutual inductances were found to be linearly proportional to the inverse square root of the frequency in the examined frequency range.

The frequency dependence of the calculable cross capacitor is calculated based on the circuit parameters. It has been found that the frequency dependence of the cross capacitance is proportional to the square of the frequency, and that the influence of mutual inductances of opposite electrodes dominate at higher frequencies. The dominant uncertainty contributions are the standard uncertainty of the mean value of the capacitances of adjacent electrodes due to an asymmetry of the electrode system and the bridge accuracy for the mutual inductance measurements. The calculable cross capacitor is normally operated at a frequency of 1592 Hz. For this frequency, the correction amounts to $(9.2 \pm 3.1)\times10^{-8}$ pF for an expanded uncertainty (k=2). In some cases, also frequencies of 1000 Hz and 1233 Hz are used. The frequency corrections for these frequencies are $(3.5 \pm 1.5)\times10^{-8}$ pF and $(5.6 \pm 2.1)\times10^{-8}$ pF, respectively.

To improve the frequency behavior of the PTB calculable cross capacitor, the use of non-magnetic material for all constructional parts of the capacitor is suggested. This will reduce the self and mutual inductances and therewith the frequency correction and its uncertainty. The standard deviation due the asymmetry of the electrode system is one of the largest uncertainty contributions for the PTB calculable cross capacitor. It can be reduced either by improving the symmetry of the electrode system or by taking the actual values of the capacitances between adjacent electrodes into consideration instead of their mean value.

The determination of the frequency dependence of the calculable cross capacitor is not only of importance for the realization of the unit of capacitance but will have great perspectives ahead. Particularly, the theory for the AC behavior of the quantum Hall effect (AC–QHE) presently being developed can be investigated. By comparing a frequency-characterized cross capacitor and an AC–QHR with a quadrature bridge, the frequency dependence being observed in AC–QHR devices can be checked. Presently, the ohm can be traced back to the farad via the AC–QHE with measurement uncertainty of $6\times10^{-9}$ (k=1) [13]. Furthermore, a capacitance standard based on a single electron tunneling (SET) device can be investigated.

In future, quantum metrology may lead to an International System of Units based on the fundamental constants and free from any artifact standards. For the units of electrodynamics, the elementary charge $e$ will be fixed instead of the present ampere definition and Planck's constant $h$ will replace the kilogram (kg). Therefore, it is a big challenge and of great importance for metrology to prove the validity of Josephson constant $K_J = 2e/h$ and the von Klitzing constant $R_K = h/e^2$. A well defined calculable cross capacitor with a small uncertainty can make a valuable contribution.

# References


[1] International Bureau of Weights and Measures, *The International System of Units*, 8th edition, 2006.

[2] P. J. Mohr, B. N. Taylor, and D. B. Newell, "CODATA recommended values of the fundamental physical constants: 2006", *Reviews of modern physics*, vol. 80, p.637, April–June. 2008.

[3] V. Sienknecht and T. Funck, "Realization of the SI Unit Volt by Means of a Voltage Balance", *Metrologia*, vol. 22, pp. 209-212, 1986.

[4] M. W. Keller, "Current status of the quantum metrology triangle", *Metrologia*, vol. 45, pp. 102–109, Jan. 2008.

[5] I. M. Mills, P. J. Mohr, T. J. Quinn, B. N. Taylor, and E. R. Williams "Redefinition of the kilogram, ampere, kelvin and mole: a proposed approach to implementing CIPM recommendation 1 (CI-2005)", *Metrologia*, vol. 43, pp. 227–246, 2006.

[6] A. Jeffery, R. E. Elmquist, J. Q. Shields, L. H. Lee, M. E. Cage, S. H. Shields, and R. F. Dziuba, "Determination of the von Klitzing constant and the fine-structure constant through a comparison of the quantized Hall resistance and the ohm derived from the NIST calculable capacitor", *Metrologia*, vol. 35, pp. 83-96, Apr. 1998.

[7] G. W. Small, B. W. Ricketts, P. C. Coogan, B. J. Pritchard, and M. M. R. Sovierzoski, "A new determination of the quantized Hall resistance in terms of the NML calculable cross capacitor", *Metrologia*, vol. 34, pp. 241-243, Jun. 1997.

[8] G. Trapon, O. Thevenot, J. C. Lacueille, and W. Poirier, "Determination of the von Klitzing constant $R_K$ in terms of the BNM calculable capacitor – fifteen years of investigations", *Metrologia*, vol. 40, pp. 159-171, Jun. 2003.

[9] K. Jones and A. C. Corney, "The PEL Calculable", *Metrologia*, vol. 24, pp. 1-11, 1987

[10] A. M. Thompson, D. G. Lampard, “A New Theorem in Electrostatics and its Application to Calculable Standards of Capacitance”, *Nature*, vol. 177, p 888, May 1956.

[11] M. W. Kelle, N. M. Zimmerman, A. L. Eichenberger, and J. M. Martinis, “A Capacitance Standard Based on Counting Electrons”, *Science*, vol. 285, pp. 1706-1709, Jul. 1999.

[12] A. L. Eichenberger, M. W. Keller, J. M. Martinis, and N. M. Zimmerman, “Frequency Dependence of a Cryogenic Capacitor Measured Using Single Electron Tunneling Devices”, *Journal of Low Temperature Physics*, vol.118, pp. 317-324, 2000.

[13] J. Schurr, V. Bürkel and B. P. Kibble, “Realizing the farad from two ac quantum Hall resistances”, *Metrologia*, vol. 46, pp. 619–628, Oct. 2009.

[14] D. G. Lampard, "A new theorem in electrostatics with applications to calculable standards of capacitance," *J. Inst. Elec. Eng*., vol. 104C, pp. 271-280, Jan. 1957.

[15] D. G. Lampard and R. D. Cutkosky, "Some results on the crosscapacitance per unit length of cylindrical three-terminal capacitors with dielectric films on their electrodes," *J. Inst. Elec. Eng*., vol.107C, pp. 112-119, Jan. 1960.

[16] A. M. Thompson, "The cylindrical cross-capacitor as a calculable standard," *Proc. Inst. Elec. Eng*. (London), vol. 106B, pp. 307- 310, May 1959.

[17] G. H. Rayner, “NPL calculable capacitor”, *IEEE Trrms. Instrum. Meas*, vol. 21, pp. 361-365, Nov. 1972.

[18] H. Bachmair, T. Funck, R. Hanke, and H. Lang, “Realization and maintenance of the unit of capacitance with the PTB cross capacitor during the last ten years”, *IEEE Trans. Instrum. Meas*, vol. 44, pp. 440 – 442, Apr. 1995.

[19] W. K. Clothier, “A Calculable Standard of Capacitance”, *Metrologia*, vol. 1, p.36, Apr. 1965.

[20] H. Bachmair, Determination of the unit of resistance and the von Klitzing constant RK based on a calculable capacitor, *Eur. Phys. J. Special Topics* , vol.172, pp. 257–266, Jun. 2009.

[21] A.M. Jeffery, L.H. Lee and J.Q. Shields, “Model tests to investigate the effects of geometrical imperfections on the NIST calculable capacitor”, *IEEE Trans*., vol 48, pp. 356-359, Apr. 1999.

[22] Agilent, *Impedances measurement handbook*, Agilent Technologies Inc, 4th ed., p 5-15, Jun. 2009.

[23] R. Hanke, A. Kölling and J. Melcher, "Inductance calibration in the frequency range 50 Hz to 1 MHz at PTB", *CPEM 2002 Conf. Dig*., pp 186–7, 2002

[24] S. Awan, B. P. Kibble and J. Schurr, *Coaxial Electrical Circuits for Interference-Free Measurements*, Institution of Engineering and Technology, pp 94–95, 2011.

[25] K. Küpfmüller, *Einführung in die theoretisch Eelktrotechnik*, Springer Berlin Heidelberg, p 93, 1973

[26] F. W. Grover, *Inductance Calculations*, Dover Publications Inc., pp 31–47, 2004

[27] Hewlett-Packard, *Operation Manual HP: 4284A Precision LCR meter*, Hewlett-Packard Japan Ltd., 6th ed., p 9-8, Aug. 1998.

[28] I. O. for Standardization, *Guide to the Expression of Uncertainty in Measurement*, GUM, 1 Rue Varamb, Case Postale 56, CH 1221, Geneva, Switzerland.

[29] "Gum workbench," http://www.gum.dk/e-wb-home/gw home.html.

[30] R. Boll, *Weichmagnetisch Werkstoffe*, Vacuumschmelze GmbH, Hanau, p. 239, 1977

# Appendix A

# Appendix

## A.1 Verification of the auto-balancing bridge

For a check of the auto-balancing bridge a circular loop inductance has been used. The inductance of such a circular loop inductor as shown in figure A.1 (a) can be calculated by $L_{circle} \approx N^2 R \mu_0 \mu_r \left[ \ln\left(\frac{8R}{a}\right) - 2 \right]$.

Figure A.1 (a): Circular loop inductor.

where
$N$ : Number of turns
$R$ : Radius of the circular loop
$a$ : Wire radius
$\mu_r$ : Relative permeability of the medium

By applying this equation, the calculated inductance and resistance of this circular loop inductor are 0.8 μH and 10 mΩ, respectively.


Figure A.1 (b): Measurement setup for measuring circular loop inductance.

Figure A.1 (b) shows the measurement setup. Before performing a measurement, open/short compensation must be used to reduce the additional errors caused by the test fixture. Open compensation capability cancels errors due to stray admittances and short compensation cancels errors due to residual impedances. The calculated and measured values agree quite well.

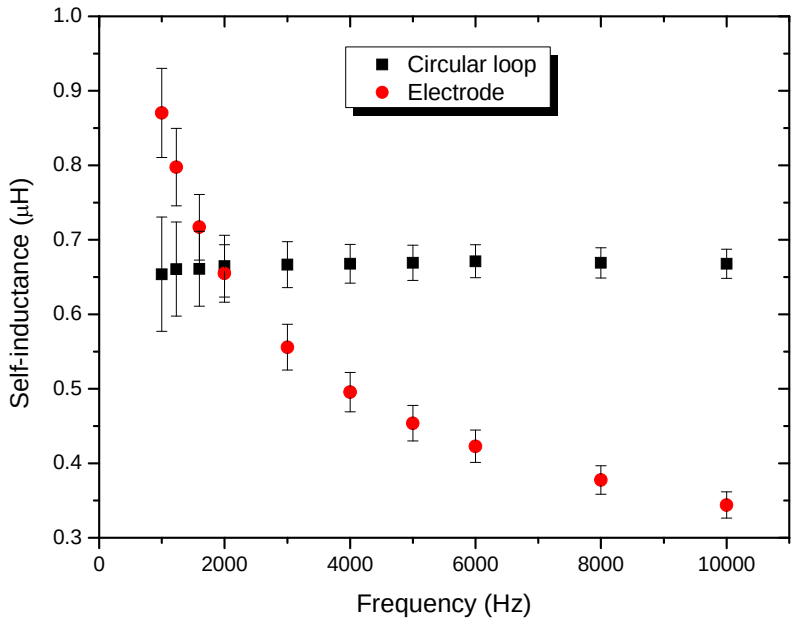


Figure A.1(c): Self-inductance of the circular loop inductor and a main electrode of the calculable cross capacitor with measurement uncertainties.

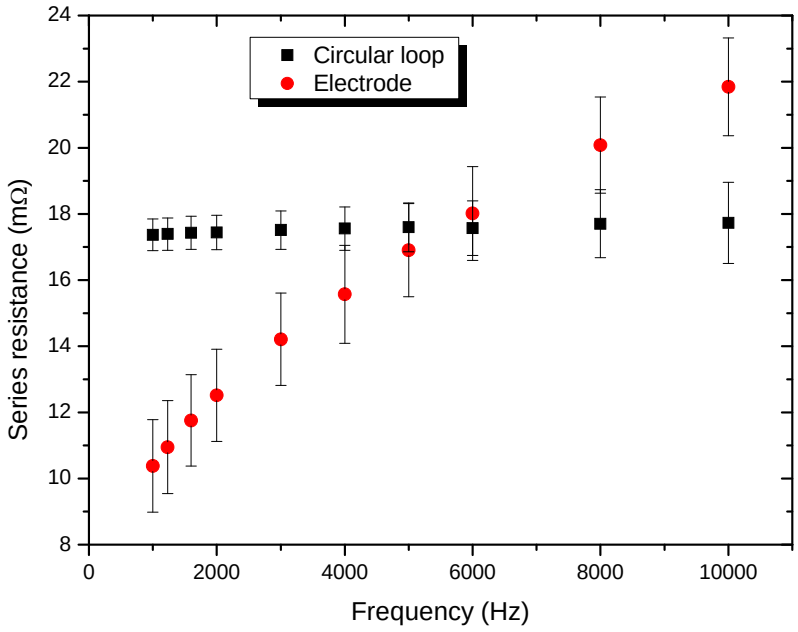


Figure A.1 (d): Series resistance of the circular loop inductor and a main electrode of the calculable cross capacitor with measurement uncertainties

As expected, the inductance and resistance of the circular loop inductor are frequency independent as shown in figure A.1 (c) and figure A.1 (d). This gives the proof that the auto-balancing bridge measures the inductances and resistances correctly, and the observed frequency dependence of the inductance and resistance of the main electrode of the calculable cross capacitor does not depend on an error of the bridge measurements but on the material properties and geometry of the main electrode.

# A.2 Investigation of the influence of the electrode material

To investigate the influence of the electrode material on the frequency behavior of the self-inductance and resistance of the electrodes, the inductances and resistances of a copper (Cu) bar with the same dimensions as the electrodes of the calculable cross capacitor and a spare electrode (material INVAR) have been measured. For measuring the very low impedances, the four-terminal measurement technique has been applied. The challenge of the measurement is to eliminate the small magnetic coupling between the current and voltage circuits. Therefore, unshielded wires have been used, and the low current ($L_C$) and high current ($H_C$) leads were tightly twisted together and kept apart from the low potential ($L_P$) and high potential ($H_P$) leads as shown in figure A.2 (a). The measurements were made on a table of non-ferromagnetic material.

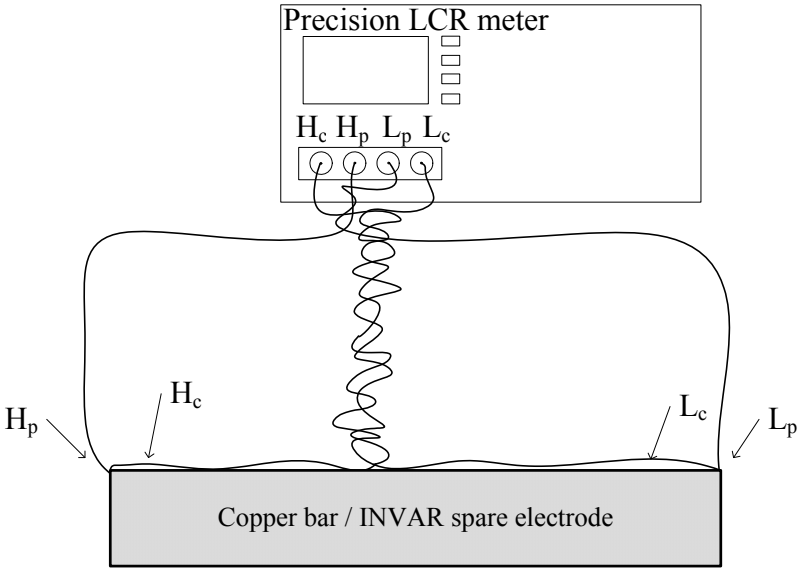


Figure A.2 (a): Measurement setup for measuring the copper bar and the INVAR spare electrode.

The inductances and resistances of the copper bar, the INVAR spare electrode and the main electrodes are measured in frequency range from 1 kHz to 10 kHz and are normalized to the value at 1 kHz as shown in figure A.2 (b) and figure A.2 (c).

The DC and AC resistance of a straight cylindrical conductor and a tubular conductor [26] are given by $R_{AC(cylindical)} = 4.15\frac{1}{\rho}\sqrt{f}\cdot 10^{-8}$ Ω/cm (only for copper!)

where ρ is radius of the cylindrical conductor, and

$R_{AC(tube)} = \frac{\sqrt{f\sigma}}{r}\left(1+\frac{1}{2}\frac{1}{\tau}\frac{t}{r}\right)\Omega/\text{cm}$ where $\tau = \frac{mt}{\sqrt{2}}$ and $m = 2\pi\sqrt{\frac{2\mu f}{\sigma}}$

$t$ : Thickness of the tube in centimeter

$r$ : Outer radius in centimeter
σ : Resistivity of material in c.g.s unit
μ : Permeability of material

**Table A2.1**: Measured and calculated resistances of the INVAR spare electrode and the copper bar.

| Resistance | INVAR spare electrode | | Copper bar | |
|---|---|---|---|---|
| | Measurement | Calculation | Measurement | Calculation |
| $R_{DC}$ | 0.3 mΩ | 0.2 mΩ | <0.01 mΩ | 0.002 mΩ |
| $R_{1kHz}$ | 2.4 mΩ | 1.9 mΩ | 0.03 mΩ | 0.025 mΩ |
| $R_{10kHz}$ | 7.2 mΩ | 5.7 mΩ | 0.13 mΩ | 0.078 mΩ |
| $R_{10kHz}/R_{1kHz}$ | 3 | 3 | 4.3 | 3.1 |

Owing to table A2.1, the measured values and the calculated value are in fairly good agreement and clearly show that the resistance increases with frequency due to the skin effect. The expanded measurement uncertainties shown in figure A.2 (b) mainly come from the resolution of the measuring bridge (0.01 mΩ).

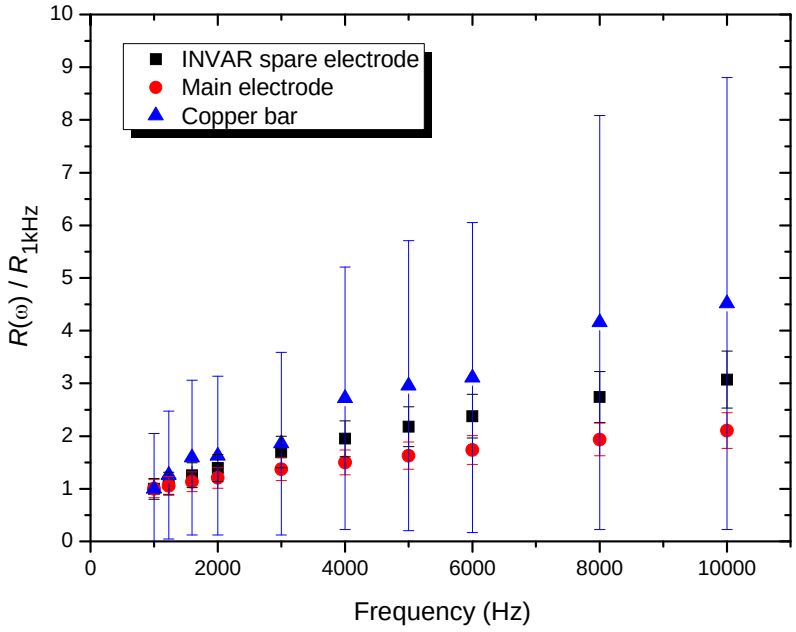


Figure A.2 (b): Normalized resistances of the copper bar, the INVAR spare electrode and the main electrodes with their measurement uncertainties.

The inductances of an isolated cylindrical conductor and an isolated tubular conductor are given by $L(\omega)=2l\left[\ln\frac{2l}{\rho}-1+\frac{\mu}{4}T\right]$nH and $L(\omega)=2l\left[\ln\frac{2l}{r}-1+\frac{\mu}{4}T\right]$nH, respectively. The

function $T$ which takes the skin effect into account is taken from the table given by Grover [26]. $r$ is a geometric mean distance and ρ is a radius of the cylindrical conductor. The permeability for a 35–40 % nickel iron alloy is about 3000 and it is frequency independent in desired frequency range [30].

**Table A2.2**: Normalized inductances of the INVAR spare electrode and the copper bar.

| Inductance | INVAR spare electrode | | Copper bar | |
|---|---|---|---|---|
| | Measurement | Calculation | Measurement | Calculation |
| $L_{10kHz}/L_{1kHz}$ | 0.35 | 0.46 | 0.85 | 0.94 |

Due to table A2.2, the measurement and calculation for normalized inductances of the INVAR spare electrode and the copper bar are fairly in agreement. In figure A.2 (c), the measurements show very clearly that the frequency behavior of inductances depends on the material properties because the inductances of the INVAR spare electrode and the main electrodes which are made from ferromagnetic material strongly depend on the frequency, while the inductance of the copper bar only shows a slight frequency dependence. The frequency behavior of inductances is mainly explained by the skin effect. The small difference in the inductance of the INVAR spare electrode and the main electrode depends on the ferromagnetic material inside the calculable cross capacitor in the neighbourhood of each main electrode (the three other main electrodes, the guard electrodes and the guard cylinder).

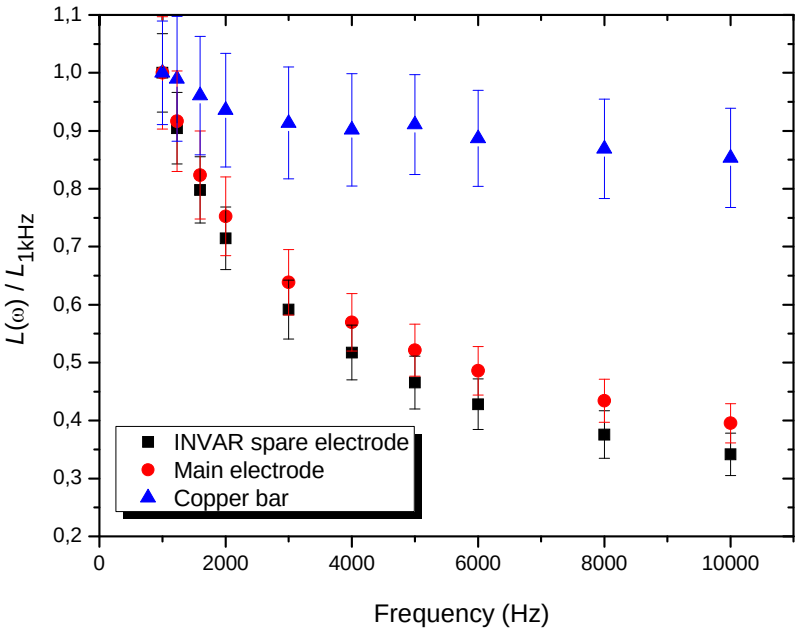


Figure A.2 (c): Normalized inductances of the copper bar, the INVAR spare electrode and the main electrodes with their measurement uncertainties.

# A.3 Sensitivity coefficients

The sensitivity coefficients can be calculated from the partial derivatives of the model function to the input quantities $C_i = \partial y / \partial x_i$.

$$C_1 = -4\omega^2 C_{eLMG}\left(L_{kwire} + L_{kcoa} + L_{kD} + \left(\frac{L_e}{3}\right)\right) - \left(\frac{2}{3}\right)\omega^2 C_{gLMG} M_{eLMG}$$

$$C_2 = 4\omega^2 C_{eUMG}\left(L_{kwire} + L_{kcoa} + L_{kD} + \left(\frac{L_e}{3}\right)\right) + \left(\frac{2}{3}\right)\omega^2 C_{gUMG} M_{eUMG}$$

$$C_3 = 2\omega^2 C_{0LMG}\left(L_{kwire} + L_{kcoa} + L_{kD}\right) + 2\omega^2 \left\{ \begin{array}{l} \left(C_{0LMG} + C_{gLMG} + \frac{C_{kwire}}{2}\right) L_{kwire} \\ + \left(C_{0LMG} + C_{gLMG} + C_{kwire} + \frac{C_{kcoa}}{2}\right) L_{kcoa} \\ + \left(C_{0LMG} + C_{gLMG} + C_{kwire} + C_{kcoa} + \frac{C_{kD}}{2}\right) L_{kD} \end{array} \right\}$$

$$C_4 = -2\omega^2 C_{0UMG}\left(L_{kwire} + L_{kcoa} + L_{kD}\right) + 2\omega^2 \left\{ \begin{array}{l} \left(C_{0UMG} + C_{gUMG} + \frac{C_{kwire}}{2}\right) L_{kwire} \\ + \left(C_{0UMG} + C_{gUMG} + C_{kwire} + \frac{C_{kcoa}}{2}\right) L_{kcoa} \\ + \left(C_{0UMG} + C_{gUMG} + C_{kwire} + C_{kcoa} + \frac{C_{kD}}{2}\right) L_{kD} \end{array} \right\}$$

$$C_5 = 2\omega^2 C_{0LMG}\left(\frac{L_{kwire}}{2} + L_{kcoa} + L_{kD}\right) - 2\omega^2 C_{0UMG}\left(\frac{L_{kwire}}{2} + L_{kcoa} + L_{kD}\right)$$

$$C_6 = 2\omega^2 C_{0LMG}\left(\frac{L_{kcoa}}{2} + L_{kD}\right) - 2\omega^2 C_{0UMG}\left(\frac{L_{kcoa}}{2} + L_{kD}\right)$$

$$C_7 = \omega^2 C_{0LMG} L_{kD} - \omega^2 C_{0UMG} L_{kD}$$

$$C_8 = -2\omega^2 C_{BLMG}\left(L_{B0} + \frac{L_{BLMG}}{3}\right) + \left(\frac{1}{6}\right)\left(1 - \frac{l_1}{l}\right)\omega^2 C_{BLMG} M_{BLMG} + \left(\frac{1}{6}\right)\omega^2 M_{BLMG}\left(C_{gLMG}\left(\frac{l_1}{l}\right) + C_{BLMG}\left(1 - \frac{l_1}{l}\right)\right)$$

$$C_9 = 2\omega^2 C_{BUMG}\left(L_{B0} + \frac{L_{BUMG}}{3}\right) - \left(\frac{1}{6}\right)\left(1 - \frac{l_2}{l}\right)\omega^2 C_{BUMG} M_{BUMG} - \left(\frac{1}{6}\right)\omega^2 M_{BUMG}\left(C_{gUMG}\left(\frac{l_2}{l}\right) + C_{BUMG}\left(1 - \frac{l_2}{l}\right)\right)$$

$$C_{10} = \left(\frac{2}{3}\right)\omega^2 C_{gLMG} M_{0LMG} - \left(\frac{2}{3}\right)\omega^2 C_{eLMG} M_{eLMG} + \left(\frac{1}{6}\right)\left(\frac{l_1}{l}\right)\omega^2 C_{BLMG} M_{BLMG} + 2\omega^2 C_{0LMG}\left(\begin{array}{l} L_{kwire} + \\ L_{kcoa} + L_{kD} \end{array}\right)$$

$$C_{10} = \left(\frac{2}{3}\right)\omega^2 C_{gLMG} M_{0LMG} - \left(\frac{2}{3}\right)\omega^2 C_{eLMG} M_{eLMG} + \left(\frac{1}{6}\right)\left(\frac{l_1}{l}\right)\omega^2 C_{BLMG} M_{BLMG} + 2\omega^2 C_{0LMG}\begin{pmatrix} L_{kwire} + \\ L_{kcoa} + L_{kD} \end{pmatrix}$$

$$C_{11} = -\left(\frac{2}{3}\right)\omega^2 C_{gUMG} M_{0UMG} + \left(\frac{2}{3}\right)\omega^2 C_{eUMG} M_{eUMG} - \left(\frac{1}{6}\right)\left(\frac{l_1}{l}\right)\omega^2 C_{BUMG} M_{BUMG} - 2\omega^2 C_{0UMG}\begin{pmatrix} L_{kwire} + \\ L_{kcoa} + L_{kD} \end{pmatrix}$$

$$C_{12} = -\left(\frac{2}{3}\right)\omega^2 C_{eLMG}^2 + \left(\frac{2}{3}\right)\omega^2 C_{eUMG}^2$$

$$C_{13} = -2\omega^2 C_{eLMG}^2 + 2\omega^2 C_{0LMG}\left(C_{0LMG} + C_{gLMG} + \frac{C_{kwire}}{2}\right) + 2\omega^2 C_{eUMG}^2 - 2\omega^2 C_{0UMG}\begin{pmatrix} C_{0UMG} + C_{gUMG} \\ + \frac{C_{kwire}}{2} \end{pmatrix}$$

$$C_{14} = -2\omega^2 C_{eLMG}^2 + 2\omega^2 C_{0LMG}\begin{pmatrix} C_{0LMG} + C_{gLMG} + C_{kwire} \\ + \frac{C_{kcoa}}{2} \end{pmatrix} + 2\omega^2 C_{eUMG}^2 - 2\omega^2 C_{0UMG}\begin{pmatrix} C_{0UMG} + C_{gUMG} \\ + C_{kwire} + \frac{C_{kcoa}}{2} \end{pmatrix}$$

$$C_{15} = -2\omega^2 C_{eLMG}^2 + 2\omega^2 C_{0LMG}\begin{pmatrix} C_{0LMG} + C_{gLMG} + C_{kwire} \\ + C_{kcoa} + \frac{C_{kD}}{2} \end{pmatrix} + 2\omega^2 C_{eUMG}^2 - 2\omega^2 C_{0UMG}\begin{pmatrix} C_{0UMG} + C_{gUMG} \\ + C_{kwire} + C_{kcoa} \\ + \frac{C_{kD}}{2} \end{pmatrix}$$

$$C_{16} = -\omega^2 C_{BLMG}^2 + \omega^2 C_{BUMG}^2$$

$$C_{17} = -\left(\frac{1}{3}\right)\omega^2 C_{BLMG}^2$$

$$C_{18} = \left(\frac{1}{3}\right)\omega^2 C_{BUMG}^2$$

$$C_{19} = \left(\frac{1}{3}\right)\omega^2 C_{gLMG}^2$$

$$C_{20} = -\left(\frac{1}{3}\right)\omega^2 C_{gUMG}^2$$

$$C_{21} = -\left(\frac{2}{3}\right)\omega^2 C_{gLMG} C_{eLMG}$$

$$C_{22} = \left(\frac{2}{3}\right)\omega^2 C_{gUMG} C_{eUMG}$$

$$C_{23} = \left(\frac{1}{6}\right)\omega^2 C_{BLMG}\left(C_{gLMG}\left(\frac{l_1}{l}\right) + C_{BLMG}\left(1 - \frac{l_1}{l}\right)\right)$$

$$C_{24} = -\left(\frac{1}{6}\right)\omega^2 C_{BUMG}\left(C_{gUMG}\left(\frac{l_2}{l}\right) + C_{BUMG}\left(1 - \frac{l_2}{l}\right)\right)$$

$$C_{25} = \left(\frac{1}{6}\right)\omega^2 C_{BLMG} M_{BLMG}\left(C_{BLMG}\left(\frac{l_1}{\sqrt{l}}\right) - C_{gLMG}\left(\frac{l_1}{\sqrt{l}}\right)\right) - \left(\frac{1}{6}\right)\omega^2 C_{BUMG} M_{BUMG}\left(C_{BUMG}\left(\frac{l_2}{\sqrt{l}}\right) - C_{gLMG}\left(\frac{l_2}{\sqrt{l}}\right)\right)$$

$$C_{26} = \left(\frac{1}{6}\right)\omega^2 C_{BLMG} M_{BLMG}\left(C_{gLMG}\left(\frac{1}{l}\right) + C_{BLMG}\left(\frac{1}{l}\right)\right)$$

$$C_{27} = -\left(\frac{1}{6}\right)\omega^2 C_{BUMG} M_{BUMG}\left(C_{gUMG}\left(\frac{1}{l}\right) - C_{BUMG}\left(\frac{1}{l}\right)\right)$$

# A.4 Uncertainty budget for a calculation of the capacitance change at 1592 Hz.



### TLK Capacitance change at 1.6 kHz

An approximate presentation of the calculable cross capacitor is shown in figure 1, and the connections apply to the measurement of a cross capacitance $C_{25}$ between electrodes 2 and 5 while electrodes 3, 4, and the guard electrodes are ground potential. The external electrical connection to the electrodes is made through coaxial connectors and ceramic feedthroughs mounted in the vacuum housing. All electrodes are connected to a feedthrough via a metal pin, a flexible piece of wire to accommodate small movements of the electrodes during adjustment, and a coaxial cable, respectively.

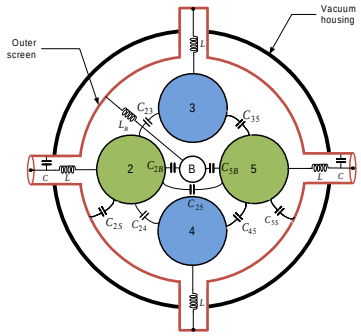


**Figure 1: An approximate presentation of the PTB's calculable cross capacitor.**

**Model Equation:**

$$\Delta C_0=(-2*\omega\text{^}2*C_{eLMG}\text{^}2*(L_{kwire}+L_{kcoa}+L_{kD}+(L_e/3))-\omega\text{^}2*C_{BLMG}\text{^}2*(L_{B0}+(L_{BLMG}/3))+$$
$$(1/3)*\omega\text{^}2*C_{gLMG}\text{^}2*M_{0LMG}-(2/3)*\omega\text{^}2*C_{gLMG}*C_{eLMG}*M_{eLMG}+$$
$$(1/6)*\omega\text{^}2*C_{BLMG}*M_{BLMG}*(C_{gLMG}*(l_1/l)+(C_{BLMG}*(1-(l_1/l))))+$$
$$2*\omega\text{^}2*C_{0LMG}*(((C_{0LMG}+C_{gLMG}+(C_{kwire}/2))*L_{kwire})+((C_{0LMG}+C_{gLMG}+C_{kwire}+(C_{kcoa}/2))*L_{kcoa})+$$
$$((C_{0LMG}+C_{gLMG}+C_{kwire}+C_{kcoa}+(C_{kD}/2))*L_{kD}))-$$
$$(-2*\omega\text{^}2*C_{eUMG}\text{^}2*(L_{kwire}+L_{kcoa}+L_{kD}+(L_e/3))-\omega\text{^}2*C_{BUMG}\text{^}2*(L_{B0}+(L_{BUMG}/3))+$$
$$(1/3)*\omega\text{^}2*C_{gUMG}\text{^}2*M_{0UMG}-(2/3)*\omega\text{^}2*C_{gUMG}*C_{eUMG}*M_{eUMG}+$$
$$(1/6)*\omega\text{^}2*C_{BUMG}*M_{BUMG}*(C_{gUMG}*(l_2/l)+(C_{BUMG}*(1-(l_2/l))))+$$
$$2*\omega\text{^}2*C_{0UMG}*(((C_{0UMG}+C_{gUMG}+(C_{kwire}/2))*L_{kwire})+((C_{0UMG}+C_{gUMG}+C_{kwire}+(C_{kcoa}/2))*L_{kcoa})+$$
$$((C_{0UMG}+C_{gUMG}+C_{kwire}+C_{kcoa}+(C_{kD}/2))*L_{kD}))$$

;$\omega=2*pi*f$

**List of Quantities:**

| Quantity | Unit | Definition |
|---|---|---|
| $\Delta C_0$ | F | Change in capacitance of the calculable cross capacitor |
| $\omega$ | rad/s | Angular frequency |
| $C_{eLMG}$ | F | Coupling capacitance between adjacent electrodes at lower position of the movable guard electrode |
| $L_{kwire}$ | H | Inductance of wire (Internal cable) |
| $L_{kcoa}$ | H | Inductance of coaxial cables (Internal cable) |

| | TLK Capacitance change at 1.6 kHz | PTB |
|---|---|---|

| Quantity | Unit | Definition |
|---|---|---|
| $L_{kD}$ | H | Inductance of feedthrough (Internal cable) |
| $L_e$ | H | Inductance of main electrode |
| $C_{BLMG}$ | F | Coupling capacitance between main electrode and movable guard electrode at lower position |
| $L_{B0}$ | H | Residual inductance of movable guard electrode for the distance between the lower end of the main electrodes and the ring of contacts |
| $L_{BLMG}$ | H | Inductance of movable guard electrode at its lower position |
| $C_{gLMG}$ | F | Coupling capacitance between electrode to ground at lower position of the movable guard electrode |
| $M_{0LMG}$ | H | Mutual inductance between opposite electrodes at lower position of the movable guard electrode |
| $M_{eLMG}$ | H | Mutual inductance between adjacent electrodes at lower position of the movable guard electrode |
| $M_{BLMG}$ | H | Mutual inductance between movable guard electrode and mian electrode at lower position |
| $l_1$ | m | length of movable guard electrode at lower position |
| l | m | length of main electrode |
| $C_{0LMG}$ | F | Cross capacitance at lower position of the movable guard electrode, 1.23 pF |
| $C_{kwire}$ | F | Capacitance of wire (Internal cable) |
| $C_{kcoa}$ | F | Capacitance of coaxial cable (Internal cable) |
| $C_{kD}$ | F | Capacitance of feedthrough (Internal cable) |
| $C_{eUMG}$ | F | Coupling capacitance between adjacent electrodes at upper position of the movable guard electrode |
| $C_{BUMG}$ | F | Coupling capacitance between main electrode and movable guard electrode at upper position |
| $L_{BUMG}$ | H | Inductance of the movable guard electrode at upper position |
| $C_{gUMG}$ | F | Coupling capacitance between electrode to ground at upper position of the movable guard electrode |
| $M_{0UMG}$ | H | Mutual inductance between opposite electrodes at upper position of the movable guard electrode |
| $M_{eUMG}$ | H | Mutual inductance between adjacent electrodes at upper position of the movable guard electrode |
| $M_{BUMG}$ | H | Mutual inductance between movable guard electrode and mian electrode at upper position |
| $l_2$ | m | length of movable guard electrode at upper position |
| $C_{0UMG}$ | F | Cross capacitance at upper position of the movable guard electrode, 0.23 pF |
| pi | | |
| f | Hz | frequency |

**$C_{eLMG}$:** Type B normal distribution
Value: $53.5 \cdot 10^{-12}$ F
Expanded Uncertainty: $1.1 \cdot 10^{-12}$ F
Coverage Factor: 3.31

| Date: 06/04/2012 | File: TLK 1.6 kHz Thesis.smu | Page 2 of 7 |
|---|---|---|

Generated with GUM Workbench Pro Version 2.4.1.392

| | TLK Capacitance change at 1.6 kHz | PTB |
|---|---|---|

**$L_{kwire}$:** Type B normal distribution
Value: $0.033 \cdot 10^{-6}$ H
Expanded Uncertainty: $0.018 \cdot 10^{-6}$ H
Coverage Factor: 2.13

**$L_{kcoa}$:** Type B normal distribution
Value: $0.059 \cdot 10^{-6}$ H
Expanded Uncertainty: $0.010 \cdot 10^{-6}$ H
Coverage Factor: 2

**$L_{kD}$:** Type B normal distribution
Value: $0.293 \cdot 10^{-6}$ H
Expanded Uncertainty: $0.02039 \cdot 10^{-6}$ H
Coverage Factor: 2

**$L_{e}$:** Type B normal distribution
Value: $0.717 \cdot 10^{-6}$ H
Expanded Uncertainty: $0.043 \cdot 10^{-6}$ H
Coverage Factor: 2

**$C_{BLMG}$:** Type B normal distribution
Value: $9 \cdot 10^{-12}$ F
Expanded Uncertainty: $0.57 \cdot 10^{-12}$ F
Coverage Factor: 2

**$L_{B0}$:** Type B normal distribution
Value: $0.0151 \cdot 10^{-6}$ H
Expanded Uncertainty: $0.0024 \cdot 10^{-6}$ H
Coverage Factor: 2.14

**$L_{BLMG}$:** Type B normal distribution
Value: $0.0326 \cdot 10^{-6}$ H
Expanded Uncertainty: $0.0047 \cdot 10^{-6}$ H
Coverage Factor: 2.25

**$C_{gLMG}$:** Type B normal distribution
Value: $273.0 \cdot 10^{-12}$ F
Expanded Uncertainty: $1.5 \cdot 10^{-12}$ F
Coverage Factor: 2.9

**$M_{0LMG}$:** Type B normal distribution
Value: $0.1061 \cdot 10^{-6}$ H
Expanded Uncertainty: $0.0053 \cdot 10^{-6}$ H
Coverage Factor: 2

**$M_{eLMG}$:** Type B normal distribution
Value: $0.1713 \cdot 10^{-6}$ H
Expanded Uncertainty: $0.0076 \cdot 10^{-6}$ H
Coverage Factor: 2

| Date: 06/04/2012 | File: TLK 1.6 kHz Thesis.smu | Page 3 of 7 |
|---|---|---|

Generated with GUM Workbench Pro Version 2.4.1.392

| | TLK Capacitance change at 1.6 kHz | PTB |
|---|---|---|

**$M_{BLMG}$:** Type B normal distribution
Value: $0.0192 \cdot 10^{-6}$ H
Expanded Uncertainty: $0.0021 \cdot 10^{-6}$ H
Coverage Factor: 2

**$l_1$:** Constant
Value: 0.065 m

**l:** Constant
Value: 0.85 m

**$C_{0LMG}$:** Constant
Value: $1.23 \cdot 10^{-12}$ F

**$C_{kwire}$:** Type B normal distribution
Value: $4.24 \cdot 10^{-12}$ F
Expanded Uncertainty: $0.28 \cdot 10^{-12}$ F
Coverage Factor: 2.7

**$C_{kcoa}$:** Type B normal distribution
Value: $10.45 \cdot 10^{-12}$ F
Expanded Uncertainty: $0.19 \cdot 10^{-12}$ F
Coverage Factor: 3.3

**$C_{kD}$:** Type B normal distribution
Value: $5.31 \cdot 10^{-12}$ F
Expanded Uncertainty: $0.018 \cdot 10^{-12}$ F
Coverage Factor: 2

**$C_{eUMG}$:** Type B normal distribution
Value: $49.5 \cdot 10^{-12}$ F
Expanded Uncertainty: $1.1 \cdot 10^{-12}$ F
Coverage Factor: 3.31

**$C_{BUMG}$:** Type B normal distribution
Value: $74 \cdot 10^{-12}$ F
Expanded Uncertainty: $4.2 \cdot 10^{-12}$ F
Coverage Factor: 2

**$L_{BUMG}$:** Type B normal distribution
Value: $.289 \cdot 10^{-6}$ H
Expanded Uncertainty: $0.042 \cdot 10^{-6}$ H
Coverage Factor: 2.28

**$C_{gUMG}$:** Type B normal distribution
Value: $325.8 \cdot 10^{-12}$ F
Expanded Uncertainty: $4.6 \cdot 10^{-12}$ F
Coverage Factor: 3.3

**$M_{0UMG}$:** Type B normal distribution
Value: $0.0993 \cdot 10^{-6}$ H
Expanded Uncertainty: $0.0052 \cdot 10^{-6}$ H
Coverage Factor: 2

| Date: 06/04/2012 | File: TLK 1.6 kHz Thesis.smu | Page 4 of 7 |
|---|---|---|

Generated with GUM Workbench Pro Version 2.4.1.392

| | TLK Capacitance change at 1.6 kHz | PTB |
|---|---|---|

**$M_{eUMG}$:** Type B normal distribution
Value: $0.1698 \cdot 10^{-6}$ H
Expanded Uncertainty: $0.0076 \cdot 10^{-6}$ H
Coverage Factor: 2

**$M_{BUMG}$:** Type B normal distribution
Value: $0.170 \cdot 10^{-6}$ H
Expanded Uncertainty: $0.019 \cdot 10^{-6}$ H
Coverage Factor: 2

**$l_2$:** Constant
Value: 0.575 m

**$C_{0UMG}$:** Constant
Value: $0.23 \cdot 10^{-12}$ F

**pi:** Constant
Value: 3.1415926535898

**f:** Constant
Value: 1591.54943091895 Hz

# A.4 Uncertainty budget for a calculation of the capacitance change at 1592 Hz



**Uncertainty Budgets:**

**$\Delta C_0$:** **Change in capacitance of the calculable cross capacitor**

| Quantity | Value | Standard Uncertainty | Distribution | Sensitivity Coefficient | Uncertainty Contribution | Index |
|---|---|---|---|---|---|---|
| $\omega$ | 10000.0 rad/s | 0.0 rad/s | | | | |
| $C_{eLMG}$ | $53.500 \cdot 10^{-12}$ F | $332 \cdot 10^{-15}$ F | normal | $-16 \cdot 10^{-9}$ | $-5.5 \cdot 10^{-21}$ F | 12.1 % |
| $L_{kwire}$ | $33.00 \cdot 10^{-9}$ H | $8.45 \cdot 10^{-9}$ H | normal | $-30 \cdot 10^{-15}$ | $-250 \cdot 10^{-24}$ F | 0.0 % |
| $L_{kcoa}$ | $59.00 \cdot 10^{-9}$ H | $5.00 \cdot 10^{-9}$ H | normal | $-28 \cdot 10^{-15}$ | $-140 \cdot 10^{-24}$ F | 0.0 % |
| $L_{kD}$ | $293.0 \cdot 10^{-9}$ H | $10.2 \cdot 10^{-9}$ H | normal | $-26 \cdot 10^{-15}$ | $-270 \cdot 10^{-24}$ F | 0.0 % |
| $L_e$ | $717.0 \cdot 10^{-9}$ H | $21.5 \cdot 10^{-9}$ H | normal | $-27 \cdot 10^{-15}$ | $-590 \cdot 10^{-24}$ F | 0.1 % |
| $C_{BLMG}$ | $9.000 \cdot 10^{-12}$ F | $285 \cdot 10^{-15}$ F | normal | $-35 \cdot 10^{-12}$ | $-9.9 \cdot 10^{-24}$ F | 0.0 % |
| $L_{B0}$ | $15.10 \cdot 10^{-9}$ H | $1.12 \cdot 10^{-9}$ H | normal | $540 \cdot 10^{-15}$ | $610 \cdot 10^{-24}$ F | 0.1 % |
| $L_{BLMG}$ | $32.60 \cdot 10^{-9}$ H | $2.09 \cdot 10^{-9}$ H | normal | $-2.7 \cdot 10^{-15}$ | $-5.6 \cdot 10^{-24}$ F | 0.0 % |
| $C_{gLMG}$ | $273.000 \cdot 10^{-12}$ F | $517 \cdot 10^{-15}$ F | normal | $1.4 \cdot 10^{-9}$ | $730 \cdot 10^{-24}$ F | 0.2 % |
| $M_{0LMG}$ | $106.10 \cdot 10^{-9}$ H | $2.65 \cdot 10^{-9}$ H | normal | $2.5 \cdot 10^{-12}$ | $6.6 \cdot 10^{-21}$ F | 17.5 % |
| $M_{eLMG}$ | $171.30 \cdot 10^{-9}$ H | $3.80 \cdot 10^{-9}$ H | normal | $-970 \cdot 10^{-15}$ | $-3.7 \cdot 10^{-21}$ F | 5.5 % |
| $M_{BLMG}$ | $19.20 \cdot 10^{-9}$ H | $1.05 \cdot 10^{-9}$ H | normal | $4.4 \cdot 10^{-15}$ | $4.6 \cdot 10^{-24}$ F | 0.0 % |
| $l_1$ | 0.065 m | | | | | |
| l | 0.85 m | | | | | |
| $C_{0LMG}$ | $1.23 \cdot 10^{-12}$ F | | | | | |
| $C_{kwire}$ | $4.240 \cdot 10^{-12}$ F | $104 \cdot 10^{-15}$ F | normal | $74 \cdot 10^{-12}$ | $7.6 \cdot 10^{-24}$ F | 0.0 % |
| $C_{kcoa}$ | $10.4500 \cdot 10^{-12}$ F | $57.6 \cdot 10^{-15}$ F | normal | $64 \cdot 10^{-12}$ | $3.7 \cdot 10^{-24}$ F | 0.0 % |
| $C_{kD}$ | $5.31000 \cdot 10^{-12}$ F | $9.00 \cdot 10^{-15}$ F | normal | $29 \cdot 10^{-12}$ | $260 \cdot 10^{-27}$ F | 0.0 % |
| $C_{eUMG}$ | $49.500 \cdot 10^{-12}$ F | $332 \cdot 10^{-15}$ F | normal | $16 \cdot 10^{-9}$ | $5.3 \cdot 10^{-21}$ F | 11.5 % |
| $C_{BUMG}$ | $74.00 \cdot 10^{-12}$ F | $2.10 \cdot 10^{-12}$ F | normal | $890 \cdot 10^{-12}$ | $1.9 \cdot 10^{-21}$ F | 1.4 % |
| $L_{BUMG}$ | $289.0 \cdot 10^{-9}$ H | $18.4 \cdot 10^{-9}$ H | normal | $180 \cdot 10^{-15}$ | $3.4 \cdot 10^{-21}$ F | 4.6 % |
| $C_{gUMG}$ | $325.80 \cdot 10^{-12}$ F | $1.39 \cdot 10^{-12}$ F | normal | $-1.8 \cdot 10^{-9}$ | $-2.4 \cdot 10^{-21}$ F | 2.4 % |
| $M_{0UMG}$ | $99.30 \cdot 10^{-9}$ H | $2.60 \cdot 10^{-9}$ H | normal | $-3.5 \cdot 10^{-12}$ | $-9.2 \cdot 10^{-21}$ F | 34.2 % |
| $M_{eUMG}$ | $169.80 \cdot 10^{-9}$ H | $3.80 \cdot 10^{-9}$ H | normal | $1.1 \cdot 10^{-12}$ | $4.1 \cdot 10^{-21}$ F | 6.8 % |
| $M_{BUMG}$ | $170.00 \cdot 10^{-9}$ H | $9.50 \cdot 10^{-9}$ H | normal | $-300 \cdot 10^{-15}$ | $-2.9 \cdot 10^{-21}$ F | 3.3 % |
| $l_2$ | 0.575 m | | | | | |
| $C_{0UMG}$ | $230.0 \cdot 10^{-15}$ F | | | | | |
| pi | 3.1415926535898 | | | | | |
| f | 1591.549430919 Hz | | | | | |
| $\Delta C_0$ | $-92.4 \cdot 10^{-21}$ F | $15.7 \cdot 10^{-21}$ F | | | | |

| | TLK Capacitance change at 1.6 kHz | PTB |
|---|---|---|

**Results:**

| Quantity | Value | Expanded Uncertainty | Coverage factor | Coverage |
|---|---|---|---|---|
| $\Delta C_0$ | $-92 \cdot 10^{-21}$ F | $31 \cdot 10^{-21}$ F | 2.00 | 95% (t-table 95.45%) |

| Date: 06/04/2012 | File: TLK 1.6 kHz Thesis.smu | Page 7 of 7 |
|---|---|---|

Generated with GUM Workbench Pro Version 2.4.1.392

# Acknowledgements

First and foremost, I would like to express my sincere gratitude and deep appreciated to Prof. Dr. Meinhard Schilling who provided the opportunity for me to take on this project and made available his support in a number of ways. I would like to express my deepest gratitude to Dr. Hans Bachmair and Dr. Torsten Funck for their valuable guidance and brilliant advices. Without their supervision this thesis would not have been possible. I offer my deepest gratitude to Dr. Jürgen Melcher for his support and useful discussions.

I would like to thank Prof. Achim Enders and Prof. Marc Tornow for offering their time to read and assess my work. Their compliments to make me very happy and I am very delighted to know that they recognize my work.

I am indebted to my many of my colleagues to Harald Bothe, Tim Thielemann, Dr. Bernd Schumacher, Dr. Jürgen Schurr, Veit Bürkel, Jürgen Kopton, Jan Kucera and Dr. Bryan Kibble. They contributed greatly to the success of this thesis and they are always very friendly and helpful to me all the time.

I would like to thank Physikalisch-Technische Bundesanstalt (PTB) for giving me the opportunity to perform my study. Also I would like to thank the international graduate school of metrology (IGSM) Braunschweig especially to Dr. Dezhen Li for supporting metrology courses and seminars.

I would like to thank my institute, National Institute of Metrology (Thailand), and Thai Government for funding and providing the opportunity for this thesis to be made possible. I offer my deepest gratitude to Ajchara Charoensook and Chalit Kumtawee who gave constant encouragement and support.

I am heartily thankful to my wife, Chompunut Jenajaroen, for her love, support and help.

Finally, to everyone who supported me in any respect during the completion of the thesis who was not stated by name here, I offer my sincerest gratitude and warmest blessings to you.

# Curriculum Vitae

| | |
|---|---|
| **Name** : | Monthol Homklintian |
| **Position** : | Metrologist, Department of Electrical Metrology |
| **Year of Birth** : | 1972 |
| **National** : | THAI |
| **Religion** : | Buddhism |
| **Higher Education** : | Master of Science (Physics) Department of Physics, Faculty of Science King Mungkut's University of Technology Thonburi Thailand |
| **Awards** : | Granted scholarship from The Royal Thai Government Scholarship (2007) |
| | Granted scholarship from National Institute of Metrology (Thailand), NIMT (2001) |
| **Principle fields of work** : | Maintain at the national impedance standard |

**Experiences**

| | |
|---|---|
| 1998(Nov) to present : | Metrologist at Electrical Laboratory, Electrical Metrology Department, National Institute of Metrology (Thailand), NIMT |
| 1994 to 1998 : | Scientist at Electrical and Electronic Standard Laboratory, Thailand Institute of Scientific and Technology Research, TISTR |

**Professional Records**

| | |
|---|---|
| Oct. 2006, Nov. 2007 : | Lecturer on the Association for Oversea Technical Scholarship (AOTS) Programme, Thailand |

# Declaration

This thesis is a presentation of my original research work. Wherever contributions of others are involved, every effort is made to indicate this clearly, with due reference to the literature, and acknowledgement of collaborative research and discussions.

I confirm that:

1. This work was done wholly or mainly while in candidature for a research degree at this University;
2. Where any part of this thesis has previously been submitted for a degree or any other qualification at this University or any other institution, this has been clearly stated;
3. Where I have consulted the published work of others, this is always clearly attributed;
4. Where I have quoted from the work of others, the source is always given. With the exception of such quotations, this thesis is entirely my own work;
5. I have acknowledged all main sources of help.